ARISTOTLE UNIVERSITY OF THESSALONIKI
FACULTY OF GEOLOGY
DEPARTMENT OF MINERALOGY, PETROLOGY,
ECONOMIC GEOLOGY

CHRISTOS L. STERGIOU

MINERALOGICAL, GEOCHEMICAL AND STRUCTURAL – CONTROL STUDY OF THE HYDROTHERMAL ALTERATIONS AND THE ORE MINERALIZATION AT VATHI PORPHYRY Cu – Au ± U ± Mo SYSTEM, N. GREECE

MASTER THESIS

THESSALONIKI
2016

CHRISTOS L. STERGIOU

Submitted at the Department of Mineralogy, Petrology, Economic Geology, Faculty of Geology, A.U.TH.

THREE-MEMBER COMMITTEE

1. Vasilios Melfos*	Assistant Professor. Department of Mineralogy, Petrology, Economic Geology, Faculty of Geology, School of Science, Aristotle University of Thessaloniki.
2. Kleopas Michailidis	Professor. Department of Mineralogy, Petrology, Economic Geology, Faculty of Geology, School of Science, Aristotle University of Thessaloniki.
3. Panagiotis Voudouris	Associated Professor. Department of Mineralogy – Petrology, Faculty of Geology and Geoenvironment, National and Kapodistrian University of Athens.

* Supervisor Professor

MINERALOGICAL, GEOCHEMICAL AND STRUCTURAL – CONTROL STUDY OF THE HYDROTHERMAL ALTERATIONS AND THE ORE MINERALIZATION AT VATHI PORPHYRY Cu – Au ± U ± Mo SYSTEM, N. GREECE.

ΟΡΥΚΤΟΛΟΓΙΚΗ, ΓΕΩΧΗΜΙΚΗ ΚΑΙ ΤΕΚΤΟΝΙΚΗ ΜΕΛΕΤΗ ΤΩΝ ΥΔΡΟΘΕΡΜΙΚΩΝ ΕΞΑΛΛΟΙΩΣΕΩΝ ΚΑΙ ΤΗΣ ΜΕΤΑΛΛΟΦΟΡΙΑΣ Cu – Au ± U ± Mo ΠΟΡΦΥΡΙΤΙΚΟΥ ΤΥΠΟΥ, ΣΤΗ ΒΑΘΗ, ΚΙΛΚΙΣ.

Table of Contents

ΠΕΡΙΛΗΨΗ

Στη Βάθη 18.5 χλμ ΒΔ του Κιλκίς στα όρια της Σερβομακεδονικής μεταλλογενετικής επαρχίας εντοπίζεται μεταλλοφορία Cu–Au±U±Mo πορφυριτικού τύπου. Ένας τραχειδακιτικός πορφύρης και διεισδύσεις χαλαζιακού μονζονίτη (18-17 Ma), η τοποθέτηση των οποίων ελέγχεται από την Τριτογενή τεκτονική της Σερβομακεδονικής Μάζας, φιλοξενούν την μεταλλοφορία. Γενετικά η μεταλλοφορία συνδέεται με τις διεισδύσεις του χαλαζιακού μονζονίτη, οι οποίες τέμνουν τον τραχειδακιτικό πορφύρη και τα περιβάλλοντα κρυσταλλοσχιστώδη πετρώματα του υποβάθρου της ενότητας Βερτίσκου. Ο τραχειδακιτικός πορφύρης χαρακτηρίζεται από μια προπυλιτική ζώνη εξαλλοίωσης, η οποία επικαλύπτεται από μια εκτεταμένη σερικιτική εξαλλοίωση. Ο χαλαζιακός μονζονίτης χαρακτηρίζεται από μια ποτασσική ζώνη εξαλλοίωσης, η οποία επίσης επικαλύπτεται από μια σερικιτίωση. Στον τραχειδακιτικό πορφύρη παρατηρούνται πλέγματα φλεβιδίων με οξειδωμένη μεταλλοφορία, παράλληλες φλέβες και D-τύπου φλέβες οξειδωμένου σιδηροπυρίτη, χαλκοπυρίτη και χαλαζία. Τοπικά μια έντονα ποτασσικά εξαλλοιωμένη τεκτονική ζώνη ελέγχει την παρουσία του χαλαζιακού μονζονίτη, ενώ αλλού συνδεόμενο με αυτόν εντοπίζεται ένα μαζώδες φρεατομαγματικό λατυποπαγές το οποίο διεισδύει στον τραχειδακιτικό πορφύρη. Διάσπαρτη και φλεβική μεταλλοφορία σιδηροπυρίτη – χαλκοπυρίτη εντοπίζεται στο χαλαζιακό μονζονίτη και σε βάθος στον τραχειδακιτικό πορφύρη. Σε μεγαλύτερα βάθη διασπορές σιδηροπυρίτη – χαλκοπυρίτη – βορνίτη – μολυβδαινίτη – μαγνητίτη – αυτοφυούς χρυσού περιγράφουν την μεταλλοφορία πορφυριτικού τύπου. Η μικροσκοπική μελέτη δειγμάτων προερχόμενων από γεώτρηση εντόπισε την παρουσία τριών ακόμη μεταλλοφοριών, μιας διάσπαρτης σιδηροπυρίτη – χαλκοπυρίτη – αντιμονίτη, και δυο φλεβικού τύπου, μία σφαλερίτη – γαληνίτη – αρσενοπυρίτη και μία μαγνητοπυρίτη – σιδηροπυρίτη – χαλκοπυρίτη. Τέλος, χαρακτηριστική είναι η επιφανειακή αλλά και σε βάθος παρουσία σιδηρούχων και χαλκούχων οξειδίων και μετα-τορβερνίτη τα οποία σχηματίζουν μια εκτεταμένη ζώνη οξείδωσης η οποία ακολουθείται βαθύτερα από μια μικρής έκτασης ζώνη δευτερογενή εμπλουτισμού αποτελούμενη κυρίως από χαλκοσίνη και κοβελλίνη. Η πορφυριτικού τύπου μεταλλοφορία της Βάθης χαρακτηρίζεται από υψηλές συγκεντρώσεις Au, αλλά και U και ορισμένων REEs το οποίο δεν είναι σύνηθες για τα πορφυριτικά συστήματα, και θα μπορούσε να αποτελέσει μελλοντικό ερευνητικό στόχο για χρυσό και REEs.

SUMMARY

The Vathi porphyry Cu–Au±U±Mo mineralization occurs in the Serbo-Macedonian metallogenic province, 18.5 km NW of Kilkis city at N. Greece. A trachydacite porphyry and quartz monzonite dikes (18-17 Ma), which emplacement was structurally controlled by the Tertiary evolution of the Serbo-Macedonian Massif, host the mineralization. Genetically the mineralization is linked to the quartz monzonite dikes which intrude the trachydacite porphyry and the crystalline basement rocks of the Vertiskos Unit. The trachydacite porphyry is affected by propylitic alteration, which is overprinted by an extended sericitic alteration. The quartz monzonite is affected by potassic alteration which is also overprinted by sericitic alteration. Stockwork, sheeted veins and oxidized pyrite, chalcopyrite and quartz D-type veins, outcrop in the trachydacite porphyry. Locally, a strongly potassically altered structural trend controls the qtz-monzonite emplacement, while elsewhere the quartz monzonite appears venting the trachydacite porphyry and creates a hydrothermally altered massive phreato-magmatic breccia. Disseminated and vein-type mineralization consisting of pyrite and chalcopyrite is found in the quartz monzonite and along the potassically altered area of the trachydacite porphyry. At depth, the most common mineralization consists of disseminated chalcopyrite – bornite – molybdenite – magnetite – native gold. The microscopic study of drill core samples revealed additionally the presence in depth of disseminated pyrite – chalcopyrite – stibnite, and of vein-type sphalerite – galena – arsenopyrite and pyrrhotite – pyrite – chalcopyrite mineralization. Along and near the surface a characteristic and extent supergene oxidation zone is developed dominated by iron and copper oxides and meta-torbernite, while deeper it is followed by a restricted secondary enrichment zone which consists mainly of chalcocite and covellite. The Vathi porphyry style mineralization bears exceptional enrichment in U and REEs which is unusual for porphyry systems. It shares several features in common to the Skouries porphyry Cu-Au deposit, in the adjacent Chalkidiki district and it could be a promising future exploration target for gold and REEs.

PREFACE

The increasing demand of modern societies for mineral resources in order to cover industrial needs, as well as the development of economic opportunities that could arise in an environment of economic depression, increased the interest of societies to reexamine their own mining potential. Geology and especially economic geology could significantly contribute to this target achievement.

Natural raw resources are subdivided into metals, industrial minerals and rocks, and energy mineral materials (coal, natural gas, oil, uranium) (PERC code). Critical and strategic minerals, also known as high technology minerals and/or metals (e.g In, Sb, Nb, Co etc), are definitions which describe the dependence of global industry to these metals (Sievers and Buijs, 2011). They are substantial to cutting-edge technological products such as lasers (gallium), super-conductors (indium), or even in more common products such as engine oil (graphite) and fire extinguishing materials (antimony). These contradict examples in terms of natural availability reveal the significance of the risk in supply shortage for some minerals which subcategorize them as critical (Sievers and Buijs, 2011). As a result, a new diplomatic field has been developed during the recent decades building and securing supply networks. Consequently, geoscientists co-working with economists and diplomats have a great responsibility to scientifically advising governments to plan a sustainable future on mineral resources policy.

Back in 2008, the European Commissioner Mr. Verheugen led a team of specialists to set a well defined working framework focusing on the European Union (EU) policy about mineral resources exploitation. Taking into consideration economic and technical feasibility factors, the Member States of EU should turn on exploring and developing their own mining potential, building a stronger economic society and securing the industrial future and independence. Since then the EU Commission has funded several projects examining the global challenges faced with respect to access to oil, gas, strategic and critical mineral resources over the next 30 years and to propose solutions (e.g POLINARES, Policy on Natural Resources - http://www.polinares.eu/). The Member States are encouraged to cooperate with geoscientists supporting their constant research efforts and utilizing the produced knowledge. Furthermore, geoscientists could secure rational exploitation and consistent in terms of environmental protection processes.

This master thesis was supported by the 2014 Society of Economic Geologists Foundation (SEGF) Student Research Grants Program and Hugh E. McKinstry Fund. It aims to reexamine the most recent theories on the hydrothermal alteration zones, the ore mineralization and the structural control of the Vathi porphyry Cu – Au ± U ± Mo deposit, at an effort to highlight the possible exploration and exploitation potentials. The Vathi porphyry-type deposit belongs to the Kilkis mining district of the Southern Serbo-Macedonian Massif in N. Greece and is an unexploited ore deposit. It bears exceptional geochemical and structural characteristics making it a target for both academic study and exploration.

I would like to gratefully acknowledge the supervisor Assistant Professor Vasilios Melfos for his valuable help and guidance to this effort. His patience, motivation and guidance were crucial in completing the fieldwork, research and writing of this thesis. Furthermore, I would like to thank Professor Kleopas Michailidis and Associated Professor Panagiotis Voudouris for providing their insight and expertise that greatly assisted the research, as well as the Assistant Professors Lambrini Papadopoulou and Nikolaos Kantiranis for their assistance with SEM and XRD analyses respectively and their constructive comments. Special thanks should be addressed to Assistant Professor Alexandros Chatzipetros for his helpful insights and revisions on the structural control of the Vathi porphyry system. I would also like to thank the PhD candidate Nikolaos Kipouros and the MSc student Aris Stamatiadis for their support in thin and polished sections preparation. Special thanks should be addressed to Constantinos Bangos and the laboratory staff of NCSR “Demokritos” for their assistance with SEM analysis of ore mineralization. Feeling immensely grateful to Eleni Tsirigoti I would like to thank her for providing technological, photographic and field work support. Finally, I would like to express my gratitude to my family for the overall support in the integration effort of my master studies, which tangible completion is this master thesis.

CHAPTER 1. INTRODUCTION

There are parts of the Earth's crust, sometimes extending thousands of kilometers, which comprise a high concentration of ore deposits of various types but with similar genetic origin and geological ages. These major ore exploration and production areas were first named metallogenic provinces by Louis de Launay (1913), a term which was later coined by Lindgren (1933), while later Petrascheck (1965) rephrased the definition of the metallogenic provinces. Accordingly, a metallogenic province is the entity of mineral deposits that formed during a tectonic-metallogenic epoch within a major tectonic Unit and which are characterized by related mineral composition, form of ore mineral bodies, and intensity of mineralization (Petrascheck, 1965). Globally, the major metallogenic provinces and the related ore deposits are associated to various geotectonic settings, for example, layered PGM and chromite deposits are connected to hot spots and continental rifting settings in cratonic areas, VMS-Cyprus type ore deposits are formed in mid-ocean ridge settings, and porphyry Cu-Mo ore deposits are linked to island and volcanic arc settings along collisional belts (Kerrich et al., 2005; Ridley, 2013).

Eurasian continent includes three major collisional zones which are associated with the Paleozoic Central Asian metallogenic belt, the Jurassic to Cenozoic Tethyan Eurasian metallogenic belt and the Jurassic to Cretaceous East Margin metallogenic belt of the Eurasian Continent (Mao et al., 2014). These enormous metallogenic belts comprise numerous metallogenic provinces with various types of porphyry ore deposits (Mao et al., 2014; Bertrand et al., 2014). The Tethyan Eurasian metallogenic belt (TEMB) extends approximately for 10,000 km from the Eastern Mediterranean to Southwestern Indonesia (Jankovic, 1977; 1986) and is subdivided into the Western and the Eastern Tethyan metallogenic belts. From SE Europe to Myanmar the TEMB hosts several major porphyry ore deposits (e.g. Rosia Poieni, Elatsite, Skouries, Kisladag, Sungun, Saindak; Mao et al., 2014; Zürcher et al., 2015). For this reason it is a significant exploration target for new deposits of this type. During the last years 50 new Cu-deposits bearing 280 Mt of Cu ore have been discovered (Singer et al., 2005; Zhang et al., 2009; Zürcher et al., 2015).

Running along the Alpine-Balkan-Carpathian-Dinaride orogen and continuing to Anatolide-Tauride orogen and to Zagros Mountains the Western Tethyan metallogenic belt (WTMB) comprises several major porphyry copper and high-

sulfidation epithermal ore deposits (Neubauer and Heinrich, 2003; von Quadt et al., 2004; de Vos et al., 2005; Yigit, 2012; Sutphin et al., 2013; Bertrand et al., 2014; Zürcher et al., 2015). The Eocene-Miocene branch of this belt comprises 46 porphyry Cu ore deposits (Carpathian–Balkan–Aegean deposits) through Romania, Serbia, Former Yugoslav Republic of Macedonia (FYROM), Greece and Turkey (Bertrand et al., 2014).

Mining has been part of the Greek civilization since antiquity, when ancient Greeks began extracting metallic mineral resources for use, mainly gold, silver, copper, lead and iron. The Vathi porphyry-type deposit was one of the targets for gold mining and the ancient underground mines are witnesses of the intense exploitation during the Kingdom of Alexander I of Macedonia (498–454 BC) and even later (Vavelidis, 2004). Since Bronze Age the auriferous deposits of Northern Greece developed and boosted a significant economic background for the future prospect of the ancient Macedonian Kingdom (Sagui, 1928; Vavelidis and Andreou, 2007). This was later capitalized by Philip II of Macedonia and Alexander the Great by financing the Macedonian campaign to Asia (Vavelidis, 2004; Vavelidis and Andreou, 2007).

Porphyry deposits are very attractive exploration and mining targets due to their high tonnage and relatively easy open pit mining. Recent research of porphyry Cu, Mo, Au deposits worldwide focuses on the refinements to the porphyry model and the new approaches and advances in geology and geochemistry and integrated interpretation, used to illustrate the state of the art of porphyry exploration (Sinclair, 2007; Seedorf et al., 2008; Sillitoe, 2010). The latest publications about Vathi date from late 1970s to early 1980s (e.g. Melidonis, 1970; Fillipidis et al., 1988; Sklavounos et al., 1992; Stergiou et al., 1993). In addition, there is not any publication targeted on the porphyry-style mineralization as most of them are focused on the U-rich mineralization occurring at the area.

The Vathi porphyry deposit belongs in the Serbo-Macedonian metallogenic province, which along with the adjacent Rhodope metallogenic province in northeastern Greece, are part of the Western Tethyan metallogenic belt and two of the most promising regions for future ore exploration projects in the south-eastern Europe (Neubauer and Heinrich, 2003; Melfos and Voudouris, 2012). Other well-known porphyry deposits in the Serbo-Macedonian metallogenic province are found in Skouries of Chalkidiki (N. Greece) (Eliopoulos and Economou-Eliopoulos, 1991; Gilg and Frei, 1994; Kroll et al., 2002), in Buchim mining area (FYROM) and in

Borov Dol (Serbia) (Serafimovski et al., 2010). Although Vathi is a small porphyry system, it is locally enriched in Cu, Mo, Au and U and has a considerable exploration potential for porphyry-style mineralization. Rough estimations show a potential of the Vathi system accounting for 15 Mt ore with 0.30 wt% Cu and 0.8 g/t Au on average (Veranis and Tsamantouridis, 1991).

In this framework of revisions of the previous investigations and new additions to scientific knowledge, this study focuses for the first time on the porphyry-style mineralization at Vathi. It aims at the study of the relations between the hydrothermal alteration zones, the ore mineralization and the structural control of the porphyry-type deposit. Furthermore, it reexamines the relations between the parent and the host rocks of the mineralization, as well as their petrology. Finally, on the base of the presented data a rough schematic model of the emplacement of the magmatic rocks, the ore mineralization and the alteration zones at Vathi is given.

CHAPTER 2. PORPHYRY TYPE DEPOSITS AND THEIR GEOTECTONIC SETTING

2.1. FROM MAGMAS TO PORPHYRY MINERALIZATION

During the last 46 years, since the establishment of the theory of porphyry ore deposits formation, many researchers continuously reexamine and evolve the principles and factors characterizing these economically fundamental ore deposits. More recent works (Sinclair, 2007; Seedorff et al., 2008; John et al., 2010; Sillitoe, 2010; Ridley, 2013; Loucks, 2015) refer on the porphyry Cu deposits comprising a long field experience and the most updated scientific knowledge. Globally, most of the regions of porphyry mineralization correspond spatially with contemporaneous or ancient subduction zones and with locations of lateral slab detachment at depth (Fig. 2.1).

Beneath the active and shaped by the ongoing collision settings geotectonic regimes, Al-rich basalts are formed, representing the parent magmas for the later calc-alkaline magmatic rock series. Geochemically they are enriched in Large-Ion Lithophile Elements (LILE), Nd, Sr and Pb isotopes deriving from the subducted slab, and in High Field Strength Elements (HFSE) deriving from the mantle wedge. According to Loucks et al. (2015), these distinguishing chemical characteristics of the copper-ore-forming calc-alkaline arc magmas are the result of accumulation of

dissolved H_2O through multiple cycles of replenishment and crystallization in high-pressure magma chambers near the Moho. Then a significant time of ponding along lower crust, in the magma reservoir follows, characterized by successive magma fractionations and assimilation of the surrounding rocks. These enriched in LILE and HFSE magmas are saturated in S, bear a significant metalliferous signature and move as diapirs towards the upper crust forming magma chambers (Fig. 2.2a,b). According to Seedorff et al. (2008) and Sillitoe (2010), the root zone of the melts forming porphyry rocks is placed at an average depth of 15 km. In this position localized fluid flows are characterized by the presence of numerous quartz veins and strong wall-rock alteration (Seedorff et al., 2008). Subsequently, these melts when extrude the batholithic cupola can intrude up to 5 km towards surface forming water-rich calc-alkaline magmatic chambers (Sillitoe, 2010).

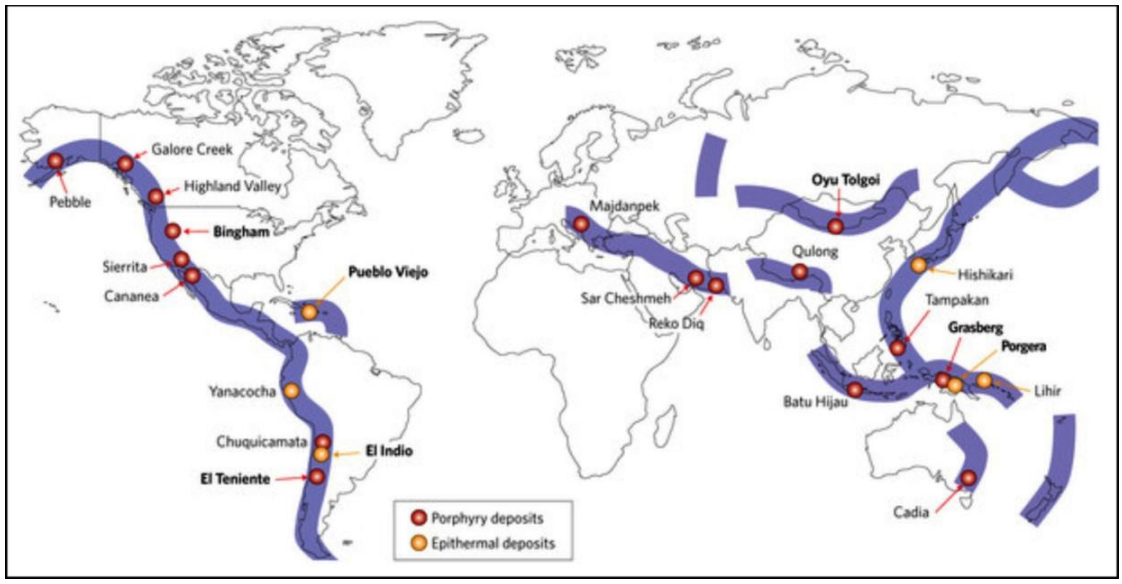

Figure 2.1. Old and contemporaneous subduction zones are the most common places where porphyry-Cu deposits are found, bearing an enormous metallic context. The old Western Tethyan Metallogenic Belt and the contemporaneous Andean Metallogenic Belt are the most important for exploration and exploitation (Richards, 2013).

At later stages, fluids and melts can exsolve in lower depths (up to <3 km) forming vertical intermediate to felsic (52-77 %wt SiO_2) intrusions, stocks and/or dikes and possibly create volcanic, mainly stratovolcanic, eruptions (Sillitoe, 2010; Ridley, 2013). Commonly these intrusions are subcategorized to early mineral, intermineral, late mineral and postmineral porphyries, and occur along the same porphyry rock stock and dike system (Gustafson, 1978). The last stages of these

evolving systems include the formation of lateral and vertical widespread hydrothermal alteration zones affecting large volumes of parent and host rocks.

Recently, many porphyry deposits are related to post-subduction procedures (Fig. 2.2c,d). These porphyry deposits exhibit many similarities compared to arc-related ones, regarding the magma composition and the ore deposit style, suggesting analogous petrogenetic and metallogenic processes (Richards, 2009). Slight differences are observed in the post-subduction magmatic settings at extensional and compressional/contractional environments related to subduction settings. For example post-subduction porphyry deposits are more enriched in Au with low Mo content compared to subduction related deposits.

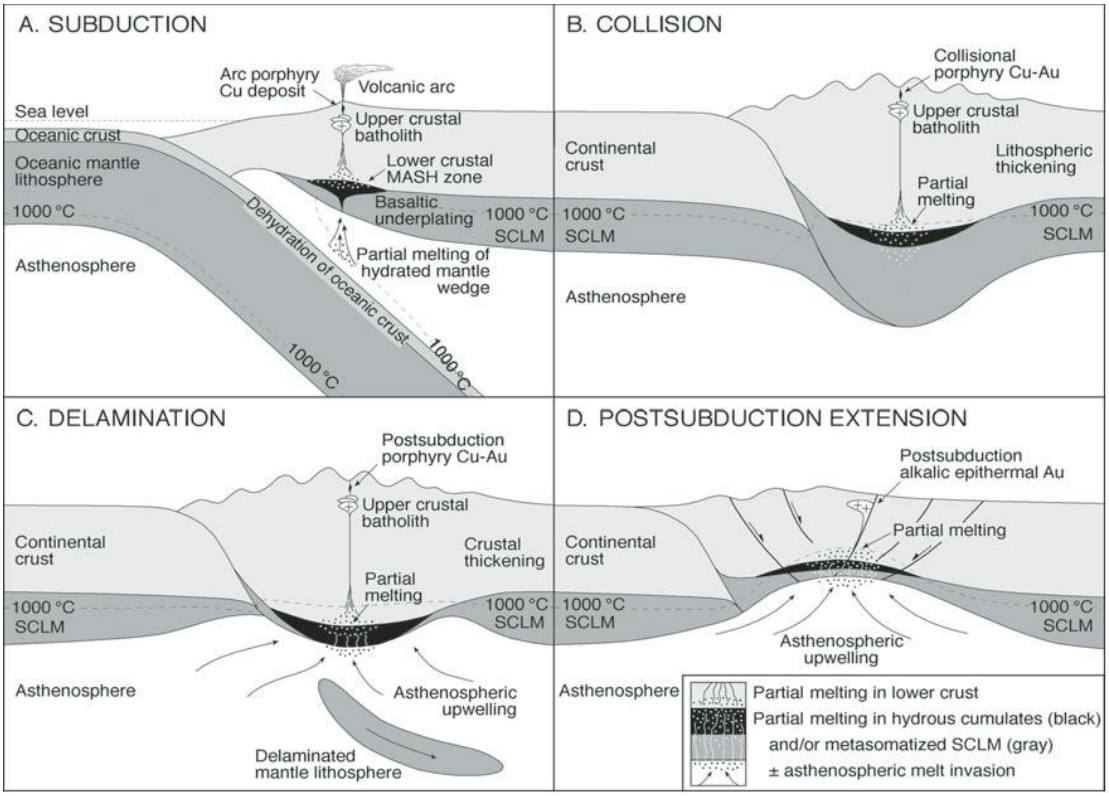

Figure 2.2. The spatial and genetical connection between porphyry deposits and geotectonic subduction (a,b) and post-subduction environments (c,d). MASH and SCLM acronyms stand for melting, assimilation, storage, and homogenization and subcontinental lithospheric mantle, respectively (Richards, 2009).

Contractional geotectonic environments are better correlated to porphyry deposits (Richards, 2009). The parent rocks of mineralizations are mildly alkaline (high-K ± Na calc-alkaline) to strongly alkaline products of small volume magmas,

spatially isolated having crustal radiogenic isotopic signatures (Davies and von Blanckenburg, 1995; John et al., 2010). These hydrous magmas show high Sr/Y, V/Sc and La/Yb ratios and a preferential partitioning of Y and middle – heavy rare earth elements into amphiboles and garnets. They have derived by partial remelting of the metasomatized lithospheric roots and hydrous cumulate zones of former arc systems and related geotectonic mechanisms. These mechanisms result in lithospheric thickening and thermal rebound, subcontinental lithospheric mantle delamination and lithospheric extension (Green and Pearson, 1985; Richards, 2009; Loucks, 2015).

Justifying the richer Au content of post-subduction magmas Richards (2005) suggested that the crystallization of arc-related Cu-rich magmas leave a significant residual melt between lower crust and lithospheric mantle, carrying sulfide phases enriched in Au as well as in PGE and Ni, due to the greater siderophile than chalcophile affinity of these elements (Richards, 2009). The dissolve of these sulfide phases with high Au/Cu ratios, forms low-sulfur magmas and eventually post-subduction porphyry deposits and low-sulfidation epithermal mineralizations (Tarkian and Stribrny, 1999; Richards, 2005).

Despite their genetic or geotectonic correlation most porphyry deposits globally are younger than 75 Ma (Ridley, 2013). The above described magmatic procedures and the porphyry Cu systems evolution have a life span ranging from 100.000 years for small individual deposits up to 10 Ma for entire porphyry belts (Sillitoe, 2010).

2.2. ANATOMY AND MORPHOLOGY OF PORPHYRY SYSTEMS

According to Sillitoe (2010) porphyry systems may be linked to co-magmatic, calc-alkaline to alkaline rocks, of intermediate to felsic compositions, which commonly erupt subaerially between 0.5 to 3 Ma prior to porphyry system intrusion. The overall time of the consolidation of individual porphyry intrusions, of the porphyry ore formation and of the major alteration events has been calculated to last between 2000 and 100.000 year (McInnes et al., 2005; Cathles and Shannon, 2007).

The porphyry deposits are subcategorized to porphyry Cu, porphyry Cu and Au and/or Mo and to porphyry Mo or Sn and Ag (Ridley, 2013). Mineralization and hydrothermal alteration occur within and at the periphery of the intrusions exhibiting an outward cylindrical to oval zoned development (Fig. 2.3B). Ore minerals form disseminations of some micrometers up to some millimeters filling fractures or veinlets and veins of some centimeters, while chalcopyrite, bornite and chalcocite are

the most important copper minerals (Sillitoe, 2010; Ridley, 2013). Molybdenum is exclusively expressed via molybdenite and when being present it occurs deeper than the Cu-Au ore body or along the periphery of the intrusion (Ridley, 2013). Native gold is present as small inclusions in bornite and chalcopyrite or as solid solutions in bornite (Berger et al., 2008; Ridley, 2013). Pyrite is increasing outwards the Cu ore body and may be spread up to few kilometers around large deposits. Galena, sphalerite, tetrahedrite and gold tellurides may be present in minor concentrations at the upper parts of the intrusion (Berger et al., 2008; Sillitoe, 2010). Finally, Re, W, Bi, In, PGEs and REEs are reported as trace constituents in many porphyry systems by Sinclair (2007) and Berger et al. (2008), and can be exploited as by-products.

Despite their varied ore context, porphyry deposits have much lesser grades than other ore types. According to Sinclair (2007), porphyry Cu deposits grades vary for Cu from 0.2 to 1.3%, for Mo from 50 to 300 g/t and for Au from 0.004 to 0.35 g/t. Mo-W and Sn porphyry deposits have grades which vary for Mo-W between 0.1 and 0.3% and for Sn between 0.2 and 0.5%. The key factor that makes porphyry deposits economically important –producing the 60-70% of Cu and 95% of Mo world's production– is their enormous sizes of hundreds or millions of tons of ore. Bearing such significant metal contents El Teniente in Chile, Bajo de la Alumbrera in Argentina, Grasberg in Indonesia and Bingham in the USA are some characteristic examples of giant porphyry deposits. The Skouries porphyry Cu-Au deposit in Greece, bearing 0.54 % Cu, 0.83 g/t Au and being enriched in Pd and Pt, has been recently characterized as a world class deposit (Kroll et al., 2002; Kesler et al., 2002; Voudouris et al., 2013; Logan and Mihalynuk, 2014).

The outward ore zoning is more efficiently described and comprehended when studied in combination with the alteration zones (Fig. 2.3B). The pioneers Lowell and Guilbert (1970) as well as more recently John et al. (2010), Sillitoe (2010) and Ridley (2013) have demonstrated a detailed description on alteration zones, which include various stages (Fig 2.3A). A progressive cooling procedure starting from >700^{o}C consecutively creates a K-feldspar and biotite (± magnetite ± amphibole ± anhydrite) rich potassic zone centered at the inner porphyry parts. Gradually an outer propylitic zone consisting of epidote, calcite, chlorite and locally albite with pyrite is formed. Sericitic –also called phyllic, argillic alterations are formed at temperatures ranging from 350 ^{o}C to below 250^{o}C, while sometimes also advanced argillic alteration is formed (600^{o}C) (Henley and Berger, 2012). Sericitic zone is represented by quartz,

sericite and pyrite, but it could also contain smectite group minerals and hematite. This zone is usually linked to feldspar-destructive phenomena and to late stage pyrite mineralization accompanied by D-type veins (Gustafson and Hunt, 1975; John et al., 2010; Ridley, 2013). Argillic zone is represented by quartz, montmorillonite, smectite, calcite, pyrite and advanced argillic by kaolintie and alunite. Sericitic and argillic alteration zones appear zoned between potassic and propylitic alterations but also overprinting them as younger, tabular or irregular alteration zones. According to Sillitoe (2010), low sulfidation-state chalcopyrite and bornite are characteristic of the potassic zone which is usually the economic significant zone, whilst higher sulfidation-state sulfide minerals, such as pyrite, enargite and covellite are connected to the outer alteration zones (Fig. 2.3B, Fig. 2.4). In some cases the sericitic alteration may include significant amounts of Cu. This, under surface weathering procedures, may result in oxidation of pyrite which produces acid sulfur fluids leaching Cu from chalcopyrite and creating a deep supergene zone enriched in Cu (Ridley, 2013).

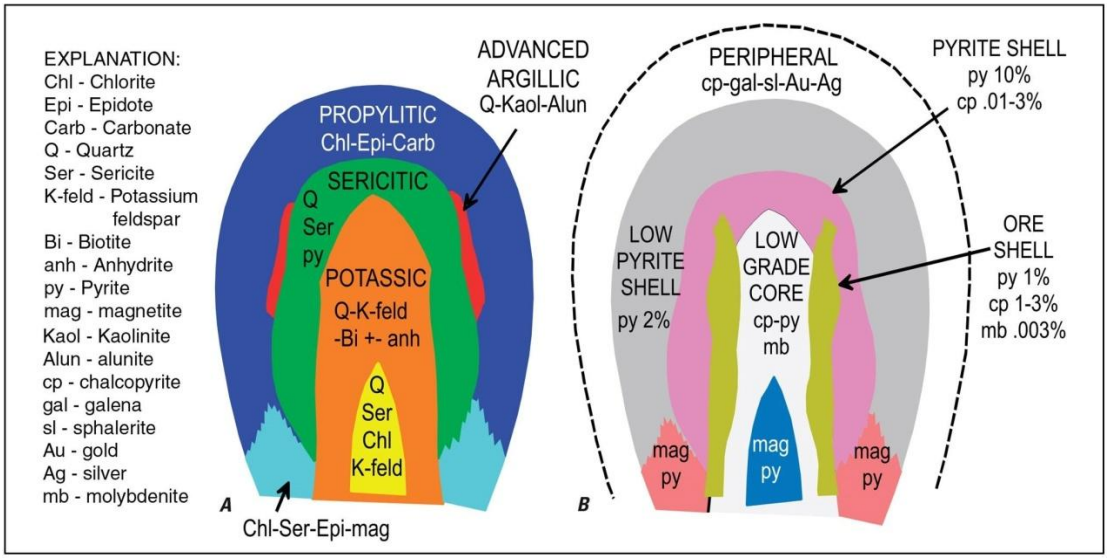

Figure 2.3. A. The general model of the lateral and vertical development of alteration zones and B. the typical outgrowth of the accompanying mineralizations in porphyry Cu (±Mo±Au) deposits (Lowell and Guillbert, 1970 modified by John et al., 2010).

Finally, some researchers describe also the calcic-sodic alteration zone (Thompson and Thompson, 1998; Ridley, 2013). The calcic-sodic alteration zone occurs peripheral to the lower limits of the ore zone and its formation requires an active fault system with saline waters at temperature of 450^{o}C which creates sodium-

and calcium-rich minerals (albite, orthoclase, actinolite) and destroys potassium- and iron-rich minerals, while minor pyrite and magnetite are often present.

Phreato-magmatic breccia eruptions are a common characteristic of the latest stages in porphyry deposits, locally remobilizing mineralization (Fig. 2.4). Interaction of magma with an external source of water creates vertical columnar breccias of up to 2 km deep and of a significant diameter, which crosscut or run the edges of the porphyry intrusions (John et al., 2010; Sillitoe, 2010). Despite that they may appear locally enriched in high-sulfidation Au mineralization, they bear poor to moderate amounts of metal content due to their late-stage character. This metal content is the result of the dilution of hypogene ore by the fluids of the pheato-magmatic breccias (John et al., 2010; Sillitoe, 2010).

The numerous veins and veinlets crosscutting a porphyry deposit have a major significance during the exploration stage (Fig. 2.5). These veins are grouped to M or EB, A, B and D veins associated with certain alteration zones and serve as hydrothermal fluid flow channels (Einaudi, 1997; Sillitoe, 2010; Ridley, 2013). The M and EB type veins, are early sulfide-free containing quartz ± actinolite ± biotite ± magnetite ± K-feldspar, lack any alteration halo and are connected to the deepest unmineralized parts of the potassic alteration zone. The A and B veins contain sulfide mineralization –mainly chalcopyrite– and granular quartz crystals, their alteration halos are not easily recognizable and are associated to potassic alteration zone. The D-type veins are late feldspar destructive veins, bearing quartz, pyrite and sericite, and are connected to sericitic alteration zone (Einaudi 1997, Sillitoe 2010, Ridley 2013). Sillitoe (2010) describes a transitional stage between M or EB veins and A and B veins which is characterized by veins consisting of quartz, sericite, K-feldspar and biotite, distinctive alteration halos of some centimeters in diameter and fine disseminated chalcopyrite ±bornite mineralization.

Furthermore, the regional and district tectonic settings should carefully be taken into consideration during studying or exploring porphyry deposits. They commonly occur at the root zones of andesitic stratovolcanoes above a continental- or island arc subduction setting but they are also related to pull-apart basins created by large post-subduction strike-slip faults (Sillitoe and Bonham, 1984; Hou et al., 2003).

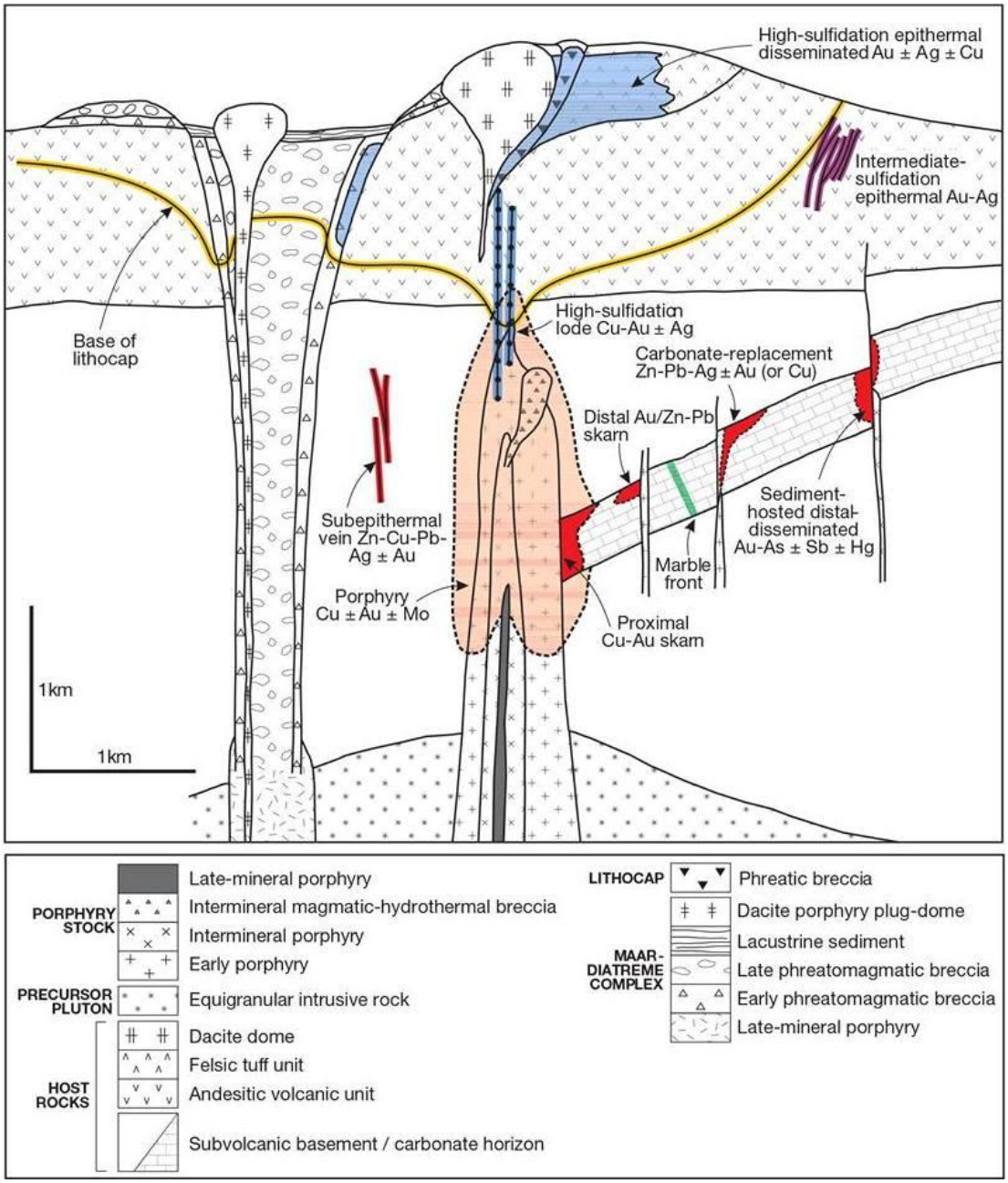

Figure 2.4. The anatomy of a telescoped porphyry Cu system comprising centrally located porphyry Cu±Mo±Au deposit (Sillitoe, 2010).

Porphyry Cu-Au deposits could be associated to alkaline intrusions at island-arc environments during periods of extension, while porphyry Au deposits appear in close relation to porphyry Cu-Au deposits (Sillitoe, 1993; MacDonald and Arnold, 1994). Porphyry Mo-W-Sn deposits are subcategorized to Endako and Climax types, related respectively to batholiths at continental rift or active extensional environments and to composite batholiths evolved in a continental subduction setting (Carten et al., 1993; Whalen et al., 2001; Ridley, 2013). Other deposits of this type are related to

subducted slab windows and gaps or to extension settings adjacent to strike-slip faults (Sillitoe, 2010).

Tectonic structures as rift settings, strike-slip faults, and pull-apart basins formed by detachment faults or between dextral strike-slip faults in extensional regimes above varied subduction or post-subduction environments are favorable areas for porphyry ore formation. They affect the morphological characteristics of the deposits and their spatial distribution in both district and regional scale. During exploration these tectonic features are described as the structural control of the intrusions and their study gives valuable information on the correlations between veins, stockworks, fractures, breccia pipes and local stress environments.

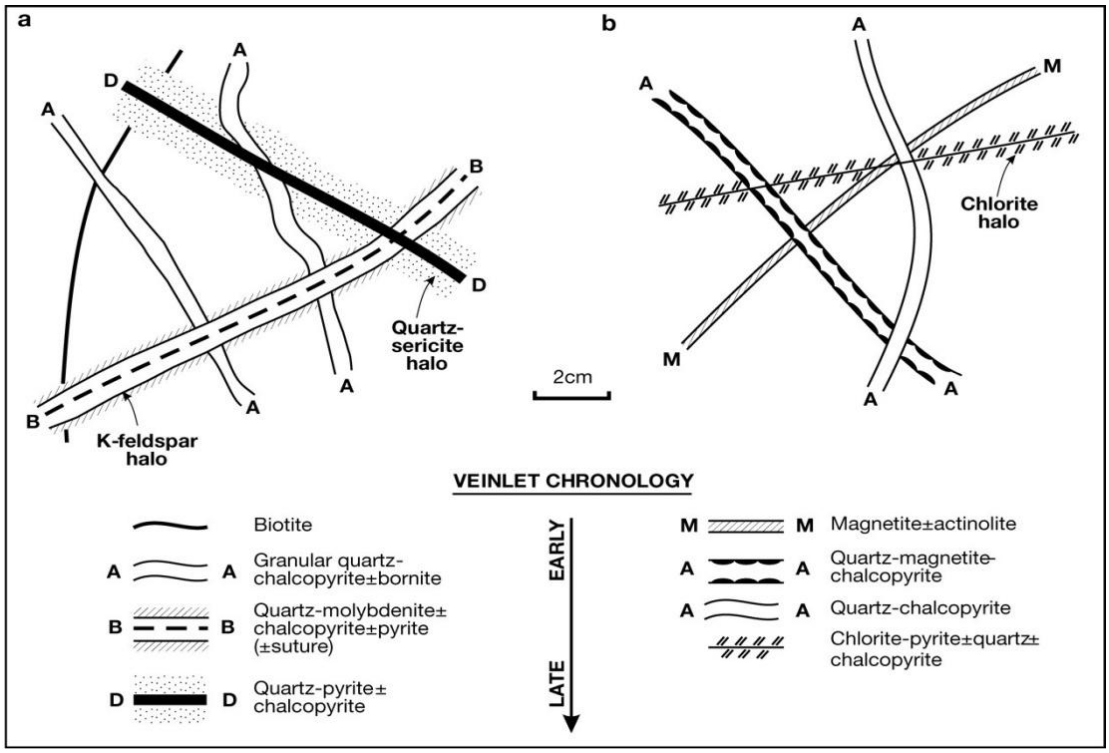

Figure 2.5. Schematic diagram depicting the chronological and morphological relations between the M- A- B- and D-type veins at porphyry systems (Sillitoe, 2010).

CHAPTER 3. GEOLOGICAL SETTING AND GEOTECTONIC EVOLUTION

3.1. TERTIARY TECTONICS AND MAGMATISM AT EASTERN MEDITERRANEAN

3.1.1. Introduction

Subduction zones are among the most complex geotectonic settings, where magmatic activity is more divergent than in spreading ridges or continental rifts, which evolve tholeitic and alkaline magmas respectively (MacDonald, 1974). At active ocean-continental margins magma is formed by partial melting of the ocean plate and/or of the overlying lerzolitic mantle wedge, caused by modified hydrated silicate fluids (MacDonald, 1974; Anderson, 2007). As far as final magma composition is concerned, four factors are very important: the initial fluids composition, the extension of mantle metasomatization, the transporting distance of the magma through overlying mantle wedge and continental crust and the timeline of the magmatic activity. On the last factor Ducea et al. (2015) add that short-term magmatic events (approx. 5-20 Ma) dwarf the volume of magmas produced. Compositionally, magmas from active continental margins, according to Nigel et al. (1986), demonstrate a wide range of low-K calc-alkaline, high-K and shoshonitic affinities (Harris et al., 1986). The same author has classified through a systematic geochemical study all the intermediate and acid rocks which occur at a continental collision zone as follows:

1. ***Pre-collision calc-alkaline (volcanic-arc) intrusions*** mostly derived from mantle, modified by a subduction component; selectively enriched in Large-Ion Lithophile Elements (LILE).
2. ***Syn-collision peraluminous intrusions (leucogranites)*** usually derived from the hydrated bases of continental thrust sheets; generally characterized by high Rb/Zr and Ta/Nb, and low K/Rb ratios.
3. ***Late or post-collision calc-alkaline intrusions*** usually derived from a mantle source undergoing extensive crustal contamination and can only be distinguished from pre-collision calc-alkaline volcanic-arc intrusions by higher Ta/Hf and Ta/Zr ratios.
4. ***Post-collision alkaline intrusions*** commonly derived from mantle lithosphere beneath the collision zones carrying high concentrations of both Large-Ion Lithophile Elements and High Field Strength Elements (hereinafter LILE and HFSE respectively).

The collision zone during the 1st and 2nd stage is characterized by climaxing dehydration reactions, volatile transfer and transient geothermal gradients (Harris et al., 1986). The 3rd stage is transitional to the 4th stage and is mainly characterized by the cease of subduction. Extensional settings, no voluminous co-temporal magmatism

and possibly slab roll-back and break-off characterize the last phases of the 3rd stage and dominate the 4th stage (de Boorder et al., 1998). Thus, the post-collision event starts with magmatic processes still influenced by subducted crustal materials. Progressively, crustal contamination of the mantle source becomes extensive, forming an enriched orogenic subcontinental lithospheric mantle (Bonin et al., 1998). As a result, the dominantly calc-alkaline series show gradual shift to alkali-calcic and then truly alkaline affinities enriched in K and LILE. It should be highlighted, that the development of this metasomatized character presupposes magma entrapment for a significant time at lower crust (Gupta and Fyfe, 2003).

The late and post-collision stages are defined by the formation of alkali-calcic monzonite – monzogranite – syenogranite alkali feldspar granite and alkaline monzonite – syenite – alkali feldspar granite associations (Bonin et al., 1998; Zhenhua et al., 2003). The alkali-calcic association is characterized by biotite and plagioclase fractionation and moderate LILE and HFSE enrichments. The alkaline association is characterized by amphibole and alkali feldspar fractionation displaying two evolutionary trends; one of peralkaline composition, sodic mafic mineralogy and higher enrichments in HFSE than in LILE and another of aluminous biotite-bearing composition marked by HFSE depletion relative to LILE due to accessory mineral precipitation (Bonin et al., 1998). Therefore, the post-collision event ends with the emplacement of bimodal post-orogenic suites along transcurrent fault zones (Bonin et al., 1998).

The K-rich magmatic rocks suite is subcategorized to high-K calc-alkaline and alkaline suites (Joplin, 1968). They include slightly silica-oversaturated to undersaturated rocks with K_2O and K_2O/Na_2O levels around 1 to 1.5 wt % for high-K calc-alkaline suite and around 1.5 to 2.5 wt % for alkaline suite (Peccerillo and Taylor, 1976). Thus, high-K basaltic andesites, andesites, dacites, rhyolites and K-trachybasalts, trachyandesites, trachytes and shoshonites are associated with high-K calc-alkaline and alkaline series respectively. Also, the subvolcanic equivalents of these volcanic rocks, such as gabbroic diorites, diorites, monzonites and granodiorites (high-K calc-alkaline suite) and quartz monzonites, monzonites (alkaline suite) follow the same classification.

Slab roll-back mechanism is commonly the main mechanism provoking extension. Slab roll-back (Fig. 3.1) occurs when the negatively buoyant slab, compared with the positively buoyant asthenosphere, sinks more rapidly than the rate

of plate convergence (Burg, 2002). The main causes for this roll-back are the length and the weight of the slab or the possible anchorage on the mantle (Condie, 1997; Anderson, 2007). Under these conditions, the slab starts to bend, away from the arc, and becomes gravitationally unstable and steeper, forcing hinge zone and bulge migration. Most commonly, such recurring events result in multiple extensional episodes in an overall convergent regime, due to the upwelling asthenosphere filling rapidly the space left by the retreating slab (Condie, 1997; Anderson, 2007).

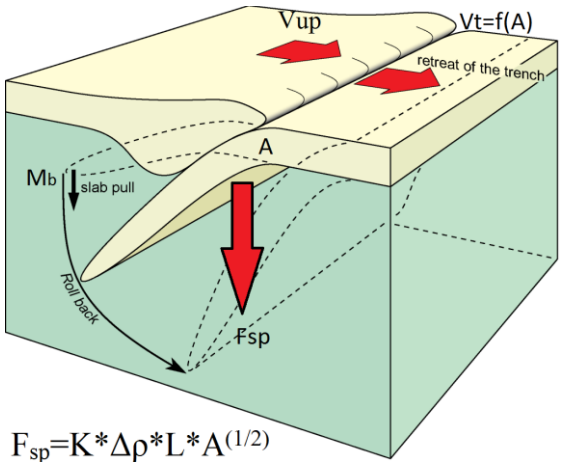

Figure 3.1. The slab roll-back model description using a mathematical equation. Where, *V*up: upper plate absolute motion, *V*t: trench absolute motion, *F*sp: slab pull force, *M*b: bending moment, *A*: age of the slab. $\Delta\rho$ defines the density difference between slab and mantle, *L* is the slab length and *K* is a constant. The upper plate is supposed to be fixed. Combined from Burg (2002), Heuret and Lallemand (2005) and Bertrand et al. (2014).

Slab roll-back defines the space of the extension, while asthenospheric material is the source of the extension (Stern, 2002; Heuret and Lallemand, 2005). Usually, slab roll-back procedure is followed by slab detachment, which is subdivided into slab break-off (tensile failure), simple shear (plastic or viscous shear zones) and necking models (Davies and von Blanckenburg, 1995; Duretz, 2012). Along strike of the trench, a fracture propagating horizontally can detach the slab from the surface part of the plate, probably after and along necking of the descending lithosphere (Davies and von Blanckenburg, 1995). Break-off usually starts from slab interior and spreads to the edges with an average rate between 150 and 800 mm/yr (van Hunen and Allen, 2011). Isostatic rebound, due to slab break-off and slab-pull suspension, characterized by a general uplift of the collision zone, follows due to the elastic unbending of the

subducting plate and the buoyant thickened crust (van Hunen and Allen, 2011). Subsequently asthenospheric material ascent to replace the dense slab and elevates the isotherms. This often leads to partial melting of both the mantle and crustal material and produces voluminous magmatism (Davies and von Blanckenburg, 1995).

According to Davies and von Blanckenburg (1995) the slab break-off may appear at shallow depths (~30 km), resulting in a shallow slab window and subsequent sudden heating and partial melting of the overriding lithosphere. However, van Hunen and Allen (2011) support that slab break-off takes place deeper than 200 km. They also, state that the time between first collision and slab break-off ranges from 10 Ma, for young and weak slabs, up to 20 Ma for old and strong slabs. Independently of the depth of the slab detachment, all researchers agree that the physicochemical mechanism leading to slab detachment is best described by viscous creep deformation theory (van Hunen and Allen, 2011; Duretz et al., 2012), where localized simple shearing and brittle fracturing are of minor importance. Despite of slab deformation variations the result is generally common, the upwelling asthenosphere gives rise to multiple magmatic rocks. Rise velocity, size, shape, volume and the surrounding frictional resistance are the factors controlling the ascent of these magmas which eventually will be emplaced in the upper crust usually forming porphyry type deposits (Winter, 2001; Dilek et al., 2009; Jolivet et al., 2013).

3.1.2. Mediterranean tectonic settings

Slab roll-back, break-off and lithospheric delamination, are pointed out by many researchers (Dugen et al., 2005; Dilek et al., 2009; Burg, 2012; Jolivet et al., 2013; Schildgen et al., 2014) as the common slab deformation procedure along the Mediterranean Alpine post-collision zone (Fig. 3.2).

In western Mediterranean, at Alboran Basin of Spain, according to Duggen et al. (2005), a slab roll-back model describes well the transition from subduction-related Si–K-rich to intraplate-type Si-poor magmatism at the Miocene–Pliocene boundary. Slab break-off settings link the Periandriatic, Adamello and Bergell melts and crustal reservoirs of calc-alkaline to ultrapotassic compositions, with an old oceanic plate subducting from Cretaceous to Eocene – Oligocene under southern Alps (Davies and von Blanckenburg, 1995; Dal Piaz et al., 2003). At the Aegean Sea, de Boorder et al. (1998) and Burg (2012) have proposed that slab roll-back settings were followed by slab detachment and asthenospheric upwelling. Finally, slab break-off deformation

and lithospheric delamination mechanisms have been proposed occurring along Arabia and Eurasia collision zone (Dilek et al., 2009; van Hunen and Allen, 2011; Schildgen et al., 2014). As an overall picture for the Mediterranean area, Duggen et al. (2005) and Dilek et al. (2009) proposed that lithospheric delamination processes followed slab roll-back or break-off. However, de Boorder et al. (1998) contradicts the lithospheric delamination process referring to evidences from a combination of seismic data tomography and predictions for lithosphere subduction through tectonic reconstructions, suggesting that a lithospheric delamination is the less likely process occurring at the European Alpine Belt. In any case, slab break-off and slab detachment mechanisms should be considered the cause of post-collision magmatism in the whole Mediterranean area (Duggen et al., 2005). Furthermore, an additional evidence for these mechanisms, especially along Aegean region, is the onset of alkaline magmatism following calc-alkaline magmatism and the exhumation of the crystalline basement rocks (de Boorder et al., 1998; Brun and Faccenna, 2008).

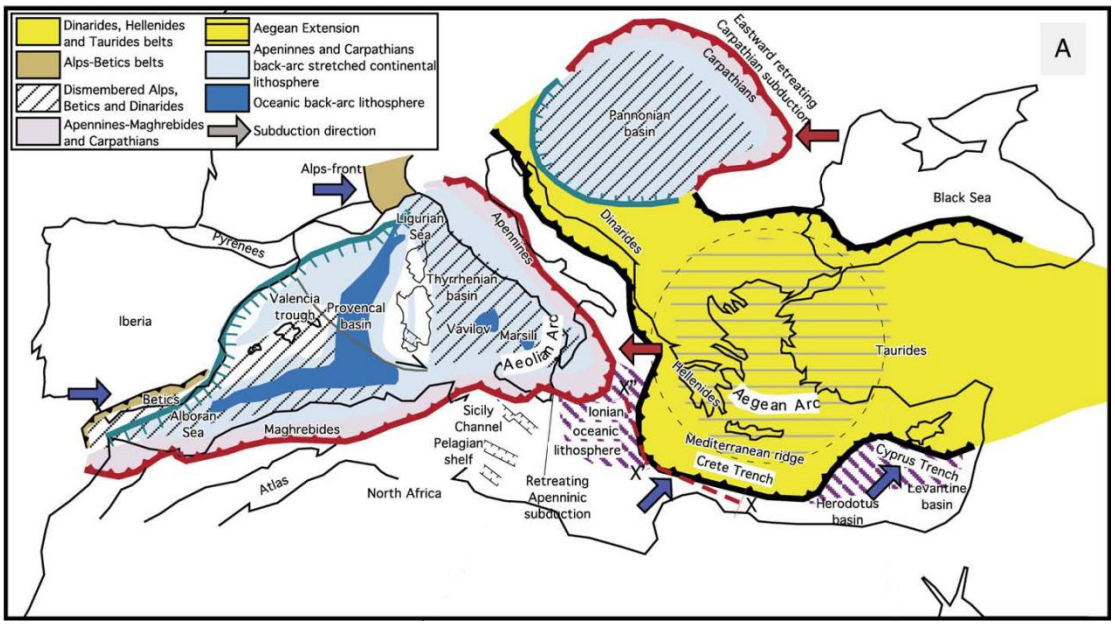

Figure 3.2. Subduction zones and major tectonic settings at the Mediterranean Alpine post collisional region (Agostini et al., 2009).

The formation of a wide range of Tertiary to Quaternary magmatic rocks characterizes the Alpine – Mediterranean region (Fig. 3.3). According to Wilson and Downes (2006), alkali basaltic magmas of anorogenic type can be found throughout the Mediterranean region, especially along the foreland of the Alps. Calc-alkaline,

potassic to ultrapotassic and silicic magmas, formed in the convergent margins, showing a geochemical composition related to subduction zones (Harangi et al., 2006). These magmatic affinities, divided by Wilson and Bianchini (1999) to orogenic and anorogenic, show a still highly controversial geodynamic and petrogenetic model (Harangi et al., 2006).

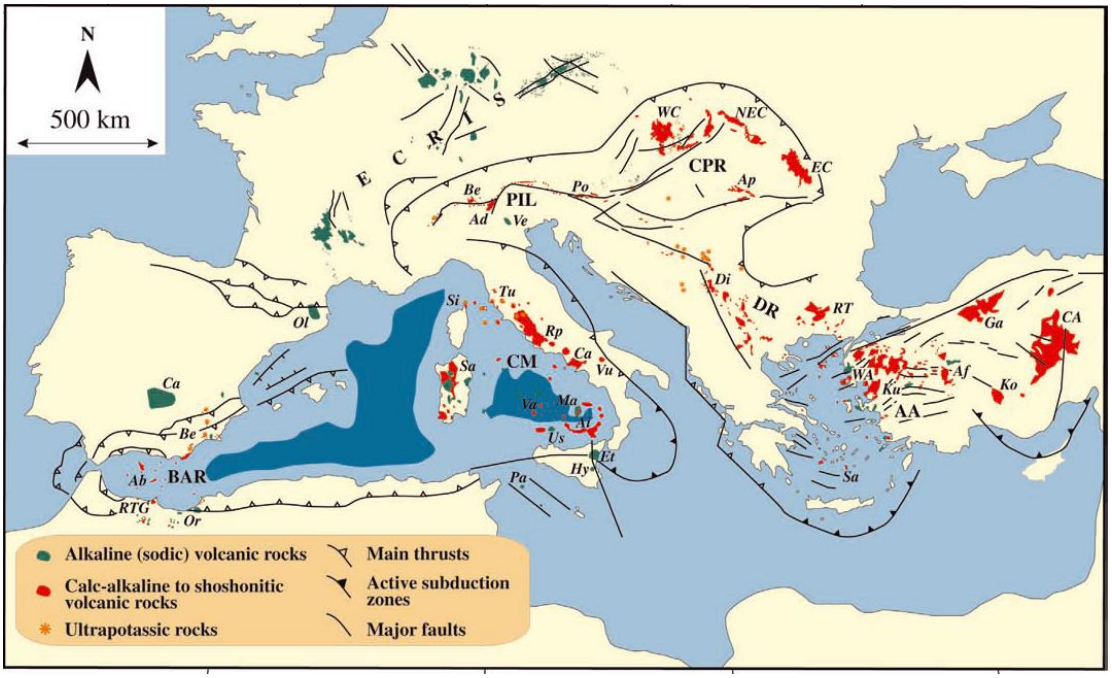

Figure 3.3. Distribution of Tertiary to Quaternary magmatic rocks in Alpine – Mediterranean region. Alkaline rocks appear mainly at intraplate and rifting environments, in contrast to calk-alkaline to ultrapotassic rocks which appear mainly at the hanging plates of the collision zones. Dark blue indicates areas with oceanic crust (Harangi et al., 2006).

3.1.3. The orogenic belt of Hellenides

The Hellenic subduction system is active since Late Cretaceous, as well as the accompanying back-arc rift developed during Upper Cretaceous-Paleocene (Agostini et al., 2010). Noteworthy are the low extension rate of the Aegean basin despite the long-lasting process, approximately 40 Ma, and the absence of oceanic crust in contrast to similar basins like Provencial and Thyrrenian (Jolivet, 2001; Doglioni et al., 2002). Running along the eastern edge of Apulia microplate, the orogenic belt of Hellenides is connected to the Alpine orogen to the north through Albanides and Dinarides orogenic belts. It displays east-directed thrusts in the internal zone and west-directed thrusts in the external zone due to Tertiary Apulia – Eurasia collision

(Dilek, 2005; 2006). This convergence has resulted in a cross-Balkan Peninsula broad dextral shear zone since Miocene and through locally well-developed transtensional zones promoted the ongoing orogenic collapse (Dumurdzanov et al., 2005; Tranos and Lacombe, 2014).

Taking place in a back-arc environment since the Late Oligocene – Early Miocene, the Western Anatolia – Aegean region is constantly subjected to extensional tectonics (Doglioni et al., 2002). Extension and magmatism (Fig. 3.4) have followed trench retreat since Eocene up to Quaternary (Harangi et al., 2006) and are tightly connected to slab roll back and slab detachment along a strongly arcuate subduction zone (Dilek, 2006; Schildgen et al., 2014). Following the complete closure of the Pindos ocean during Rupelian (30 Ma), caused by a convergence acceleration between 50 and 42 Ma, the subduction zone migrated southwards (Bertrand et al., 2014). Later, during Langhian (15 Ma), a significant decrease of the convergence rate was caused by the collision of the Arabian plate to Eurasia, which resulted in the formation of the Miocene magmatic rocks of Northern Greece and Aegean (Bertrand et al., 2014). These magmatic rocks are characterized by high-K calc-alkaline to potassic affinities and by significant ore mineralization occurences.

Slab roll-back theory, according to Doglioni et al. (2002) and Jolivet et al. (2000; 2013), is boosted by data showing that the southern Aegean moves southward relatively faster than the Anatolia microplate moves westward (Agostini et al., 2010), as well as by the fact that numerous high-pressure rocks are exhumed along trench retreat (Brun and Faccenna, 2008). Two more exceptional characteristics of this setting are the non-existence of seismicity deeper than 180 km and the low subduction angle, approximately 16°, along 200 km of subducting lithosphere resulting in a northward flattening (Agostini et al., 2010). Furthermore, Makris (1985) and Tirel (2004) have suggested that the upper continental plate range in thickness from 25 to 50 km. Also, according to Agostini et al. (2010), magmatic sources along Aegean are placed around the depth of 100 km. Taking into consideration the slab isobaths at active Aegean subduction (Papazachos et al., 2000), it is pointed out that mantle wedge beneath Aegean consists mainly of continental lithospheric mantle and a thin asthenospheric layer (Agostini et al., 2010).

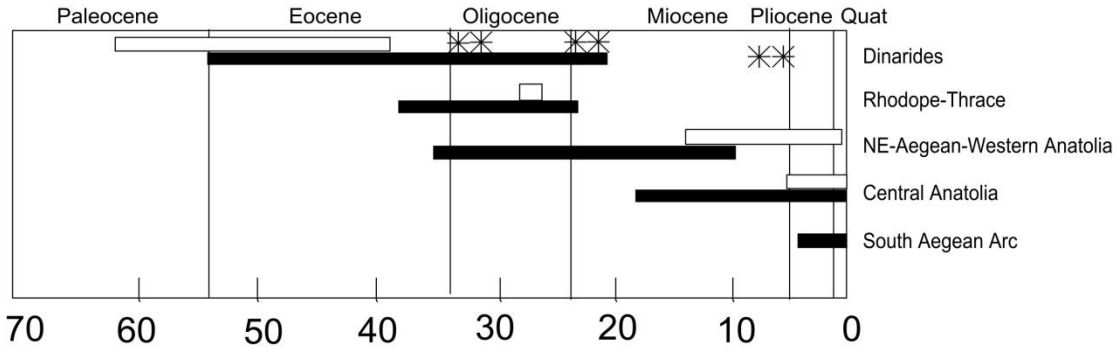

Figure 3.4. The timeline of magmatism at the Hellenic arc. The black and white lines correspond to calc-alkaline/shoshonitic and alkaline magmatisms respectively, while the radial symbols mark the ultrapotassic magmatic episodes. It seems that magmatism follows a pattern, possibly being connected to slab retreat (Harangi et al., 2006).

Thus, summing up and taking into account the above theories, some fundamental constraints can be listed (Pe-Piper, 2006; Dilek, 2006; Harangi et al., 2006; Agostini et al., 2010):

1. The hydrous melting of the mantle wedge during Eocene gave rise to magmas emplaced in a shear zone tectonic environment.
2. During Oligocene shoshonitic magmatism, probably related to slab detachment (Vardar Ocean) and set in an extensional regime was emplaced along northern Greece.
3. Early Miocene shoshonites of northeastern Aegean are probably related to a slab detachment from the Pindos Ocean. This is also the starting point of the modern geotectonic environment occurring along south Aegean.
4. During Early-Middle Miocene (Fig. 3.5A) magmas evolved from calc-alkaline to high K and ultrapotassic affinities, which implies a non-convective mantle wedge and magmas generation after partial melting of the same mantle domain.
5. B-Li negative signatures suggest that the almost stagnant, slow moving slab was almost completely dewatered. Li isotopes point out a limited interaction between slab fluids and mantle, which reveals a low-volume mantle wedge.
6. Finally, asthenosphere extensional partial melting suffering no interaction with slab fluids is the cause of the later Na-alkaline magmas (Fig. 3.5B). On the contrary, where K-alkaline magmas occur, the sub-slab magmas and residual

slab fluids, interaction should be implied, as well as the existence of a vestigial slab window due to slab tearing (Fig. 3.5).

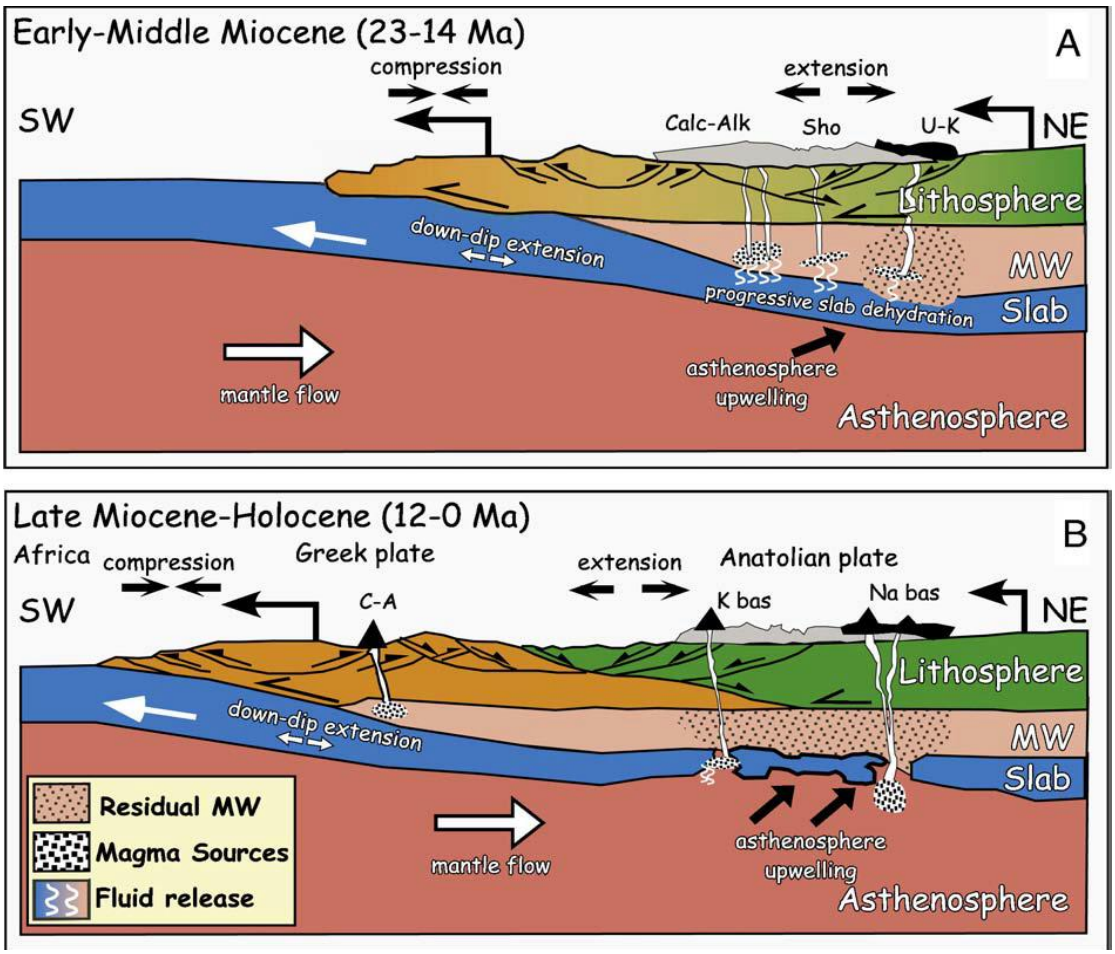

Figure 3.5. Early to Middle Miocene mantle wedge metasomatization due to slab dehydration resulted in the formation of calc-alkaline to shoshonitic and ultrapotassic magmas. Later on, since Late Miocene, the ongoing extensional tectonics led to asthenospheric upwelling affecting the whole subduction setting. OIB type magmas formed and reached the surface (Agostini et al., 2010).

These constraints along with those by Ducea et al. (2015) suggest that the continuous retreat to S-SE of the subducted plate drastically controlled the volume and the spatial distribution of the magmatism, while brief periods of decrease in the convergence rate affected the magmatism magnitude and the metalliferous content of the ore deposits (Bertrand et al., 2014). Due to this unstable geotectonic environment the Hellenides orogenic belt is characterized by variability in magmatic compositions, widespread spatial distribution and no high-voluminous magmatism. The Tertiary magmatism of the Northern Greece is characterized by dwarf magmatic volumes (Pe-

Piper and Piper, 2002; Serafimovski et al., 2010). Thus, the contradicting relation between the duration of the magmatic "flare-up" events and the high-volume magmatism with the periodic subduction retreat is highlighted (Ducea et al., 2015).

3.2. GEOLOGY AND GEOTECTONIC EVOLUTION OF THE SERBO-MACEDONIAN MASSIF

The long-debated Serbo-Macedonian Massif belongs to the complex tectonomagmatic terrain which forms the northern area of Hellenides or the North Aegean Domain (Kydonakis et al., 2015). The Serbo-Macedonian Massif (Fig.3.1) spreads from southern Serbia to northern Greece through Kosovo and the Former Yugoslav Republic of Macedonia (FYROM).

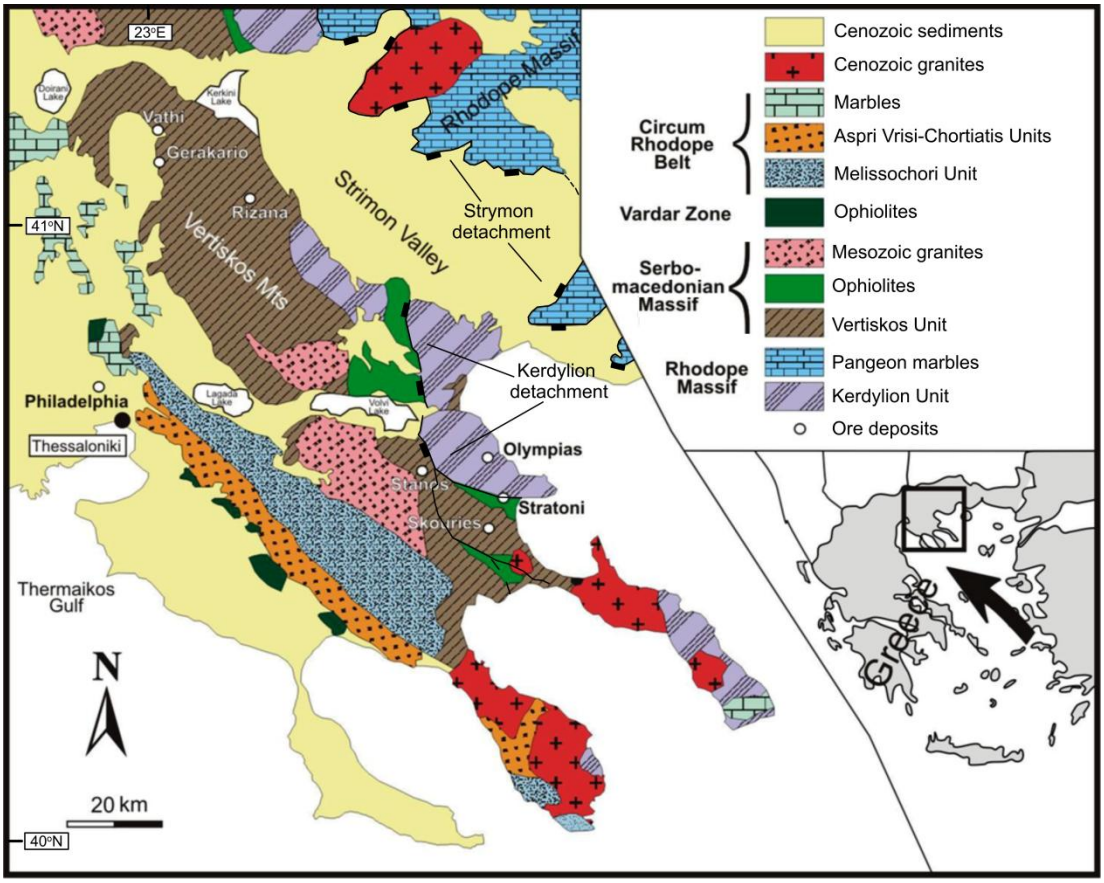

Figure 3.6. Simplified geological map of the Serbo-Macedonian Massif in northern Greece, with the major ore deposits and ore occurrences (modified after Melfos and Voudouris, 2012).

In Greece it appears as a large, elongated geotectonic zone comprising a metamorphic basement, with a NW-SE direction from the northern Greek borders to Chalkidiki peninsula (Kilias et al., 1999; Himmerkus et al., 2006; Kilias et al., 2015).

It borders to the east with the Rhodope Massif along the Strymon and Kerdylion low angle detachment fault zones (Kilias et al., 2013; Kydonakis et al., 2014; Kilias et al., 2015), and to the west with the Circum Rhodope belt along a border which is strongly debated between researchers (Kilias et al., 1999; Tranos et al., 2008). Vertiskos and Kerdylion Units are part of a Paleozoic (Kockel et al. 1968; 1972), or even Precambrian (Himmerkus et al. 2006), metamorphic napple pile (Kilias et al., 1997; 1999). During Late Cretaceous and Middle Eocene (68.5 ± 3.8 to 46.6 ± 3.6 Ma) it was exposed and subsequently extensionally collapsed until Late Eocene to south-southwest (Krohe and Mposkos, 2002; Kydonakis et al., 2014).

The lower Kerdylion and the upper and younger Vertiskos Units being separated by Kerdylion detachment fault used to be considered as the two Units building up the Serbo-Macedonian Massif (Kilias et al., 1999). In contrast to previous theories, recently the Kerdylion Unit has been regarded as part of the Rhodope Massif (Brun and Sokoutis, 2007; Kydonakis et al., 2014; Kilias et al., 2015). According to Himmerkus et al. (2007) the Greek Serbo-Macedonian Massif could be subdivided into Pirgadikia, Vertiskos, Arnea and Kerdillion Units, while according to Kydonakis et al. (2015) it is subdivided into Vertiskos Unit, the Circum–Rhodope belt, the Chortiatis Magmatic Suite and the eastern Vardar Ophiolites. However, all researchers agree that the Vertiskos Unit of the Serbo-Macedonian Massif is most probably the westernmost extreme of the Rhodope Metamorphic Province or the Rhodope Core Complex (Himmerkus et al., 2009a; 2009b; Kydonakis et al., 2014; Kilias et al., 2015). Moreover, Himmerkus et al. (2009a) suggest that the Vertiskos Unit is an exotic terrene, previously belonging to Hun-Terrene, which was incorporated and accreted on Internal Hellenides during the closure of a branch of the Tethys Ocean and the subsequent Alpine Hellenic Orogeny.

The Vertiskos Unit is divided in two sequences, one with migmatites, augen orthogneisses, mica schists and thin marble layers and another with metagabbros – metadiabases and orthoamphibolites derived from magmatism of basic igneous rocks, appearing as intercalations in orthogneisses (Sidiropoulos, 1991; Kourou, 1991; Himmerkus et al. 2009a). In addition, mafic to ultramafic bodies, known as the Therma-Volvi-Gomati (TVG) complex are tectonically interposed in the sequences of the crystalline metamorphic rocks (Dixon and Dimitriadis, 1986; Bonev et al., 2012).

Three groups of magmatic rocks intruding Serbo-Macedonian Massif have been described (Himmerkus et al., 2009b). The older group consists of the feldspar-

microclinic gneisses of Vertiskos Unit and represent granites, most probably of Silurian age (Himerkus et al., 2006). The second group is built up by the massive A-type granites of Arnea type, intruding according to Himmerkus et al. (2009b) the Serbo-Macedonian Massif at an average age of 228.3 ± 5.6 Ma (Middle Triassic). The same researchers mention that these granites along with the Triassic ultramafic amphibolitic intrusions of Vertiskos Unit are related with a contemporaneous rifting responsible for the formation of a Neo-Tethys branch.

The third group of the magmatic rocks was formed during Eocene – Oligocene – Miocene, as a result of a "leopard skin" mantle wedge evolved by forwarding metasomatism fluids released from the two subducted slabs of Pindos and Vardar Oceans (Perugini et al., 2004). Products of this process ranging from calc-alkaline to ultra-potassic affinities, following the extensive events, interacted with the crustal calc-alkaline anatectic melts and finally were impelled into Serbo-Macedonian Massif mainly as final intrusions (Fig. 3.7) (Perugini et al., 2004). In contrast to contemporaneous magmatic rocks of central Rhodope Massif (Tranos et al., 2009; Kaiser-Rohrmeier et al., 2013), the magmatic rocks of the Serbo-Macedonian Massif do not exhibit wide mylonitic structures (Fig. 3.7). Along the Serbo-Macedonian Massif the plastic deformation was replaced early during Eocene by brittle deformation, which drastically controlled the later intrusions (Kilias et al., 1999). The cause for this change was the early exhumation of the Serbo-Macedonian Massif during Late Cretaceous to Eocene (Kydonakis et al., 2014; Kilias et al., 2013; 2015).

Three metamorphic events are displayed in the Serbo-Macedonian Massif: an old Erkynian or Silourian eclogitic-facies (Himmerkus et al., 2006), a dominant amphibolitic-facies probably expanding from Late Paleozoic to Cretaceous partly affecting retrogradely the eclogitic-facies and finally a locally appearing retrograde greenschist-facies taking place between Cretaceous and Early Tertiary (Dimitriadis and Godelitsas, 1991; Himmerkus et al., 2006; Kydonakis et al., 2014). Two extensional events are reported by Kilias et al. (1997; 1999). The older is contemporaneous to the amphibolitic metamorphic facies, ductile extensional event of Cretaceous age, exhibiting ENE-WSW steering tensions and eastward sheering movements. The younger is placed during Eocene it was expressed superficially by brittle deformations; it was contemporaneous to the greenschist metamorphic face and characterized by normal faults of NE-SW direction. However the estimated

extensional ages, associated with the Tertiary magmatism, are not in absolute accordance with the above metamorphic ages.

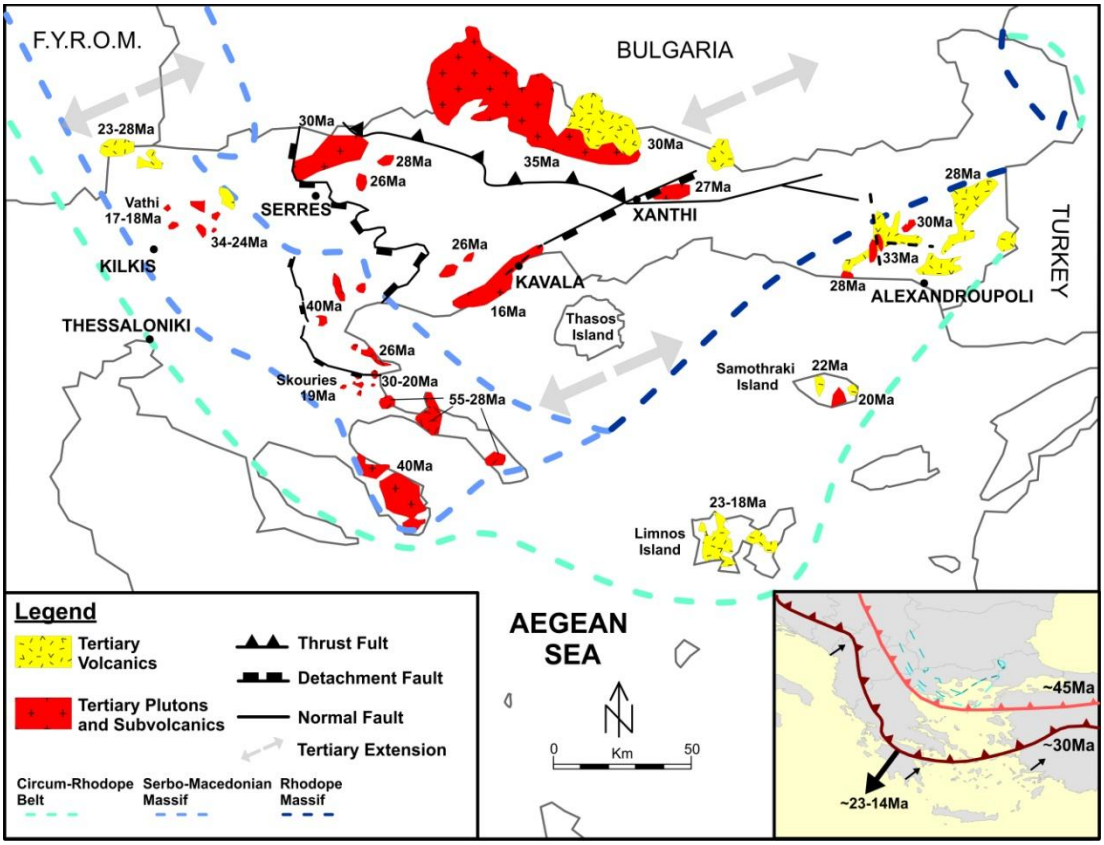

Figure 3.7. Schematic map depicting the spatial distribution of numerous Tertiary plutonic, subvolcanic and volcanic rocks through Serbo-Macedonian and Rhodope Massifs. The progressive southward retrieve of the subduction zone due to slab roll-back mechanism (bottom right image) is the main cause producing various magmatic rocks since Early Tertiary. Data from Frei (1992), Gilg and Frei (1994), Soldatos et al. (2001), Harangi et al. (2006), Agostini et al. (2010), Hahn et al. (2012) and Bertrand et al. (2014).

3.3. TERTIARY MAGMATISM IN THE SERBO-MACEDONIAN MASSIF

Several authors have mentioned the linkage between geotectonic settings and Tertiary magmatism occurring along north Greece (Pe-Piper and Piper, 2006; Dilek, 2006; Harangi et al., 2006; Agostini et al., 2010). Set in a complex extensive geotectonic environment Tertiary Serbo-Macedonian Massif magmatism is characterized by I-type plutonic rocks with calc-alkaline to high K-calc-alkaline to shoshonitic affinities, while volcanism is characterized by andesitic and dacitic rocks (Pamic et al., 2002; Pe-Piper and Piper, 2006). According to Kockel et al. (1975)

throughout the Greek Serbo-Macedonian Massif 85 magmatic rocks of intrusive and extrusive characters are mainly concentrated in three regions: the Eastern Chalkidiki peninsula (southern region), the Kerdylion and Vertiskos mountains (central region) and the Krousia mountains (northern region).

In the southern region, 60 stocks and major dikes were first reported by Kockel et al. (1975) (Fig. 3.8). Granodiorites, monzonites, diorites of sub-alkaline to shoshonitic affinities are mainly arranged in a narrow (10 km wide) NNE-SSW-striking extension belt, crosscutting the crystalline rocks without being affected by the regional deformation (Hahn et al., 2012). The Stratoni-Varvara and the Megali Panaghia-Gomati faults control this extension belt to the north and to the south respectively (Hahn et al., 2012). Stratoni granodiorite and Jerissos granite are placed to the east of the belt (Kalogeropoulos, 1990; Frei, 1996). According to Gilg and Frei (1994) the Stratoni granodiorite is the largest post-tectonic intrusion of the area, which intruded first in the Stratoni fault footwall and was followed by the other granodioritic to dioritic intrusions of the region (Kalogeropoulos, 1990). The diorite and the granodiorite porphyries of Fisoka, the granodiorite and the monzodiorite porphyries of Tsikara and the diorite and the granodiorite porphyries of Dilofon are among the most significant intrusions of the area (Gilg and Fre, 1994; Siron et al., 2016). Finally, probably the most significant intrusions of the area are the monzonites of Skouries (Kroll et al., 2002).

In the central region comparatively very few intrusions have been described. Kockel et al. (1975) and Panagos et al. (1978) reported a granodiorite and a diorite of significant size forming the Strymon magmatic complex near Strimonikon and Triantafyllia villages as well as, a diorite and two small granitic dikes near Stephanina village at the eastern part of the central Serbo-Macedonian Massif (Fig. 3.8).

In the northern region, 20 mainly porphyritic stocks are hosted within the Serbo-Macedonian metamorphic formations at Krousia and Kerkini mountains (Kockel et al., 1975; Frei, 1992) (Fig. 3.8). Crosscutting the regional schistosity, diorite and granodiorite porphyries are among the most common rock types. Subvolcanic and volcanic rocks exhibit a wider presence than plutonic rocks, while pipe breccias and tuffaceous rocks set in extent hydrothermally altered areas are common (Kockel et al., 1975).

Following another classification Pe-Piper and Piper (2002) subcategorized these intrusions in two major groups: the Northern and the Southern cluster zone.

According to Kockel et al. (1975), the petrographic and geochemical affinities of the three regional magmatic groups do not show any essential difference. Moreover, they are similar geochemically to the Paleogene intrusions and granitoids of the Pirin-Pangaion structural zone in SW Bulgaria (Zagorchev, 2007). Thus, this geographic classification serves only in spatial distribution and presentation needs. On the other hand, Frei (1992) summarizing his results of the U-Pb age determinations of zircon and uranothorite fractions from various Cenozoic intrusions in the Serbo-Macedonian Massif described four distinctive intrusive cycles spanning in: Eocene, Oligocene, Miocene, and Late Miocene-Pleistocene (Fig. 3.8). This classification is generally accepted and attested also by recent authors (Hahn et al., 2012; Siron et al., 2016). In addition, it has a major scientific interest, as it correlates time, spatial distribution and geotectonic settings with petrology and ore mineralization.

The first Cenozoic magmatic cycle is characterized by barren intrusions being related to the early stages of the Apulian plate subduction beneath the Eurasian plate which took place during Early to Middle Eocene. Major intrusions are the Jerissos granite (Frei, 1992), the Sithonia plutonic complex (Christofides et al., 1990) and the Ouranopolis granodiorite (de Wet and Miller, 1990). The second cycle was formed during Oligocene, when the whole region of the Serbo-Macedonian Massif, as well as the adjacent Rhodope Massif, were affected by an E-W trending calc-alkaline magmatism occurring along an active thick continental margin (Fytikas et al., 1984; Pe-Piper and Piper, 2002). This magmatic cycle throughout the Serbo-Macedonian Massif lacks any significant mineralization; an example of this cycle is the Stratoni granodiorite complex (Frei, 1992).

The third cycle started at Early Miocene and is characterized by an extensive subvolcanic activity with many porphyritic magmatic rocks. The most porphyry intrusions, such as those in Vathi, Skouries, Fisoka and Gerakario, were emplaced between Late Aquitanian and Middle Burdigalian (17-22 Ma) (Frei, 1992; Gilg and Frei, 1994; Kroll et al., 2002). In addition, many hidden deep-seated intrusions could be linked with a variety of vein type, shear-zone hosted and Pb-Zn carbonate replacement deposits (Frei, 1992). One of the most important ore mineralization of this category is the Stanos Miocene shear-zone hosted Cu-Au-Bi-Te deposit (Bristol et al., 2015). Other mineralizations which may be associated with this magmatic cycle are the Cu-Ag±Au±Bi quartz vein types which occur in Nea Madytos (Vavelidis and Tarkian, 1995), Drakontio (Vavelidis et al., 1999), Stephanina (Melfos et al., 2001)

and Koronouda (Vavelidis et al., 1996). However, accurate ages have not been estimated so far and therefore the exact determination of these mineralizations is still open.

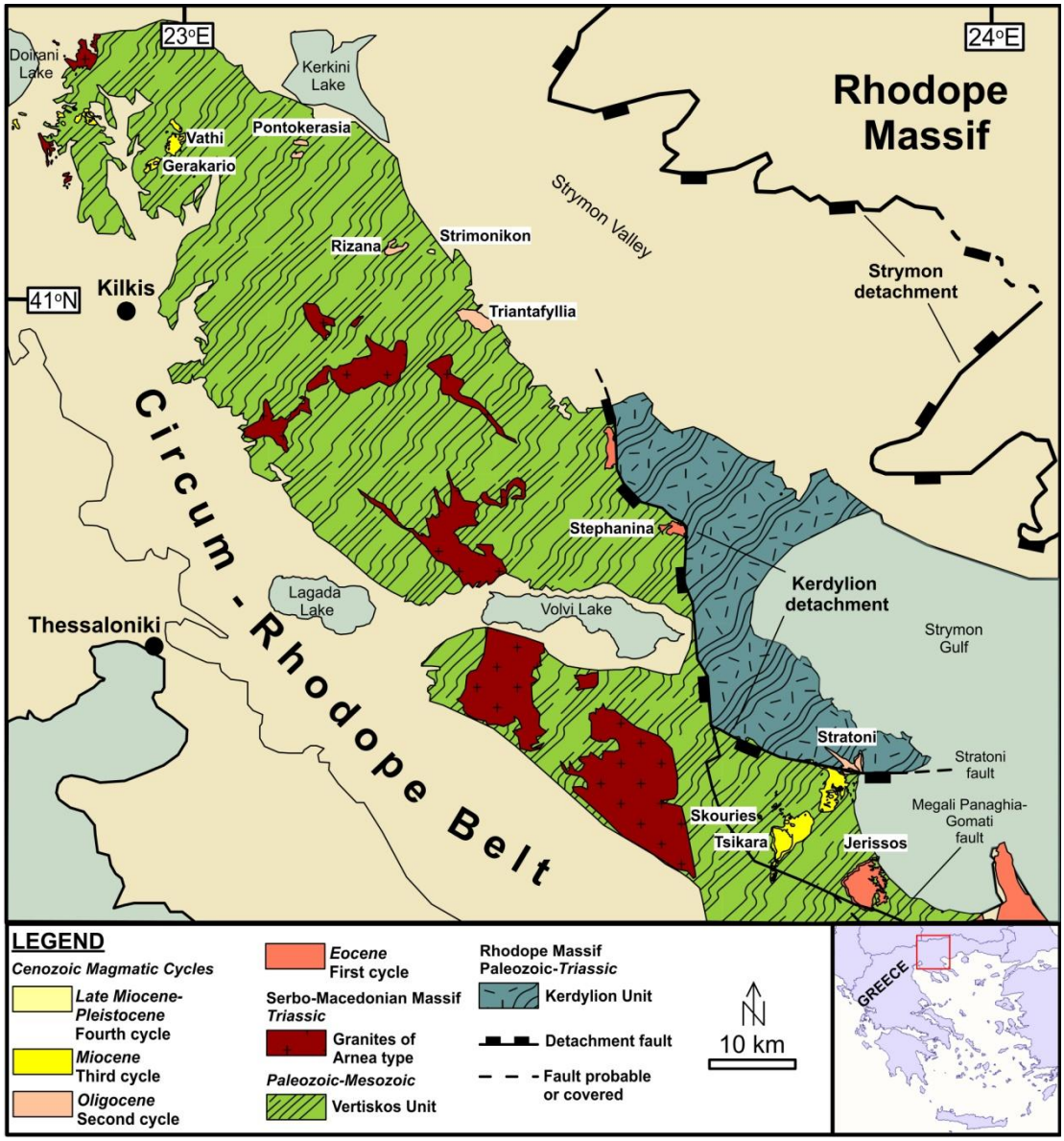

Figure 3.8. Sketch map showing the Vertiskos Unit of the Serbo-Macedonian Massif and the adjacent Kerdylion Unit in N. Greece along with the four Cenozoic magmatic cycles (Based on IGME 1:50.000 map sheets: Walther et al., 1970; Kockel et al., 1972; Kockel et al., 1978a.; Kockel et al., 1978b; Kockel et al., 1978c; Kockel et al., 1978d; Kockel, et al., 1979a; Kochel et al., 1979b; Kockel et al., 1979c. Data from Kockel et al., 1975; Frei, 1992; Melfos and Voudouris, 2012).

The last cycle is very limited and expands from Late Miocene to Pleistocene. It is represented by the Aspros Lakkos trachydacite dikes dated at 6±2/3 Ma (Frei, 1992) and the Strymonikon rhyolitic dome, dated between Late Pliocene to Early Pleistocene (Kockel and Walther, 1967). They are the only reported intrusions of this age through the whole Serbo-Macedonian Massif.

These four cycles intruded the Serbo-Macedonian crystalline rocks and inherited geochemical characteristics from the surrounding rocks. Lead isotopes of the Vertiskos Unit indicate an evolved, quite homogeneous upper sialic crust composed of rock formations becoming younger from NW to SE (Frei, 1992; Gilg, 1993). The inherited radiogenic Pb isotope components in zircons indicate the existence of a Precambrian (between 648 and 399 Ma) crustal component in the northern part (Frei, 1992). Through leaching and assimilating processes caused by the activity of hydrothermal fluids this Pb isotope content was transferred to the intrusions from the metamorphic basement rocks. This is well confirmed by the same isotopic characteristics of the unaltered gneisses and schists of the Vertiskos Unit adjacent to the intrusions (Frei, 1992). In contrast to Pd isotopes the Sr isotopes are diffusing. According to Frei (1992) this suggests that anatectic events in the lower crust, strongly affected by meta-igneous and meta-sedimentary heterogeneous crustal rocks, were the main process producing the intrusions and not magma mixing. Frei (1992) also linked the elevated Sr isotopic ratios of the intrusions characterized by extensive sericitic alteration halos to hydrothermal leaching of radiogenic Sr from the surrounding rocks.

Conclusively, magma differentiation, fractionation and assimilation of surrounding rocks during ponding at the lower crust gave rise to the various Tertiary intrusions of Serbo-Macedonian Massif and are the primary causes of their distinctive and varying geochemical characters.

3.4. TERTIARY ORE MINERALIZATION OF THE SERBOMACEDONIAN METALLOGENIC PROVINCE

The Serbo-Macedonian metallogenic province (SMMP) along with the Rhodope metallogenic province forms a continuous terrain containing significant ore deposits and mineralization (Neubauer and Heinrich, 2003; Melfos et al., 2002; Marchev et al., 2005; Melfos and Voudouris, 2012; Sutphin et al., 2013) (Fig. 3.9). Some examples include the skarn/carbonate replacement Pb-Zn-Ag-Au ore deposit of Trepca in

Kosovo, as well as the porphyry ore deposits of Buchim in FYROM and of Vathi, Pontokerasia, and Skouries in Greece (Tompouloglou, 1981; Kalogeropoulos et al, 1989; Frei, 1992; Kroll et al., 2002; Serafimovski et al., 2010; Hahn et al., 2012).

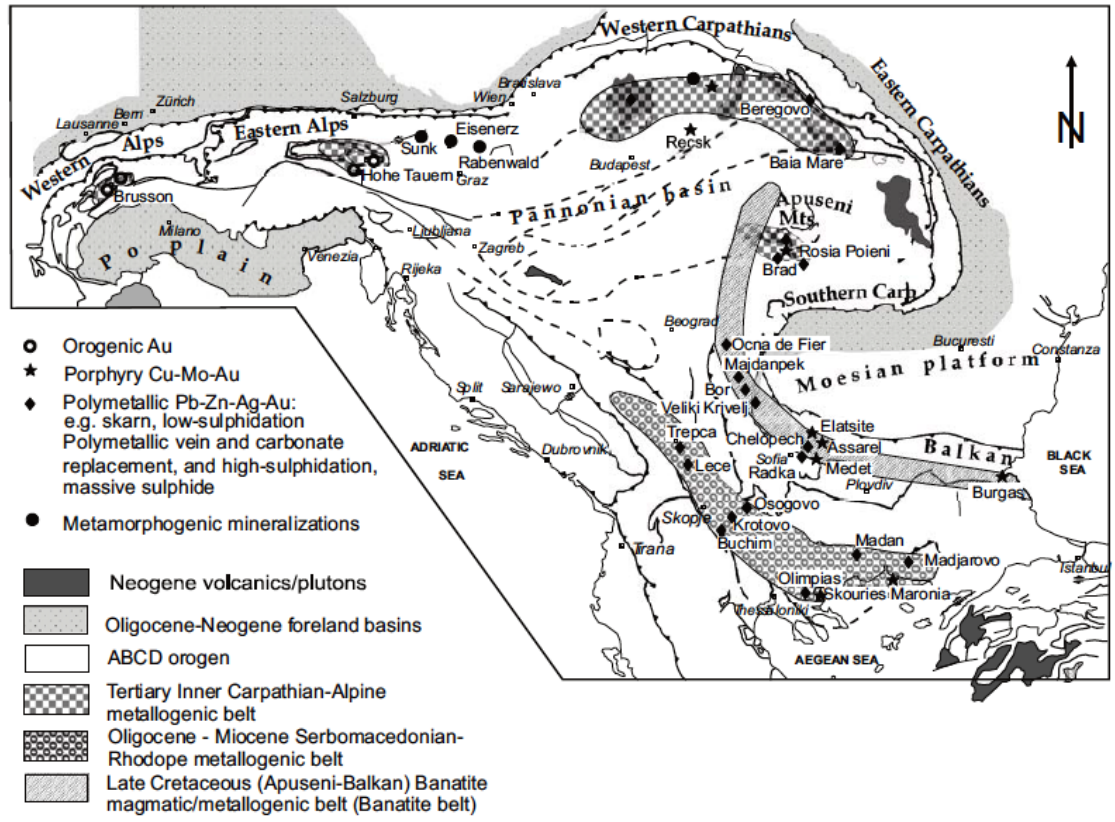

Figure 3.9. Schematic map showing the Late Cretaceous-Tertiary metallogenic provinces of the Western Tethyan Metallogenic Belt including the Serbo-Macedonian and the Rhodope metallogenic provinces. Major tectonic Units and the distribution major ore deposits are also displayed (Neubauer and Heinrich, 2003).

At the Greek part of the SMMP (Fig. 3.8) Kockel et al. (1975) were the first to study and report the close spatial association of the Tertiary magmatic rocks and the accompanying mineralization. According to these authors, 48 ore deposits and occurrences are located throughout the Vertiskos Unit and the adjacent Kerdylion Unit of the Rhodope Massif. Porphyry, epithermal, skarn/carbonate replacement, and intrusion-related vein ore types are associated with the Oligocene-Miocene intrusions. The mineralization of the Vertiskos Unit are mainly distributed spatially along the southern and the northern part of the Serbo-Macedonian Massif forming the NE Chalkidiki (or Kassandra) and the Kilkis (or Krousia) mining districts (Kockel et al., 1975; Hahn et al., 2010). Subsequently, they are classified as northern, central and

southern ore districts, which is a geographical classification proposed by Kockel et al. (1975).

At the northern part of the Greek SMMP there are porphyry (Vathi, Palatiano, Gerakario, Pontokerasia, Doirani), skarn/carbonate replacement (East and West Myriofyto, Petrades, Monolithi) and epithermal (Rodonas) ore type occurrences (Fig. 3.10). The most important mineralization include the Gerakario Cu-Au-porphyry deposit (Resources: 0.13 Mt with 0.33% Cu and up to 1.4 ppm Au) hosted in a calc-alkaline syenite and a granodiorite intrusion, the Pontokerasia Cu-Mo-Au-porphyry deposit (Resources: up to 0.26% Cu and up to 0.16 ppm Au) associated with a calc-alkaline syenite intrusion and the Vathi Cu-Au-U±Mo porphyry deposit (Resources: 0.15 Mt with 0.3% Cu and 0.8 ppm Au in average) associated with a high-K calc-alkaline monzonite (Veranis and Tsamantouridis, 1991; Frei, 1992; this study).

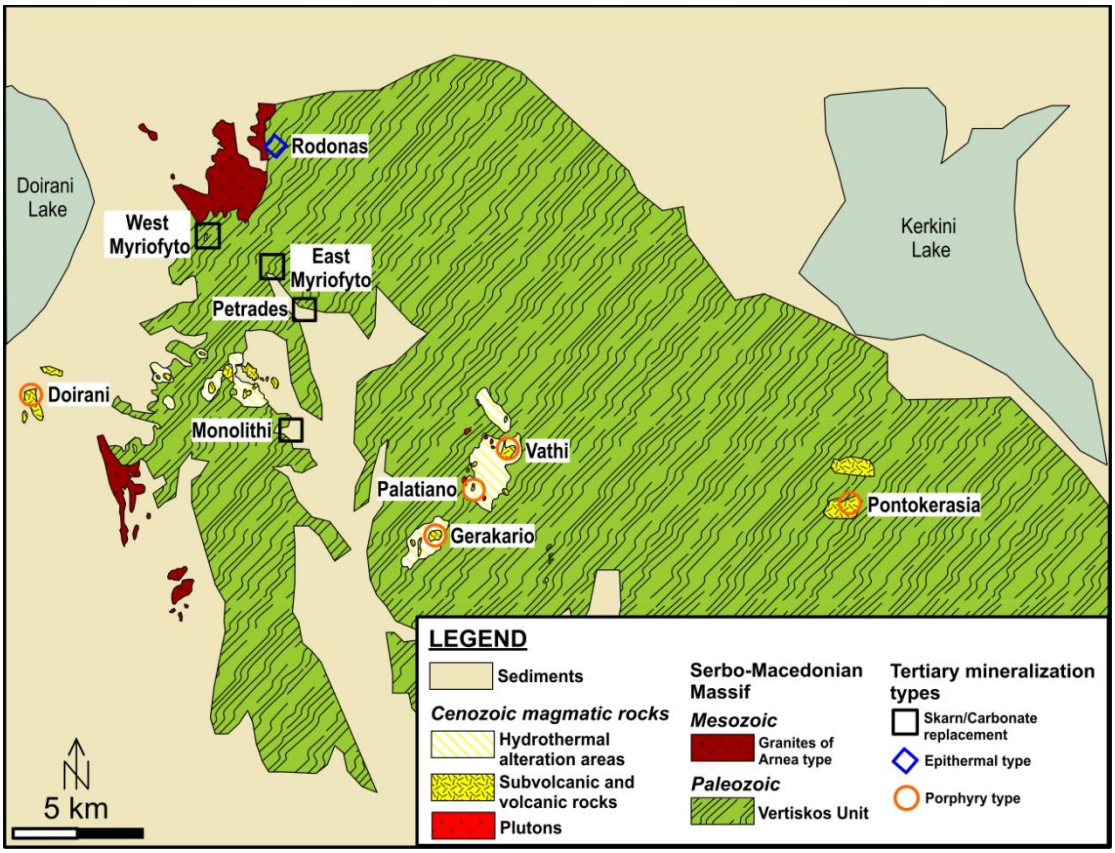

Figure 3.10. The northern part of the Greek Serbo-Macedonian metallogenic province (Geological map based on IGME 1:50.000 map sheets: Ioannidis and Kelepertzis, 1974; Kockel and Ioannidis, 1979a).

Throughout the central part of the SMMP a small number of ore mineralization occur comprising shear-zone vein hosted type (Arethousa, Drakontio, Koronouda,

Laodikino, Stephanina), metamorphic-hosted quartz vein type (Philadelphio, Rizana) and epithermal (Askos) mineralizations (Mposkos, 1983; Thymiatis, 1995; Vavelidis et al., 2000; Melfos et al., 2001; Bristol et al., 2015) (Fig. 3.11). They are not directly connected to any intrusive or extrusive magmatic rocks, which are scarce in the region. Structural mechanisms such as strike-slip faults induce the circulation of the hydrothermal fluids which have controlled the ore mineralization formation (Vavelidis et al., 1999; Bristol et al., 2015). Examples of the ore mineralization of the district are the shear-zone hosted Cu-Au-Sb-Bi-Te mineralization at Drakontio quartz vein system (up to 22.5 ppm Au, 45.1 ppm Ag and 0.1% Cu), the Koronouda veins with up to 28.30 ppm Au and 735 ppm Ag (Vavelidis et al., 1996) and the Laodikino veins bearing Cu, Au, Fe, As, Zn, Pb, Te, Co, Ni, Sb, and Bi (Thymiatis, 1995). Finally, a significant vein type Sb mineralization is located near Rizana village. The underground mine was active until late 1950s producing a total 22.5 Mt of ore at a grade of 30% Sb (Paraskevopoulos, 1958; Dimou, 1989).

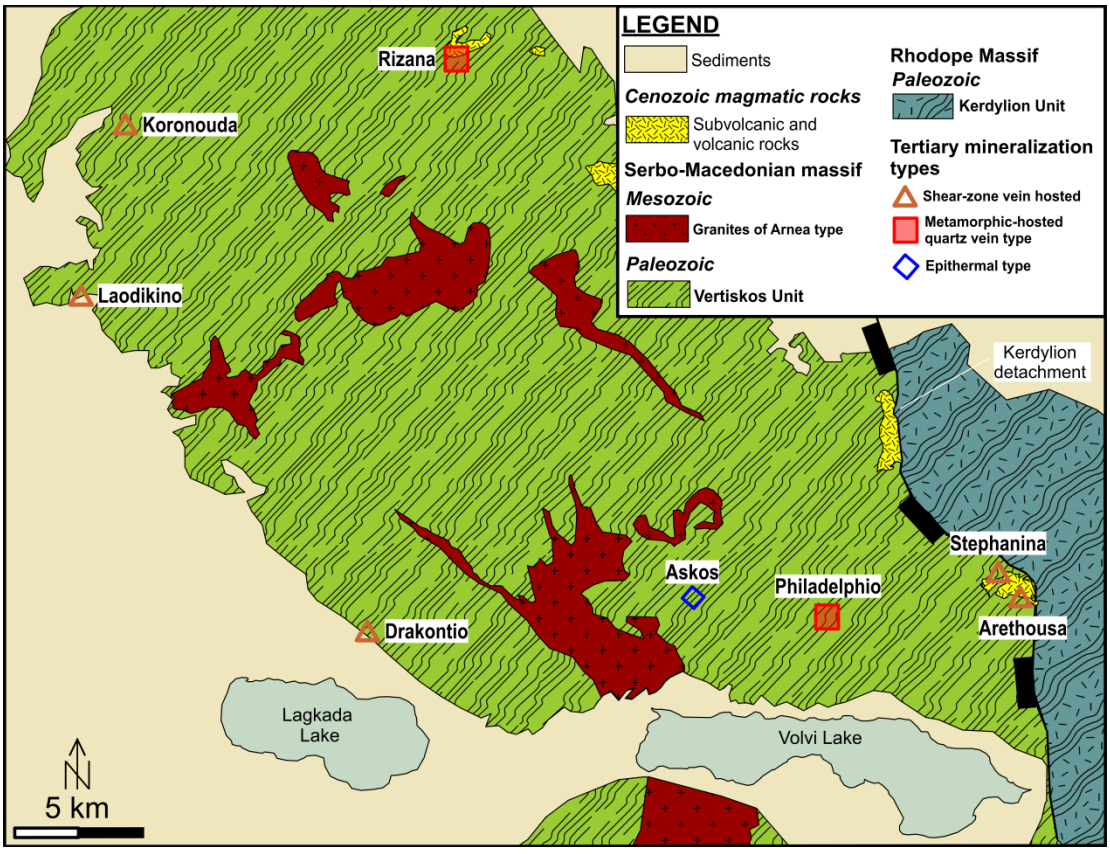

Figure 3.11. The central part of the Greek Serbo-Macedonian metallogenic province and part of the adjacent Kerdylion Unit of the Rhodope Massif (Geological map based on IGME 1:50.000 map sheets: Walther et al., 1970; Kockel et al., 1972; Kochel et al., 1979a; Kockel et al., 1979b; Kockel et al., 1979c).

The southern Chalkidiki area belongs to the southern part of the Greek SMMP. It is also known as the Kassandra mining district. It hosts several ore deposits and occurrences and comprises one of the oldest mining districts of Europe (Sagui, 1928; Kockel et al., 1975; Frei, 1992). In the southern Greek SMMP and at the adjacent Kerdylion Unit, shear-zone vein hosted (e.g. Nea Madytos, Stavros, Stanos), porphyry (e.g. Aspra Chomata, Fisoka, Tsikara, Skouries), epithermal (e.g. Zepko, Vina, Papades, Gyftissa, Giannovos) and skarn/carbonate replacement (e.g. Olympias, Varvara, Piavitsa, Mavres Petres, Madem Lakkos) mineralization occur in an area of approximately 484 km^2 (Fig. 3.12). Most ore mineralization are linked to intrusions which were emplaced within a narrow belt (<10 km), set in an extensional regime controlled by the southeastwards extensions of the Kerdylion detachment fault and the Stratoni-Varvara and Megali Panaghia-Gomati normal to oblique faults (Hahn et al., 2012). Nea Madytos and Stanos shear-zone hosted ore mineralization are linked to NW–SE shears and strike–slip brittle faults (Bristol et al., 2015).

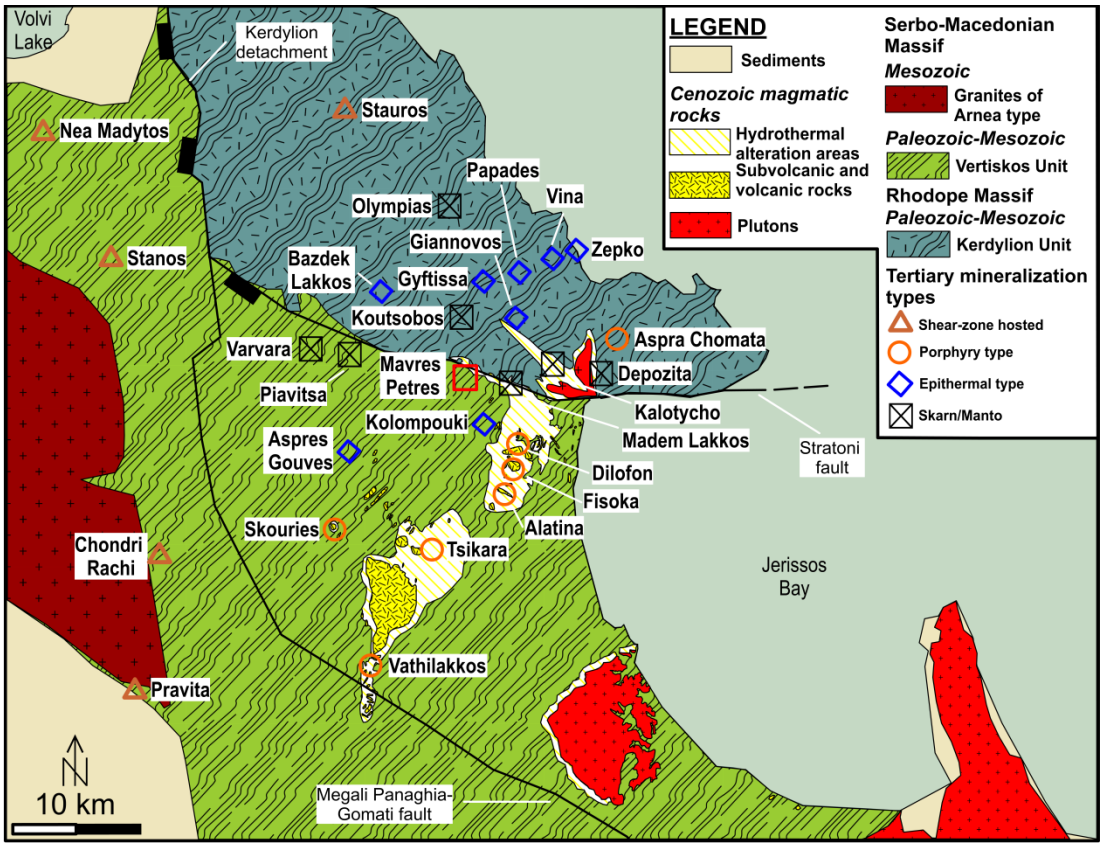

Figure 3.12. The southern part of the Greek Serbo-Macedonian metallogenic province and the adjacent Kerdylion Unit (Geological map based on IGME 1:50.000 map sheets: Kockel et al., 1978a; Kockel et al., 1978b; Kockel et al., 1978c; Kockel et al., 1978d).

A world-class ore deposit of this area is the Skouries Cu-Au-porphyry type mineralization comprising four different alkaline monzonitic porphyries (Kroll et al., 2002). This ore deposit comprises in total 146.2 Mt of ore with 0.83 g/tn Au and 0.54 wt% Cu (Eldorado Gold SA, 2016). Furthermore, the Cu-Au-porphyry ore type of Dilofon, Alatina, Fisoka and Tsikara hosted in calc-alkaline monzodiorites and diorites (with more than 0.4 ore Mt of 0.4 to 0.55% Cu) as well as the Piavitsa manto polymetallic Ag-Pb-Zn-(Au) ore mineralization are characterized as prospective yet undeveloped ore deposits (Tompouloglou et al., 1986; Gilg, 1993; Gilg and Gilg, 1994; Eldorado Gold SA, 2016).

CHAPTER 4. SAMPLING AND METHODOLOGY

During the field work in August 2014 a detailed geological mapping and sampling of the Vathi porphyry system took place at Ragian 1 and Ragian 2 Hills as well as at the surrounding area at the north of the Vathi village. The studied mineralization, spanning between and around Ragian 1 and 2 Hills, covers an area of ~3 km^2. Sampling was targeted to Ragian 1 Hill and the site to the east (Fig. 4.1). Due to the regional outcrop pattern which is generally obscured by vegetation and weathering the sampling frequency was denser or more sporadic. In total 33 surface mineralized and non-mineralized samples were collected of which 25 are from the trachydacite, 3 are from the qtz-monzonite, 2 are from the breccia formation and 3 are from the surrounding metamorphic rocks. Twenty eight of them were chosen for optical and scanning electron microscopy, X-ray powder diffractiometry and geochemical analyses.

In addition, old drill core samples, logging data and exploration results were taken into consideration and were re-assessed. During late 1960s and early 1970s an exploration program was conducted in the area and it was targeted at the U mineralization. The Institute of Geology and Mineral Exploration (IGME) carried out an exploration drilling project during 1968 on behalf of the Greek Atomic Energy Commission (EEAE) and four drillings (D1, D2, D3, D5; Fig. 4.1) of a total length of 512.90 m were drilled (Markoulis, 1970). Later another exploration drilling project was carried out by the mining company Bauxites of Parnassos S.A. Geological mapping and geophysical exploration were commenced by Andronopoulos (1967), Melidonis (1968) and Thanasoulas (1979). Eight polished sections sampled from D1

drilling between the depths of 43 to 166 m and 7 polished sections sampled from D5 drilling between the depths of 53 and 73 m were studied.

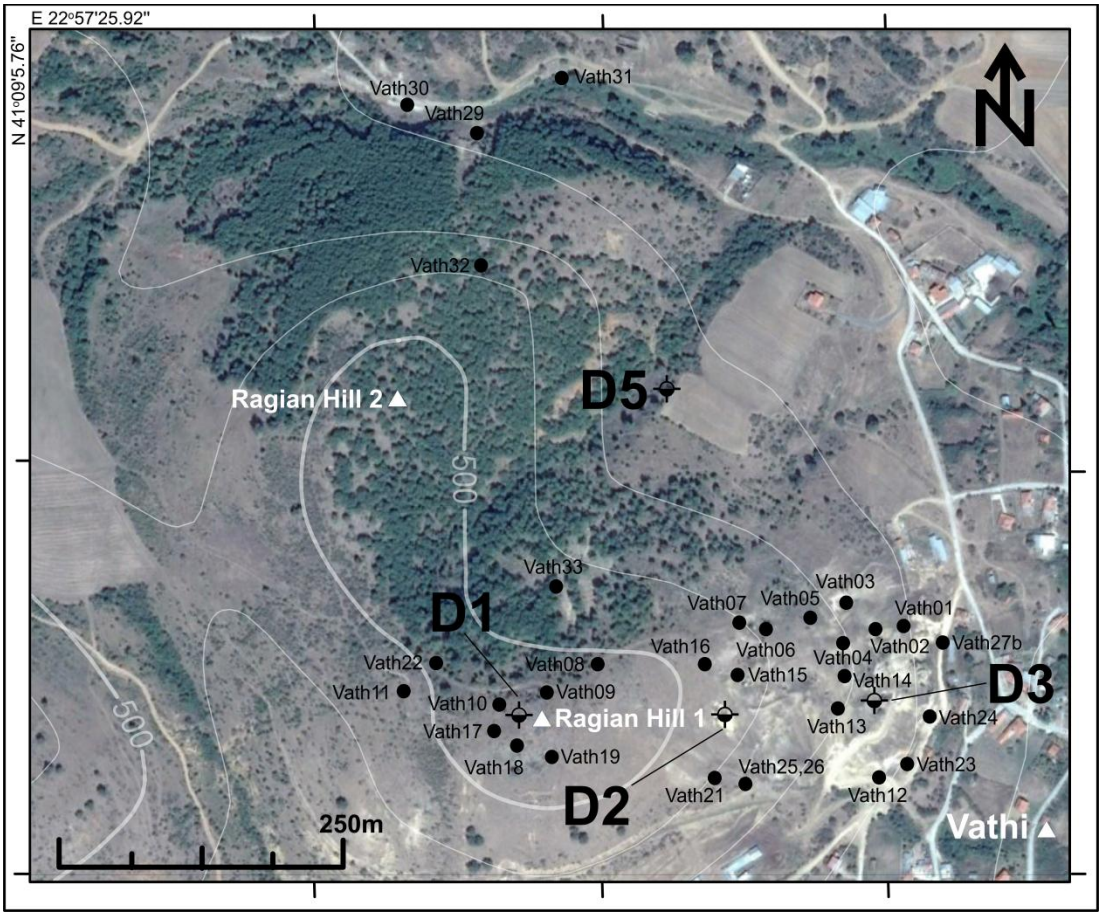

Figure 4.1. Merged topographic map and satellite image of Ragian 1 and 2 Hills showing the 33 sampling points of the Vathi porphyry system.

For the purposes of optical microscopy in addition to these polished sections, a total of 16 thin, 20 polished and 4 thin-polished sections were prepared from the surface samples and were studied under a Leitz SM-LUX dual reflected-transmitted light polarizing microscope at the Department of Mineralogy, Petrology, Economic Geology, at the Faculty of Geology, Aristotle University of Thessaloniki.

The mineralogical composition of 16 representative samples was determined by X-ray diffraction (XRD), by means of a Philips PW 1820/00, equipped with PW 1710/ 00 controller at the Department of Mineralogy, Petrology, Economic Geology, at the Faculty of Geology, Aristotle University of Thessaloniki. CuKα radiation was used producing radiation with a wavelength of 1.54056Å. The scanning speed was 0.5 sec, in a continuous scanning mode and the scanning area of the goniometer was fixed

between 3°-63°. The characterization of the mineral phases as major, minor, and traces was performed semi-quantitatively on the basis of the intensity (counts) of specific reflections, the density, and the mass absorption coefficient (CuKα) of the identified mineral phases. Also, on four comparatively less altered samples, two from the trachydacite porphyry and two from the quartz-monzonite a quantification of the major and minor minerals was carried out using the computer software "CRYST" (Stergiou, 1995).

Four thin-polished sections were studied by Scanning Electron Microscopy (SEM), using a JEOL 840 equipped with an ISIS 300 OXFORD energy dispersive spectrometer (EDS) at the School of Science, Aristotle University of Thessaloniki. Three polished sections from the drillholes were also studied by scanning electron microscopy in order to determine the chemical composition of the ore minerals, under a FEI/Quanta Inspect D8334 scanning electron microscope, coupled with an energy-dispersive X-ray spectrometer (SEM-EDS) at National Center for Scientific Research "Demokritos", Athens.

Finally, to identify the major and the trace elements of the mineralization and the host rock, 6 samples were analyzed by X-ray fluorescence (XRF) and 24 by Inductively Coupled Plasma–Mass Spectrometry (ICP-MS) at the ACME Laboratories in Vancouver, Canada.

CHAPTER 5. LOCAL GEOLOGY

The crystalline rocks at the Vathi area consist mainly of Paleozoic two-mica gneisses and schists of the Vertiskos Unit and have been metamorphosed at the amphibolitic phase (Fig. 5.1) (Ioannidis and Kelepertzis, 1974; Sidiropoulos, 1991). The gneisses are medium-grained leucocratic rocks with plagioclase (An=25-30%), quartz, K-feldspars, muscovite, biotite mostly replaced by chlorite and epidote, while garnet and sphene are the main accessory minerals (Sidiropoulos, 1991; Himmerkus et al., 2009a). The schists consist of quartz, plagioclase, muscovite and biotite and are intercalated within the gneisses. Lenses of amphibolites and amphibolitic schists occur at the west side of the Ragian 1 Hill (Melidonis, 1968). They consist of hornblende, plagioclase, epidote, sphene and traces of pyroxene (Ioannidis and Kelepertzis, 1974). Metamorphic milky quartz and pegmatoid veins often crosscut the crystalline rocks. Sometimes, thin quartz lenses occur parallel to the scistosity of the

rocks. These rocks exhibit a NNE-SSW trending, dipping to ESE at an average angle of 65^{o} (Melidonis, 1968; Sidiropoulos, 1991; Himmerkus et al., 2006).

To the northwest of the study area a Paleozoic serpentinized peridotite occurs intercalated in the gneisses (Fig. 5.1). The easternmost outcrop of this rock has been hydrothermally affected by the intrusion of the trachydacite porphyry. As a consequence, at this area the peridotite appears schistose with oxidized mineralization. Radial talc crystals occur in the rock mass and magnesite veins in fractures.

About 200 m to the west of Ragian 2 Hill seven small barren intrusions of Tertiary age occur (Fig. 5.1). Melidonis (1968) describes them as granites, contemporaneous with the subvolcanic intrusions, forming oval to round shaped dikes with the largest of them reaching in size 15 m^2. They exhibit granitic to granodioritic compositions and two rock types have been distinguished, an altered coarse-grained biotite granite and an almost unaltered fine-grained amphibole granite (Melidonis, 1968).

The main Tertiary magmatic rocks at the Vathi ore mineralization comprise subvolcanic stock-like and dyke intrusions of porphyritic texture intruding the basement rocks. Two rock types can be distinguished: a trachydacite porphyry and a quartz monzonite (hereinafter referred to as qtz-monzonite) (Fig. 5.2). Frei (1992) demonstrated two emplacement ages for the quartz monzonite based on U-Pb zircons ratios at 18±0.5 Ma and 17±1 Ma. At the surface the qtz-monzonite occurs as small (~30 m^2) outcrops, while the larger outcrop of the trachydacite porphyry covers an area of 0.251 km^2 (680 x 370 m in size) (Fig. 5.1). Andronopoulos (1967) and Melidonis (1968) characterize it as rhyodacite, although Frei (1992) classifies it as latite. Additionally, preliminary geophysical results revealed that the trachydacite porphyry dips to the east deeper than 240 m (Thanasoulas, 1979). The qtz-monzonite intrudes both the basement rocks and the trachydacite porphyry and is linked to a phreato-magmatic breccia formation. The qtz-monzonite intrusions exhibit similar mineralogical and petrological characteristics with another qtz-monzonite intrusion NW of the studied area described by Filippidis et al. (1988) and Frei (1992). The reassessement of the old drill core logging data during the present study supports the suggestion that despite all intrusions are terminated upwards, few of them reached the paleosurface level. Consequently, more intrusions are expected in depth (see Chapter 7).

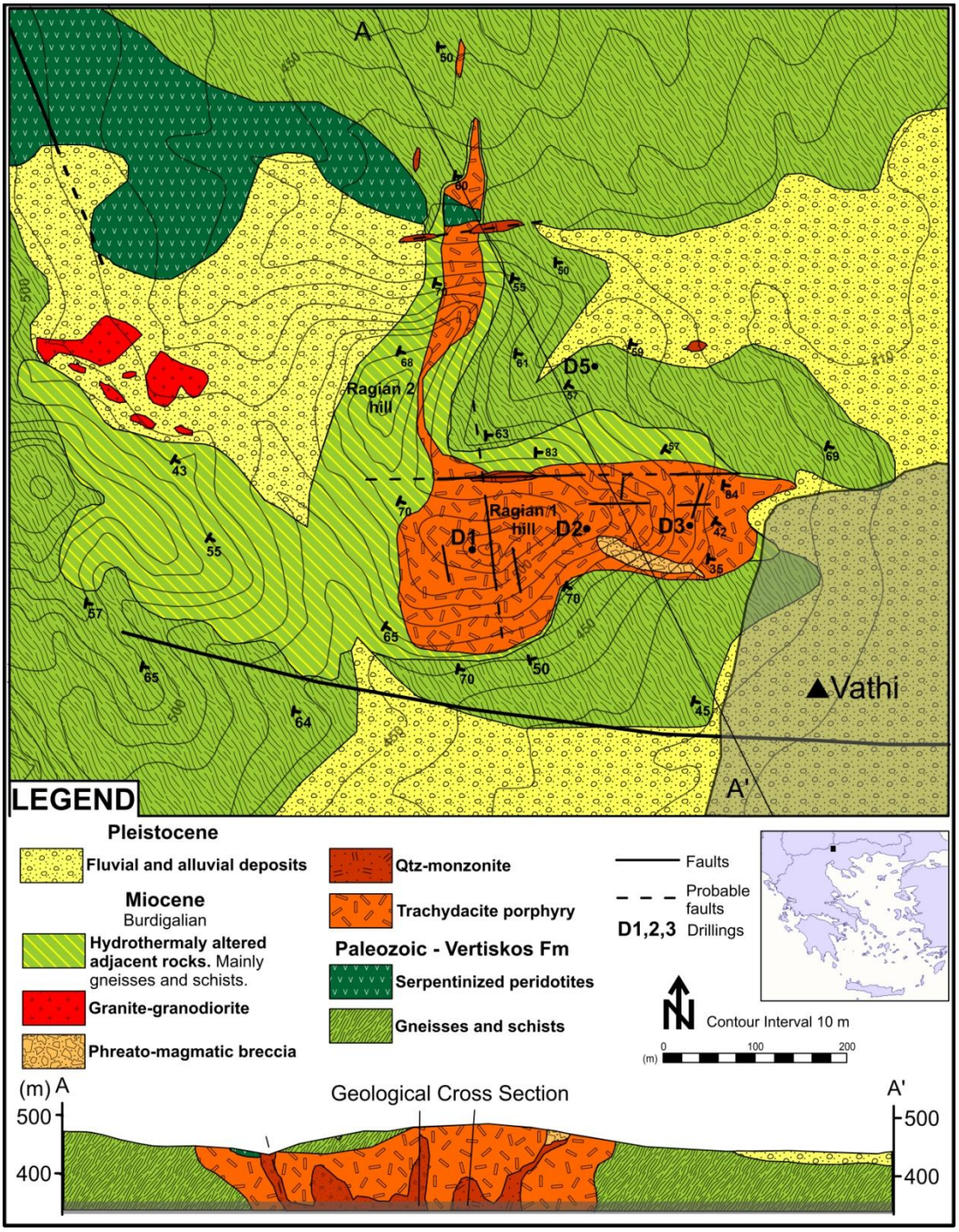

Figure 5.1. Geological map of the Vathi porphyry system modified after Melidonis (1968) and Ioannidis and Kelepertzis (1974).

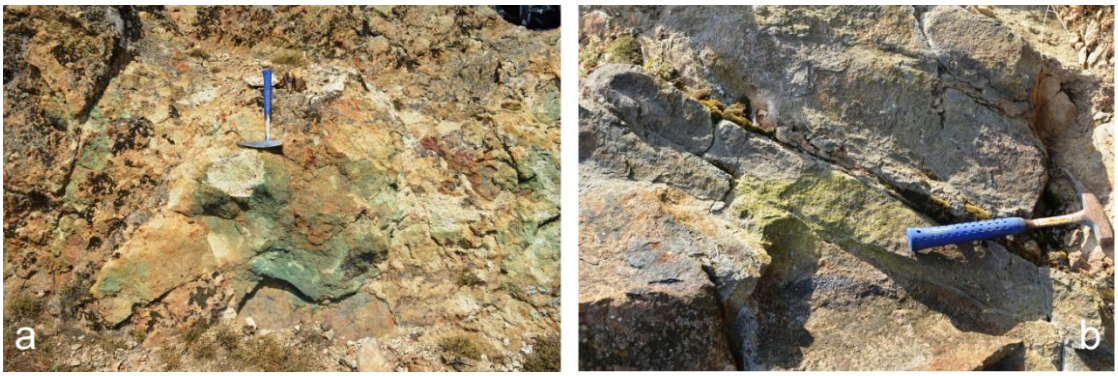

Figure 5.2. a. Trachydacite porphyry at Ragian 1 Hill. b. Qtz-monzonite north of Ragian 2 Hill.

5.1. TRACHYDACITE PORPHYRY

The trachydacite porphyry is generally fine to medium grained and only locally contains coarse grains. It has a crowded porphyritic texture and is strongly altered (Fig. 5.1; 5.3). A restricted propylitic alteration overprinted by an intense sericitic alteration were observed affecting the tracydacite porphyry. The trachydacite porphyry contains up to 40 vol% phenocrysts of K-feldspars, mainly orthoclase (<15 mm), as well as quartz (<400 μm), and minor hornblende, plagioclase and apatite set mainly in a fine grained K-feldspar, quartz and white mica dominated ground mass (Fig. 5.4a). The main accessory minerals are zircon, ilmenite, sphene, and minor monazite.

The main alteration minerals are biotite, K-feldspar, quartz, and minor magnetite (potassic zone in depth), epidote, clinozoisite, chlorite, and albite (propylitic zone), and sericite, quartz, pyrite, kaolinite, dolomite and rutile (sericitic alteration; Fig. 5.4b,c,d). The trachydacite porphyry contains a significant amount of mineralization which is totally oxidized. Hematite, goethite, malachite, azurite, chysocolla, turqoise, torbernite, and meta-torbernite are the main minerals formed during oxidation.

XRD quantification estimations showed that the average mineralogical composition (mass/mass%) of two surface trachydacite porphyry samples is: 62% quartz, 9% K-feldspar, 14% sericite, 3% chlorite, 3% kaolinite, 1% dolomite, 1% turqoise and 11% amorphous SiO_2 and Fe-oxides.

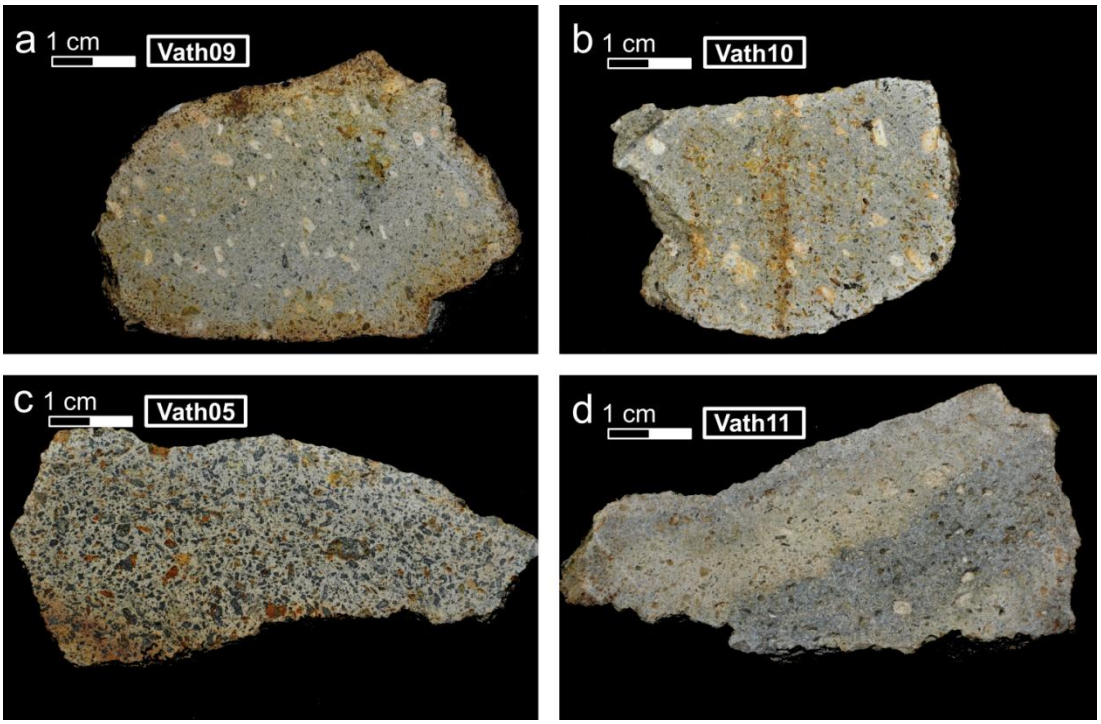

Figure 5.3. Selected rock samples of the trachydacite porphyry from Vathi. a,b. Fine grained sample exhibiting crowded porphyritic texture with K-feldspars phenocrysts. c. Medium grained propylitized sample. d. Silicified sample with vuggy texture.

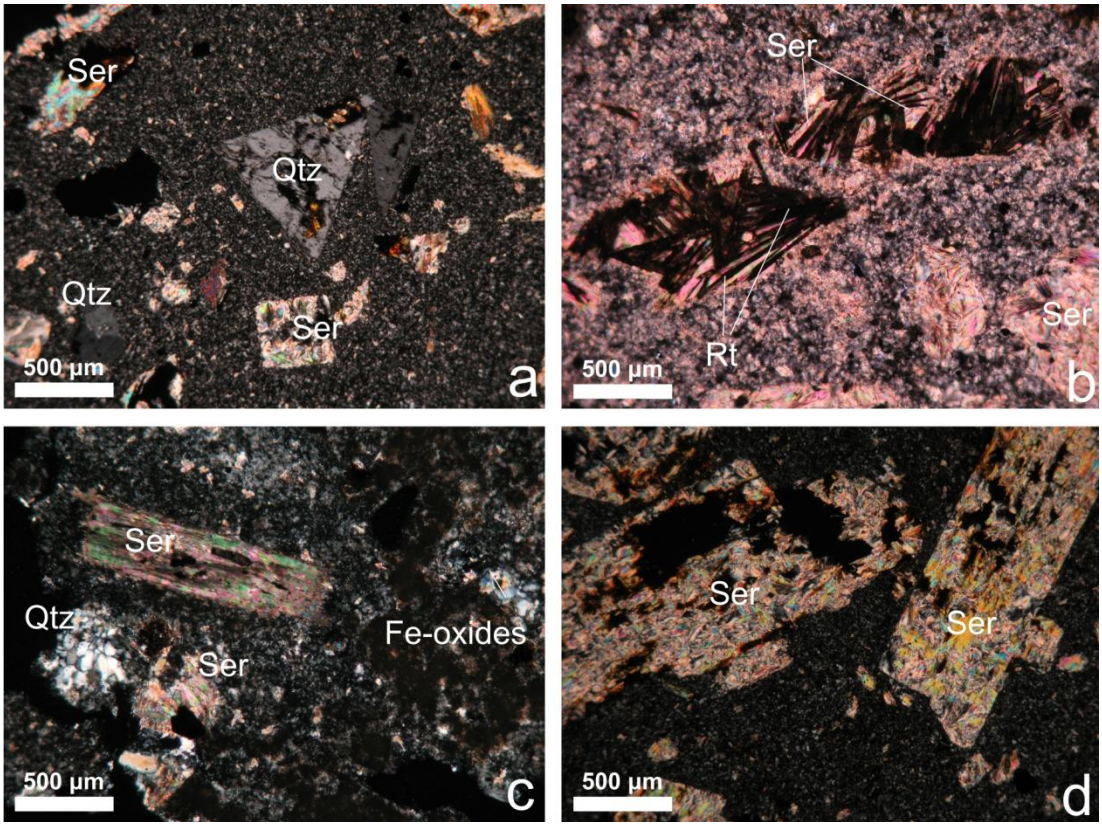

Figure 5.4. Photomicrographs showing typical mineralogical paragenesis and alteration textures of the trachydacite porphyry from Vathi (Nicols X). a. Euhedral quartz (Qtz)

and altered K-feldspar to sericite (Ser) set in a medium to fine grained ground mass composed of white mica and quartz. b. Assemblages of rutile (Rt) and sericite (Ser) in a brownish and blurry rock matrix. c. Quartz and sericite association in a fine ground mass with Fe-oxides and kaolinite. d. Complete sericitization of euhedral coarse K-feldspars.

5.2. QTZ-MONZONITE

The qtz-monzonite is a micro- to equi- granular intrusion which intersects the trachydacite porphyry (Fig. 5.1; 5.6). It appears as narrow, elongated, oval-shaped and structurally controlled intrusion, grey to light brown in color. It mainly consists of quartz, orthoclase, biotite and hornblende (Fig. 5.7a). Zircon and apatite are the main accessory minerals. Macroscopically these minerals do not exceed 2 mm in sizes. In addition, both felsic and femic minerals exhibit an equal distribution.

A weak potassic overprinted by a sericitic hydrothermal alteration have affected the rock. As a result a secondary mineral assemblage consisting of biotite, sericite, sphene and chlorite occurs (Fig. 5.7b). Veinlets (1-3 mm wide) with quartz are widespread crosscutting the rock (Fig. 5.6b; 5.7c). Locally, angular quartz crystals, micro-veins with green-brown hydrothermal biotite and relict K-feldspars altered to sericite are observed related to the potassic alteration which is developed along structural discontinuities (Fig. 5.7b,d). Sporadic sericite is present as the result of the later sericitic alteration, which overprinted the potassic alteration. Primary and oxidized mineralization is found in the qtz-monzonite consisting mainly of pyrite and Fe-oxides.

XRD quantification estimations of two samples revealed the following mineralogical composition (mass/mass%): 39% quartz, 9% K-feldspar, 18% biotite, 3% chlorite, 11% pyrite and 22% amorphous SiO_2 and Fe-oxides.

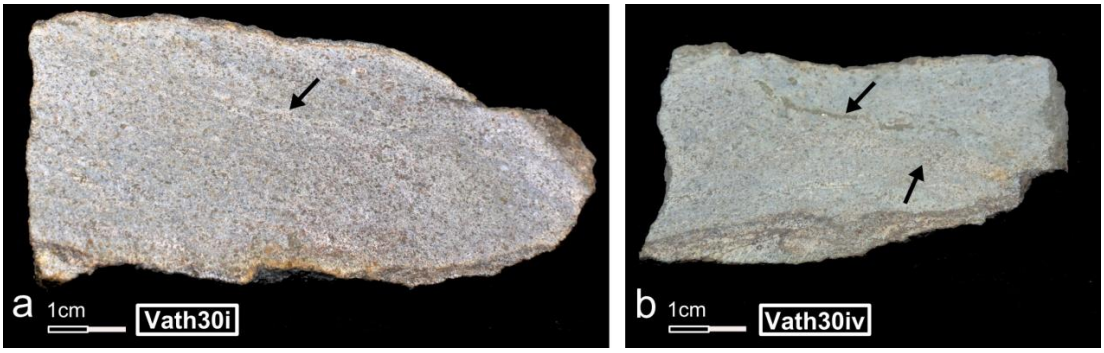

Figure 5.6. Selected rock samples of the qtz-monzonite from Vathi. a. Veinlets bearing secondary quartz are highlighted. b. Mineralized veinlets (upper arrow) and quartz-K-feldspars veinlets (lower arrow) crosscut the rock.

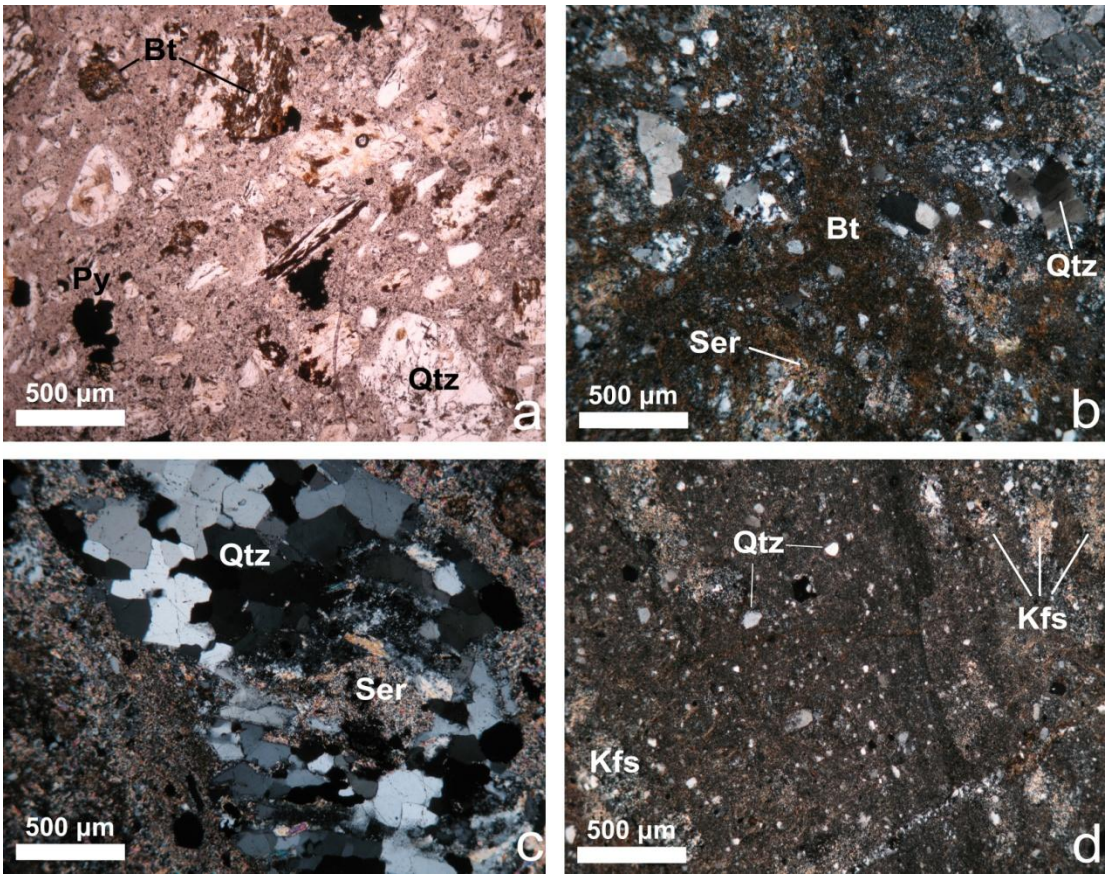

Figure 5.7. Photomicrographs showing the mineralogical paragenesis and alteration minerals of the qtz-monzonite from Vathi (Nicols //: a, Nicols: X: b,c,d). a. Biotite (Bt), quartz (Qtz) and disseminated opaque minerals –mainly pyrite (Py). b. Secondary biotite (Bt), quartz (Qtz) and sericite (Ser) in a potassically altered sample. c. A quartz (Qtz) vein with sericite (Ser) crosscuts the rock. d. Angular quartz (Qtz), secondary biotite (Bt) in micro-veins and relict K-feldspars (Kfs) from a sample along a structural discontinuity.

5.3. PHREATO-MAGMATIC BRECCIA

A breccia formation, approximately 120 m in length, 25 m in width and more than 10 m in thickness at the surface, intrudes the trachydacite porphyry at the southeastern part (Fig. 5.1; 5.8). It has also been previously described as phreato-magmatic breccia by Andronopoulos (1967) and Melidonis (1968). This formation consists of medium to strongly hydrothermally altered fragments of gneiss, schist and trachydacite porphyry (Fig. 5.9) of various sizes (up to 30 cm long) and shapes (Fig. 5.9). The most angular fragments occur closer to the marginal areas of the breccia. The breccia appears well cemented by an argillaceous matrix. XRD analysis revealed that it is composed of hydrothermal illite, kaolinite, white mica and quartz. Secondary ore minerals, mainly hematite and goethite with minor malachite also exist in the matrix. The breccia shares the same E-W trend with the qtz-monzonite intrusion, which probably reveals their common structural control. Qtz-monzonite fragments have not been found within the breccia. Thus, it is suggested that this breccia is possibly a product of the late stages of the qtz-monzonite intrusion, occurring at the upper and marginal parts of the porphyry system. This is further supported by the descriptions given on the phreato-magmatic breccias formation and characteristics, as well as by the connections presented between the late stages of a porphyry system activity and the development of phreato-magmatic breccias (Tămaș et al., 2002; Sillitoe, 2010).

Figure 5.8. The phreato-magmatic breccia at the southern part of the Ragian 1 Hill. It appears massive, extensively oxidized and well cemented.

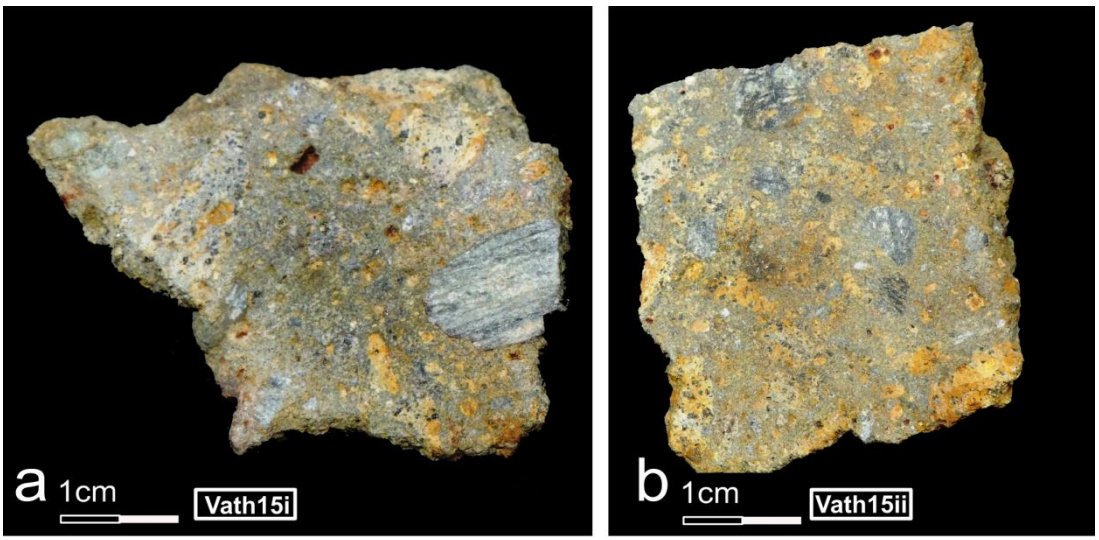

Figure 5.9. Angular and rounded fragments of gneiss and trachydacite within a well cemented argillaceous, oxidized matrix, being relatively rich in gold.

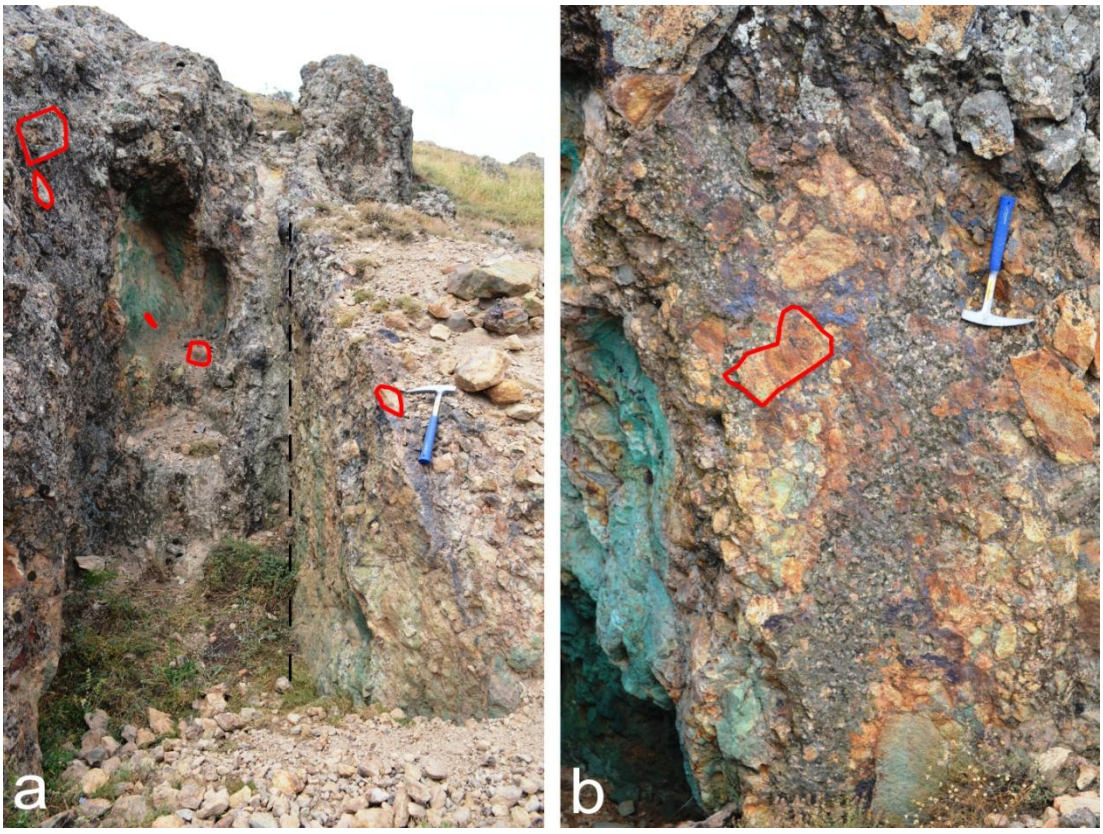

Figure 5.10. a. Fragments are getting more angular and large from the centre to the margins of the formation. b. Large, up to 25 cm long, totally cemented trachydacite porphyry fragments. The dashed line highlights the contact between the phreato-magmatic breccia and the trachydacite porphyry.

CHAPTER 6. HYDROTHERMAL ALTERATION

Spatial distribution and the special characteristics of the alteration assemblages and zones around Ragian 1 and 2 Hills have been constrained from detailed field mapping and assay results. In addition, drill core logging data by Markoulis (1970) and the study of the drillcore polished sections, as well as results from Filippidis et al. (1988) and Frei (1992) are incorporated here. Following the emplacement of the qtz-monzonite, three main hydrothermal alteration zones are recognized within the porphyry stock and the country rocks: a potassic, a propylitic and a late sericitic alteration zone (Fig. 6.1). The sericitic alteration zone is locally characterized by intense feldspar destructive phenomena which outline a distinctive sub-area in the sericitic alteration zone. The distribution of the alteration zones does not exhibit any symmetrical pattern but follows the qtz-monzonite intrusion as well as the regional structural control settings.

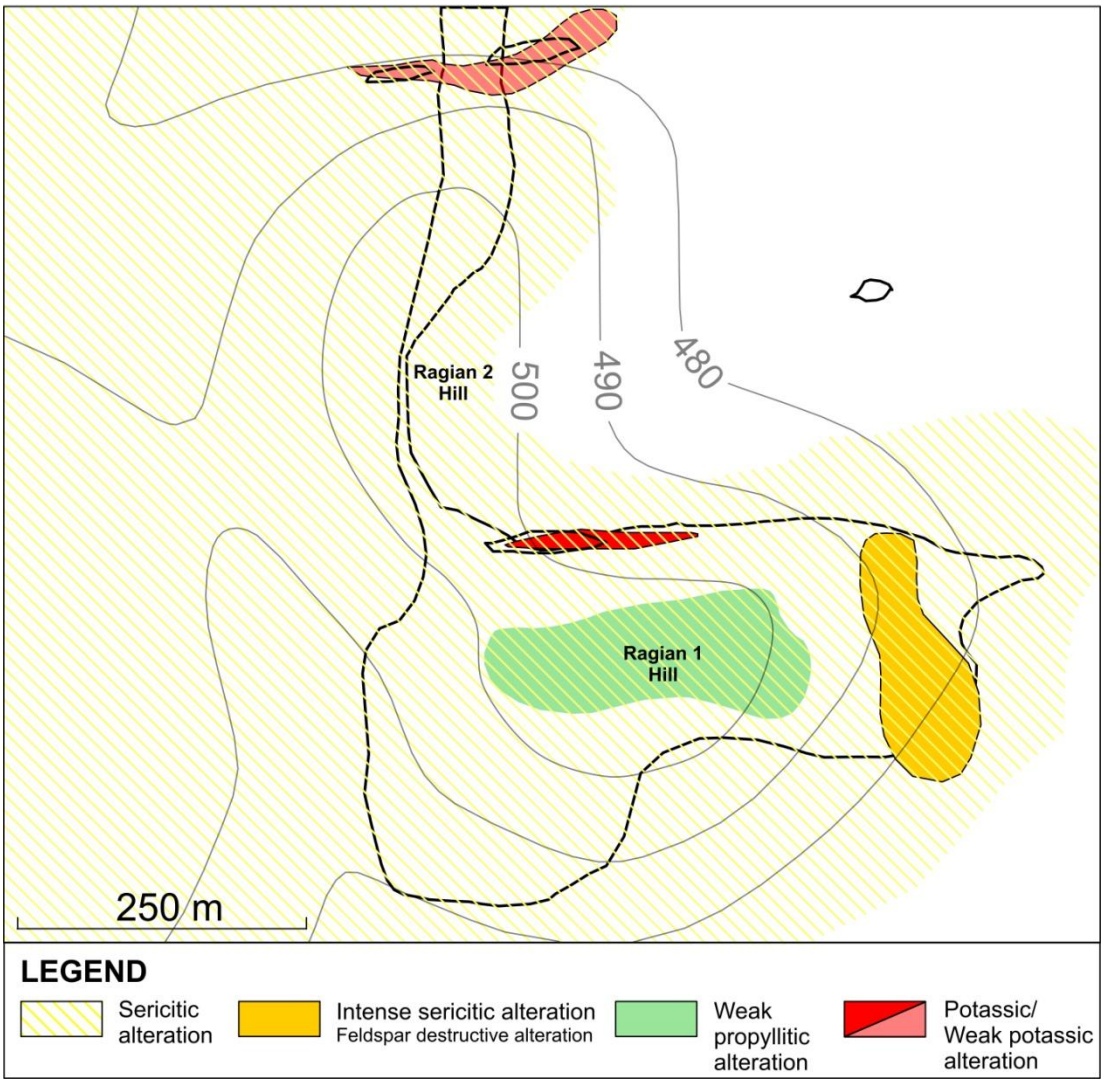

Figure 6.1. Schematic map depicting the spatial distribution of the alteration zones along Ragian 1 and 2 Hills.

The potassic alteration is overprinted by the sericitic alteration and is closely related to the fault controlled, elongated qtz-monzonite dikes. A weak potassic alteration is documented within the trachydacite porphyry in depth along the D1 drilling. The characteristic minerals of the zone are hydrothermal biotite, K-feldspar, quartz and minor magnetite, closely coinciding. This paragenesis of alteration minerals is also reported by Filippidis et al. (1988) from a drillhole set at the qtz-monzonite intrusion occurring NW of Ragian 1 Hill. Biotite occurs in clusters or in veins and it is widespread in depth. Quartz veinlets (1-3 mm wide) locally crosscut the qtz-monzonite and even intrude the surrounding rocks. Potassic alteration was

observed within the cataclastic material at a fault-controlled area sharing the same E-W trend with the qtz-monzonite dikes.

The propylitic alteration zone is present throughout Ragian 1 Hill and affects mainly the trachydacite porphyry. It was not observed in the qtz-monzonite. It demonstrates an oval-shaped distribution, covering approximately 0.20 km^2 and is overprinted by the sericitic alteration. The characteristic minerals assemblage consists of hydrothermal epidote, clinozoisite, chlorite and traces of albite (also reported by Frei, 1992). Oxidized sulfide mineralization lacks from the propylitic alteration zone.

The sericitic alteration is complete and dominant throughout the whole Vathi porphyry system affecting both the magmatic and the metamorphic rocks. In the qtz-monzonite this alteration exhibits a modest presence and the texture of the rock remains unaffected. Sericite is the only mineral characterizing this zone. It is mainly observed in the ground mass and more rarely on K-feldpsars. In the trachydacite porphyry the sericitic alteration overprints the propylitic alteration zone and locally results in the complete feldspar destructive phenomena. These phenomena are more intense at the outcrops of the tracydacite porphyry at the eastern Ragian 1 Hill (Fig. 6.1). The main mineral linked to sericitic alteration, in the trachydacite porphyry, is sericite along with minor quartz and pyrite and traces of kaolinite, dolomite and rutile. Fine-grained sericite spreads throughout the rock mass reflecting the circulation of the hydrothermal fluids. Sericite is often spatially closely related to hematite disseminations and aggregates. The K-feldspars replacement by sericite is mainly controlled by the distribution of the micro-cracks. In these cases, only the initial tabular crystal habit of the K-feldspars remains when the sericitization totally destructs K-feldpsars forming vugs of different sizes. Usually, this vuggy texture is filled by malachite and chrysocolla. Where intense sericitic alteration occurs, secondary hydrothermal quartz forms veinlets crosscutting the ground mass or fills cavities as clusters of euhedral crystals (<30 μm wide). Sometimes this zone is characterized by the local development of kaolinite, dolomite and acicular rutile. Acicular to prismatic assemblages of rutile are the result of the Ti removal of the parental mica during alteration (Rimsaite, 1973). Consequently, most often rutile is present within sericite.

CHAPTER 7. GEOCHEMISTRY

7.1. ROCK GEOCHEMISTRY

Geochemical study of the magmatic rocks was focused mainly on the rock classification, although they were affected by the intense hydrothermal alteration. Representative chemical analyses of 11 samples of the trachydacite porphyry, three samples of the qtz-monzonite and one of the phreato-magmatic breccia are presented in Table 1.

Concentrations of SiO_2 vary from 55.79 to 71.99 wt% and Al_2O_3 from 13.05 to 16.88 wt%. Samples with SiO_2 over 70 wt % are from the intense feldspar destructive parts of the sericitic alteration zone, while the less altered rock samples are characterized by lower SiO_2, ranging between 55.79 and 63.82 wt%. Thus, the two rock types are characterized as generally silica-saturated. Almost all samples demonstrate high alkali and low Fe_2O_3, CaO, MgO, and NaO_2 contents. Exceptions are the samples which bear significant iron oxides contents, such as Vath17 and sample Vath33. The Vath33 sample represents cataclastic material from a fault area related to the qtz-monzonite intrusions and exhibits higher values in calcium, magnesium and sodium. Alkali enrichment ($K_2O + Na_2O > 7$ wt%) and K_2O/Na_2O ratios >1.0 characterize the slightly altered ore bearing magmatic rocks (e.g. Vath10, Vath33). The K_2O contents vary from 4.22 to 8.79 wt% and are similar to the alkaline rocks of Skouries porphyry Cu-Au deposit (Kroll et al., 2002).

The enrichment in large ion lithophile elements (LILE; K, Rb, Ba) of the slightly altered samples suggest that the source of the magma represents a mixture of mantle and crustal materials highly enriched in LILE (Bonin et al., 1978). The low contents of the high field strength elements (HFSE; Zr, Hf, Nb, Ta, U, and Th) imply a contaminated by crustal rocks ascending magma. The relative low Nb and Ta contents are attributed to small-scale contamination (Bonin et al., 1978).

Based on the discrimination diagram Co vs Th of Hastie et al. (2007) both rock types are classified as high-K alkaline and shoshonitic rocks (Fig. 7.1). This classification is in agreement with the suggestions of Dilek (2006), Harangi et al. (2006), Pe-Piper and Piper (2006) and Agostini et al. (2010) on the magmatic evolution at Northern Aegean area during Early to Middle Miocene (see Chapter 2) who emphasize the shift of the magmatic geochemical affinities during this time period from calc-alkaline to high-K alkaline affinities.

Table 1. Chemical analyses for major and trace elements of the Vathi porphyry system. Ph.-m. br. = phreato-magmatic breccia, n.a. = not analyzed, bdl = below detection limit, adl = above detection limit.

	Vath 19	Vath 10	VTH 6	VTH 11	VTH 12	VTH 14	Vath 17	Vath 01	VTH 03	VTH 04	Vath 27b	Vath 15	Vath 30	Vath 32	Vath 33
	Trachydacite porphyry											Ph.-m. br	Qtz-monzonite		
	Propylitic alteration		Sericitic alteration										Potassic-Sericitic alteration		
wt%															
SiO_2	n.a.	66.73	7.58	59.58	63.82	56.93	67.09	71.99	56.83	55.79	69.35	n.a.	n.a.	69.69	66.70
Al_2O_3	n.a.	16.53	4.45	14.27	15.03	13.56	14.80	15.91	13.05	13.08	16.88	n.a.	n.a.	15.67	16.67
Fe_2O_3	n.a.	3.38	73.31	10.98	5.65	0.69	8.26	2.67	19.22	20.95	2.40	n.a.	n.a.	3.14	3.34
CaO	n.a.	0.26	0.07	0.29	0.13	0.09	0.03	0.05	0.05	0.09	0.16	n.a.	n.a.	0.05	1.11
MgO	n.a.	0.32	0.17	0.28	0.27	0.25	0.59	0.53	0.29	0.50	0.51	n.a.	n.a.	0.50	1.85
Na_2O	n.a.	0.36	bdl	0.70	0.42	0.25	0.09	0.14	0.07	0.10	0.15	n.a.	n.a.	0.15	3.06
K_2O	n.a.	8.79	0.80	5.90	7.69	5.19	5.22	5.12	4.32	4.55	4.94	n.a.	n.a.	6.84	4.22
MnO	n.a.	0.02	0.02	0.01	bdl	bdl	0.02	0.01	0.01	0.03	bdl	n.a.	n.a.	0.01	0.03
TiO_2	n.a.	0.48	0.05	0.41	0.44	0.44	0.42	0.48	0.38	0.40	0.54	n.a.	n.a.	0.48	0.84
P_2O_5	n.a.	0.35	0.73	0.53	0.22	0.06	0.12	0.08	0.33	0.27	0.07	n.a.	n.a.	0.05	0.13
LOI	n.a.	2.21	bdl	5.70	3.60	9.20	2.77	2.62	5.1	3.90	4.36	n.a.	n.a.	2.82	1.98
SUM	n.a.	99.59	97.89	98.64	97.25	86.66	99.43	99.62	99.67	99.67	99.44	n.a.	n.a.	99.50	100.13
ppm															
Mo	5.16	1.88	adl	57.4	39.3	62.1	29.97	319.1	49.3	1.9	20.9	340.7	2.20	4.96	1.77
Cu	88.18	85.04	adl	9297	adl	adl	1502	403.7	1449.8	1277	611.7	722.3	17.31	15.33	109.19
Pb	306.7	51.06	977.3	39.9	99.1	89.1	10.50	93.44	23.8	41.1	98.63	27.51	137.2	17.89	20.43
Zn	20.4	22.0	39	38	28	9	37.0	39.5	115	212	67.2	33.5	155.5	19.0	32.5
Ag	0.7	0.6	4.2	0.3	2.4	4.6	0.1	3.0	0.8	1.0	0.8	3.51	0.3	0.07	0.3
Ni	1.7	2.0	46.7	5.7	2.3	1.2	4.2	2.0	6.7	6.3	5.6	3.7	91.9	3.9	41.4
Co	0.7	0.9	41.7	3.4	0.6	1.1	3.3	0.9	1.6	2.5	2.5	1.0	103.3	1.9	6.8
Mn	58	75	n.a.	n.a.	n.a.	n.a.	191	90	n.a.	n.a.	49	61	6798	93	165
As	4.0	2.7	472.6	2.4	1.4	8.4	3.3	5.4	2.9	2.4	2.3	61.1	132.3	4.8	4.8
U	9.8	9.6	262.6	20.4	32.4	14.3	11.8	9.4	71.3	14.0	11.2	40.5	14.9	21.4	2.7
Th	44.4	45.5	75.2	38.9	40.4	39.7	37.3	37.4	37.0	37.2	41.3	36.2	34.4	55.1	13.0
Sr	208	196	64.4	290.7	268.9	320.8	10	28	61.8	10.7	150	47	131	128	187
Cd	0.02	0.06	6.9	2.4	2.5	bdl	bdl	bdl	0.8	7.7	0.21	bdl	0.15	bdl	0.03
Sb	2.93	3.76	18.7	0.2	0.1	0.2	3.51	5.37	0.1	0.3	2.37	11.20	1.09	1.65	0.52
Bi	2.93	12.04	5.8	3.0	8.0	1.2	8.99	6.76	4.5	239.4	4.61	18.32	2.43	2.68	0.41
V	85	82	bdl	42	46	62	72	52	91	72	101	205	81	64	148
Cr	4.0	4.0	n.a.	n.a.	n.a.	n.a.	4.0	4.0	n.a.	n.a.	5.0	18	7.0	5.0	69
Ba	1330	1219	74	1266	1876	5043	78	159	341	99	478	176	59	208	1645
W	23.1	8.2	13.9	6.2	8.9	4.7	10.4	11.5	10.6	123.6	7.7	43.6	72.6	12.1	6.4
Zr	64.7	63.5	25.5	175.5	192.0	192.6	44.7	52.8	176.3	162.4	53.5	38.2	52.1	58.7	1.1
Sn	7.6	7.3	3	9	5	5	8.3	15.4	8	32	12.7	8.3	8.4	2.0	3.6
Be	4.0	3.0	2	1	5	bdl	5.0	5.0	3	1	5.0	3.0	5.0	4.0	2.0
Hf	2.54	2.47	0.8	5.0	4.9	5.7	1.78	2.01	4.6	4.3	2.12	1.46	2.21	2.39	0.02
Li	13.9	11.4	n.a.	n.a.	n.a.	n.a.	10.4	9.6	n.a.	n.a.	23.9	17.2	7.2	10.5	12.8
Rb	261.4	287.2	63.4	169.9	267.2	189.9	367.3	420.4	241.1	339.1	213.3	321.4	317.9	89.2	159.2
Ta	1.0	0.9	0.1	0.9	0.9	1.6	0.5	0.6	0.8	0.8	1.0	0.3	0.8	0.3	0.5
Nb	12.98	11.31	0.2	11.5	11.2	14.7	5.85	9.45	9.7	15.9	13.06	3.75	10.08	4.67	5.70
Cs	7.0	8.1	3.0	10.8	7.7	7.8	5.6	8.6	7.9	5.4	10.0	13.1	6.4	7.6	6.3
Ga	19.81	19.70	5.8	15.9	15.0	15.2	19.70	21.87	14.9	15.2	21.29	23.08	18.77	18.83	24.34
In	0.14	0.19	n.a.	n.a.	n.a.	n.a.	0.63	0.20	n.a.	n.a.	0.21	0.81	0.19	0.49	0.04
Re	0.003	bdl	n.a.	n.a.	n.a.	n.a.	bdl	bdl	n.a.	n.a.	bdl	0.003	bdl	bdl	Bdl
Se	1.4	0.5	47.4	10.5	0.5	8.3	0.5	0.6	0.7	bdl	bdl	bdl	0.4	2.3	Bdl
Te	0.10	bdl	3	Bdl	bdl	bdl	0.05	0.09	bdl	bdl	bdl	0.09	0.49	0.17	0.09
Tl	4.64	5.72	0.3	0.6	0.8	0.6	4.19	5.44	0.9	0.9	4.12	4.34	4.41	5.23	2.38
Hg	n.a.	n.a.	0.86	0.01	bdl	0.11	n.a.	n.a.	0.01	bdl	n.a.	n.a.	n.a.	n.a.	n.a.
ppb															
Au	6	08	6996	135	98	26	30	20	103	1170	4	724	20	4	7

Total rare earth elements (REEs) concentrations in Vathi magmatic rocks are enriched relative to chondrite values both in light REEs (LREEs) and heavy REEs (HREEs) (Table 2; Fig. 7.2). However LREEs are significantly enriched relatively to HREEs. The qtz-monzonite and the phreato-magmatic breccia are more enriched in REEs than the trachydacite porphyry suggesting a possible same source. Among the trachydacite porphyry samples the concentrations of REEs exhibit variations. In general from west to east along Ragian 1 Hill the concentrations of REEs are diminished (Fig. 7.2). The trachydacite porphyry exhibits negative Tb anomalies, while positive Tm anomalies are observed in all the analyzed samples. A slight negative Eu anomaly in all samples, suggests a restricted fractionation of hornblende and plagioclase during the formation of the trachydacite porphyry and the qtz-monzonite.

Table 2. Rare earth elements (REEs) chemical analyses of the Vathi magmatic rocks. Ph.-m. br. = phreato-magmatic breccias.

	Vath 19	Vath 10	VTH 6	VTH 11	VTH 12	VTH 14	Vath 17	Vath 01	VTH 03	VTH 04	Vath 27b	Vath 15	Vath 30	Vath 32	Vath 33
	Trachydacite porphyry											Ph.-m. br.	Qtz-monzonite		
	Propylitic alteration		Sericitic alteration										Potassic-Sericitic alteration		
ppm															
Sc	6.7	4.8	7	6	7	7	5.2	4.3	9	9	6.2	10.0	6.1	6.4	16.8
Y	15.7	15.0	28.5	31.1	35.7	16.3	7.5	9.5	19.5	53.9	13.8	27.0	20.8	6.7	22.3
La	35.2	59.3	22.8	54.3	53.4	42.7	65.2	5.5	31.4	45.6	35.7	613.1	68.0	32.8	33.8
Ce	77.68	107	39.6	101	119	94.4	122	12.9	75.1	139.1	75.8	894	144.5	63.73	69.13
Pr	8.7	12.7	3.69	10.6	12.8	11	13.5	1.7	9.11	20.26	9.1	79.1	17.6	7.4	8.8
Nd	30.3	38.8	13.9	40.6	45.9	38.6	45.9	8.4	37.3	93.1	31.5	211.1	61.2	26.4	32.9
Sm	5.0	6.2	2.93	7.51	8.73	6.92	6.5	2.2	6.00	17.40	4.9	23.4	10.9	4.5	6.2
Eu	1.2	1.7	0.95	1.99	1.96	1.24	1.9	0.5	1.38	3.59	1.1	5.1	2.3	1.0	1.1
Gd	4.3	4.1	3.86	6.46	7.43	4.98	3.8	2.0	4.38	13.67	4.0	12.7	7.2	2.9	5.7
Tb	0.5	0.4	0.80	1.00	1.09	0.69	0.3	0.2	0.60	1.96	0.4	1.3	0.8	0.1	0.6
Dy	3.2	3.2	5.35	5.82	6.39	3.41	1.9	2.1	3.44	10.43	2.6	5.5	4.1	1.3	3.8
Ho	0.7	0.6	1.14	1.19	1.35	0.60	0.4	0.4	0.60	1.90	0.6	0.9	0.8	0.3	0.8
Er	1.8	1.8	3.10	3.77	3.86	1.69	0.9	1.0	2.06	5.09	1.8	2.1	1.8	0.7	1.8
Tm	0.3	0.3	0.52	0.54	0.59	0.27	0.2	0.2	0.33	0.77	0.3	0.4	0.3	0.1	0.3
Yb	1.8	1.9	3.29	3.51	3.87	1.69	1.4	1.2	2.11	3.83	1.8	2.2	1.7	0.9	1.6
Lu	0.2	0.3	0.45	0.51	0.60	0.29	0.2	0.2	0.35	0.61	0.3	0.3	0.3	0.2	0.2

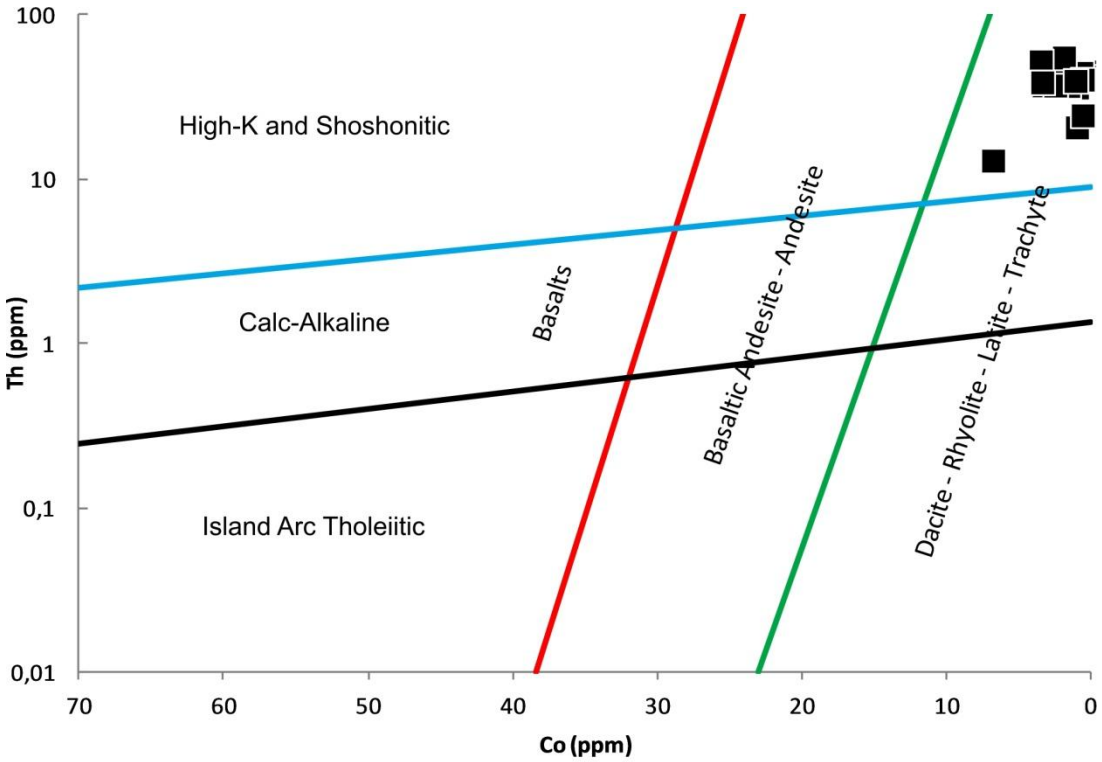

Figure 7.1. The magmatic rocks of Vathi are characterized by high-K alkaline geochemical affinities at the Hastie et al. (2007) classification diagram. Solid squares represent 17 altered samples of the trachydacite porphyry and the qtz-monzonite which exhibit a close spatial distribution.

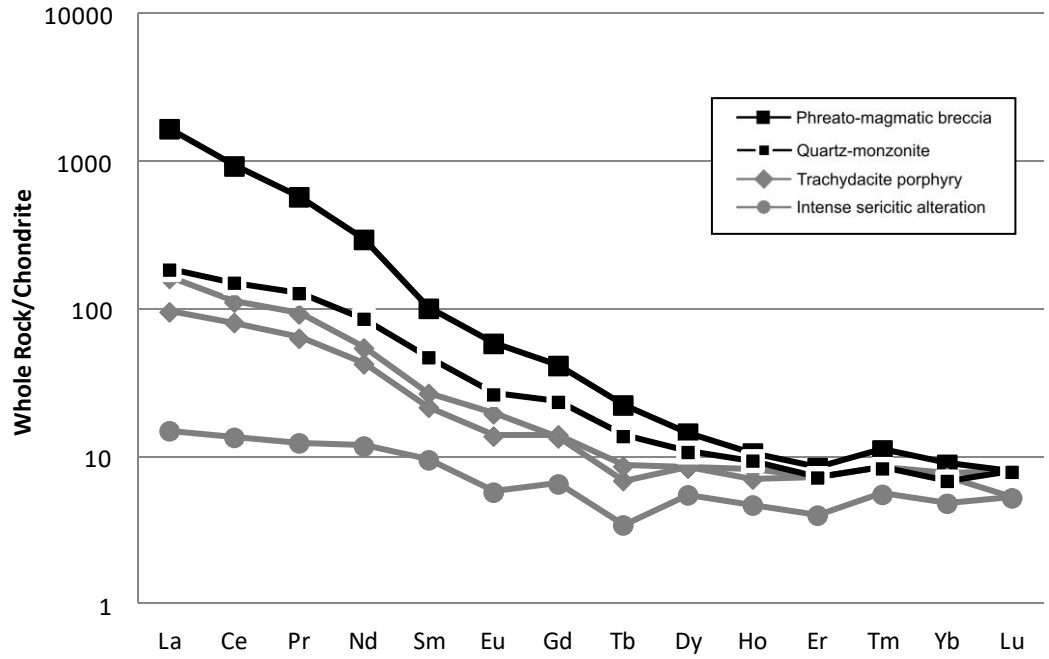

Figure 7.2. A rare earth element discrimination diagram for the Vathi magmatic rocks. Values are normalized to chondrite after Taylor and McLennan (1985).

CHAPTER 8. ORE MINERALIZATION

8.1. DESCRIPTION OF ORE MINERALIZATION

Ore mineralization at Vathi porphyry system is hosted in the qtz-monzonite dikes, in the trachydacite porphyry and the surrounding metamorphic rocks, e.g. two-mica gneisses, schists and amphibolites. It is preferentially localized along the Ragian 1 Hill covering an area of approximately 0.02 km^2. At the surface the primary ore minerals are almost totally oxidized and are associated with the distribution of the potassic-sericitic alteration. The intensity of the mineralization decreases towards the propylitic and the sericitic alteration zones. Primary mineralization is also present at the qtz-monzonite intrusion north of the Ragian 2 Hill. An extensive supergene mineralization covers Ragian 1 Hill and fades away towards Ragian 2 Hill. It reaches 90 to 100 m in depth, from the surface up to a level between +430.90 and +394.30 m a.s.l (Fig. 8.1). Approximately, at the depth of 90 m, a narrow, 2 m thick, secondary enrichment zone is developed (Markoulis, 1970; this study).

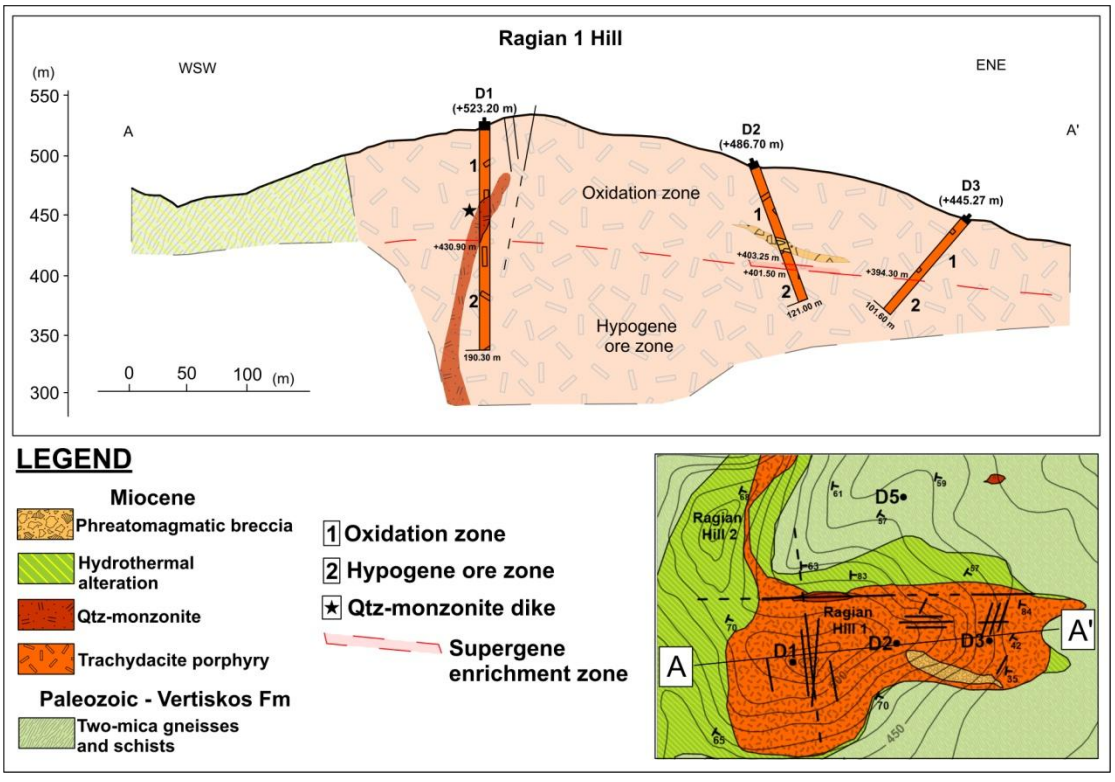

Figure 8.1. A cross section demonstrating the vertical distribution of the ore zones at Ragian 1 Hill. The qtz-monzonite dike is interpretation of this study based on drill core logging data (Markoulis, 1970; modified).

Based on the observations of the drillcore D5 samples, an oxidation zone, 35 m deep underlain by a weak primary ore zone consisting of pyrite with minor chalcopyrite, pyrrhotite, ilmenite and rutile extends at the surrounding two-mica gneisses, schists and amphibolites. The mineralization forms disseminations and veinlets (Markoulis, 1970; this study).

The porphyry style mineralization occurs as disseminations, veins, and small intergrowths. It mainly consists of pyrite and chalcopyrite with minor molybdenite, magnetite and bornite, while in depth and at the outer parts of the porphyry system galena, sphalerite, arsenopyrite and pyrrhotite occur.

The primary mineralization in the qtz-monzonite is associated with the potassic-sericitic alteration forming veins and disseminations (up to 30 vol %) and consist mainly of pyrite. Disseminated pyrite crystals reach 3 mm in sizes and in some cases make up the 30 % of the total rock volume. The veins contain quartz and pyrite and their width is up to 4 mm. This mineralization style in the qtz-monzonite is mainly observed at the surface and along the drilling D1 at a depth between 66 and 75 m (Markoulis, 1970; this study) (Fig. 8.1). Along the contact zone with the trachydacite porphyry tiny euhedral pyrite crystals are found along cracks and cavities (<0.5 cm in diameter) of the rock accompanied by hydrothermal quartz.

The phreato-magmatic breccia also contains a significant metal content, mainly anhedral pyrite up to 80 μm in size. Pyrite occurs mostly throughout the matrix of the phreato-magmatic breccia and in the brecciated rock fragments. Due to the intense surface oxidation the phreato-magmatic breccia hosts abundant hematite, goethite, malachite and minor azurite.

Trachydacite porphyry contains a weak primary sulfide mineralization consisting of pyrite and chalcopyrite, although the majority of the ore minerals are oxidized. The mineralization occurs as disseminations of euhedral crystals, as irregular aggregations and as veinlets along cracks and fractures of the rock. The mineralization is manifested at the surface and in the drillings D1, D2, and D3. The drillcores data showed that the mineralization is hosted in the trachydacite porphyry in the form of disseminations, small intergrowths and quartz veins beneath the depth of 90 m (Markoulis, 1970; this study). At the depth of 139.50 m pyrite and chalcopyrite are equally present, while at the depth of 166 m pyrite is absent and chalcopyrite and molybdenite were only observed. Numerous faults and fractures in the trachydacite porphyry are filled with massive oxidized mineralization, up to 50 cm wide, which

occur mainly at the surface (Markoulis, 1970; this study). Additionally, an extensive vuggy texture characterizes the trachydacite porphyry. This oxidation zone is described by disseminations and impregnations of secondary Cu and Fe minerals, and also contains minor native Au (Markoulis 1970; this study). Other minerals found in the oxidation zone are turqoise, torbernite and meta-torbernite. Torbernite forms disseminations and aggregations of crystals mainly within a narrow zone between 72 and 75 m in depth (Markoulis, 1970). Beneath the oxidation zone a narrow, up to 2 m thick, supergene enrichment zone has been developed. It consists of chalcocite, covellite and minor cuprite, and native copper (Markoulis 1970; this study).

Some parts of the Vathi porphyry system demonstrate a dense system of quartz – sericite – pyrite veins with an E-W trend crosscutting the trachydacite porphyry. These veins correspond to the morphology and mineralogy of the D-type veins (Sillitoe, 2010). They are thin sharp-edged veins, usually up to 1 cm wide (reaching locally 5 cm in width), and occur along the sericitic zone. Pyrite has been oxidized to limonite. In many cases they occur as fault-hosted sheeted veins and as stockworks which also contain malachite impregnations suggesting primary Cu-sulfides, which is typical to the D-type veins (Sillitoe, 2010) (Fig. 8.2a,b). Field observations did not reveal any systematic age relations between these veins.

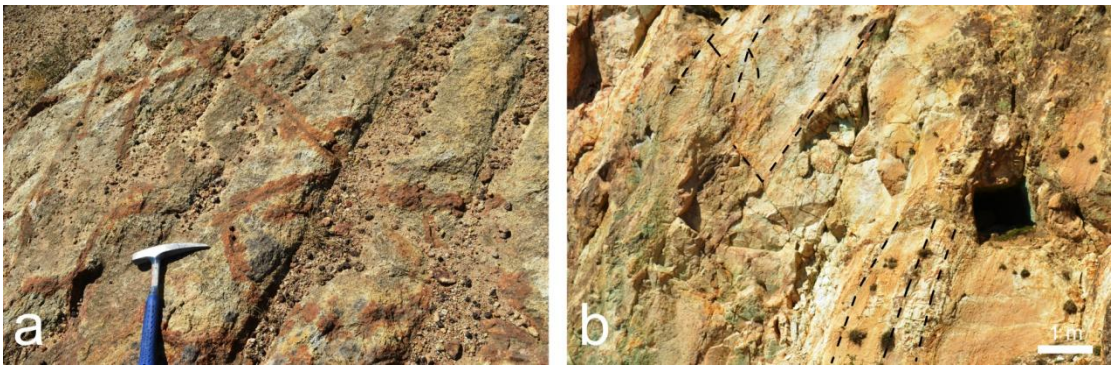

Figure 8.2. a. Narrow (1 cm wide) D-type veins crosscut the trachydacite porphyry. (a) E-W trending fault-hosted sheeted and stockwork vein systems occur at the east hillside of Ragian 1 Hill.

8.2. ORE MINERALOGY

8.2.1. Primary ore mineral assemblages

Based on field observations and microscopic studies four broad ore mineral assemblages were identified in the Vathi porphyry system. They include the following

ore assemblages (1) pyrite + chalcopyrite + bornite + molybdenite + magnetite + native gold, (2) chalcopyrite + pyrite + molybdenite ± stibnite, followed by vein-type (3) pyrite + pyrrhotite + chalcopyrite, and (4) sphalerite + galena ± arsenopyrite (Table 3). The ore assemblages pyrite + pyrrhotite + chalcopyrite and sphalerite + galena ± arsenopyrite are mainly observed below the depths of 166 and 73 m, respectively.

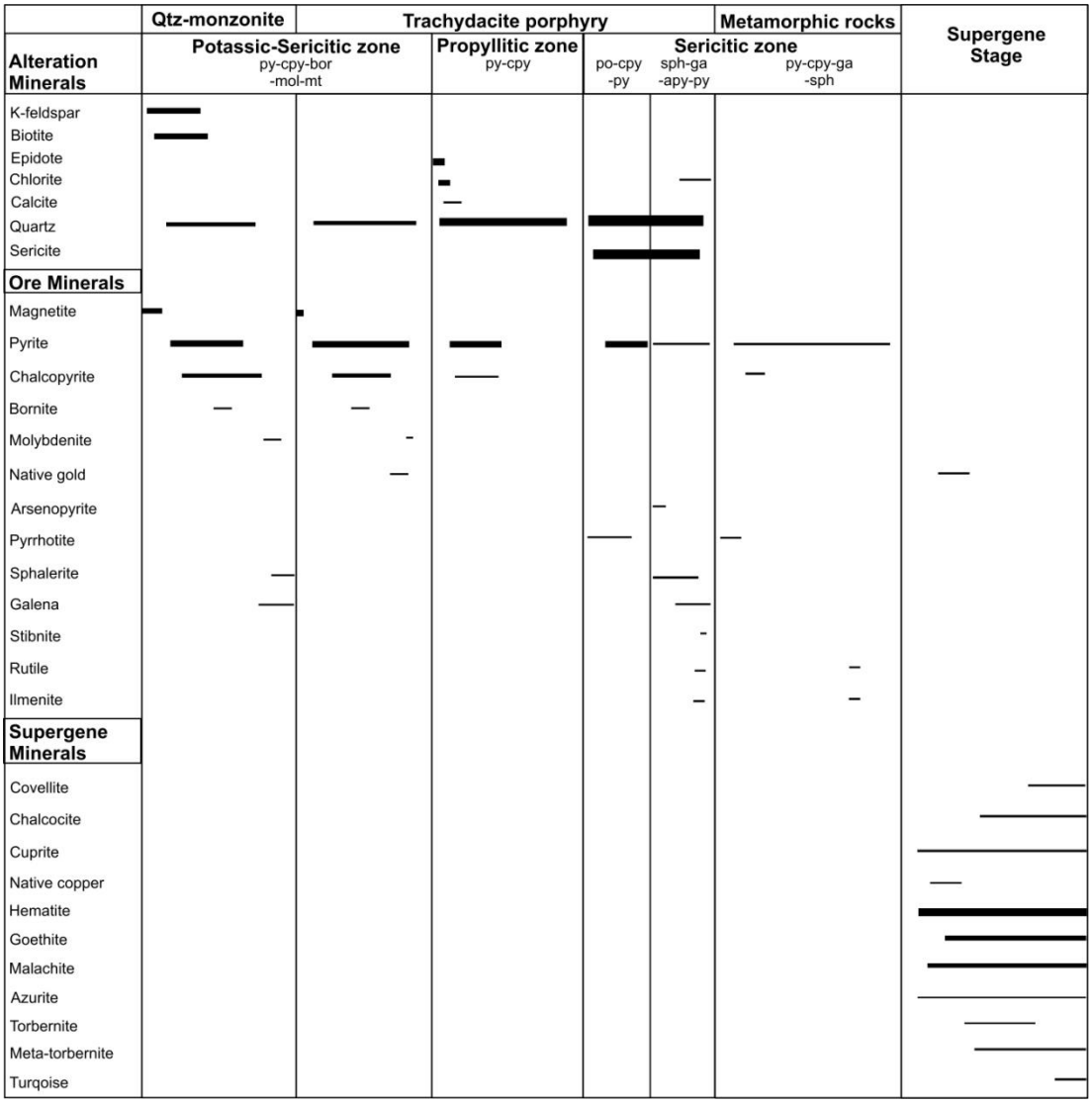

Table 3. Ore and alteration minerals corresponding to each alteration zone in the Vathi porphyry Cu-Au-U±Mo deposit. Line thickness depicts the relative abundances of the minerals. Py: pyrite; mt: magnetite; cpy: chalcopyrite; mol: molybdenite; apy: arsenopyrite; po: pyrrhotite; sph: sphalerite; ga: galena.

The crystallization sequence of the minerals forming the porphyry style mineralization follows in general the following paragenetic sequence: magnetite,

pyrite + chalcopyrite, pyrite, chalcopyrite + bornite + pyrite, molybdenite + pyrite + pyrrhotite + chalcopyrite and arsenopyrite + sphalerite + galena. Magnetite was the first mineral to form along the potassic and the propylitic alteration zones. Chalcopyrite and pyrite formations were continuous events throughout the various mineralizing stages. Chalcopyrite in depth occurs in quartz veins with mica in the altered wall rocks, while towards the surface it forms disseminations. The later sphalerite and galena formation post-dates in general the late-stage pyrite+chalcopyrite formation.

The supergene enrichment paragenetic sequence includes chalcocite, covellite, cuprite and native copper rimming chalcopyrite while the oxidation zone is characterized by the presence of hematite + goethite + malachite + azurite + cuprite.

Within the potassic-sericitic alteration zone of the qtz-monzonite only the first ore assemblage was observed, although native gold was not found. In contrast, all of the above mentioned ore assemblages were observed being hosted in the trachydacite porphyry. Within the potassic-sericitic zone of the trachydacite porphyry the pyrite + chalcopyrite + bornite + molybdenite + magnetite + native gold ore assemblage was found. This ore assemblage is mainly manifested below the depth of 130 m. The propylitic alteration zone of the trachydacite porphyry hosts only minor pyrite and chalcopyrite mineralization. The chalcopyrite + pyrite + molybdenite ± stibnite (between 53 and 60 m in depth), the pyrite + pyrrhotite + chalcopyrite (below the depth of 166 m in D1 drilling), and the sphalerite + galena ± arsenopyrite (below the depth of 73 m in D5 drilling) ore assemblages were observed at the sericitic alteration zone (Fig. 8.3).

8.2.2. Mineral description

Pyrite is the most dominant sulfide mineral of the Vathi porphyry system and is associated with all the alteration zones. It is intergrown with chalcopyrite, bornite, sphalerite, galena and pyrrhotite. It forms disseminations and small intergrowths of anhedral to euhedral (cubic to hexagonal sections) grains ranging in size from 25 μm to 200 μm (Fig. 8.4a). It is slightly to strongly oxidized exhibiting a stained texture which decreases from the periphery to the center or follows the crystal habit. In some cases it is covered by a goethite crust (Fig. 8.4b; 8.4c). Pyrite in the qtz-monzonite is less oxidized and forms veinlets ranging in width between 400 μm and 3 mm, where galena appears in interstices (Fig. 8.4d).

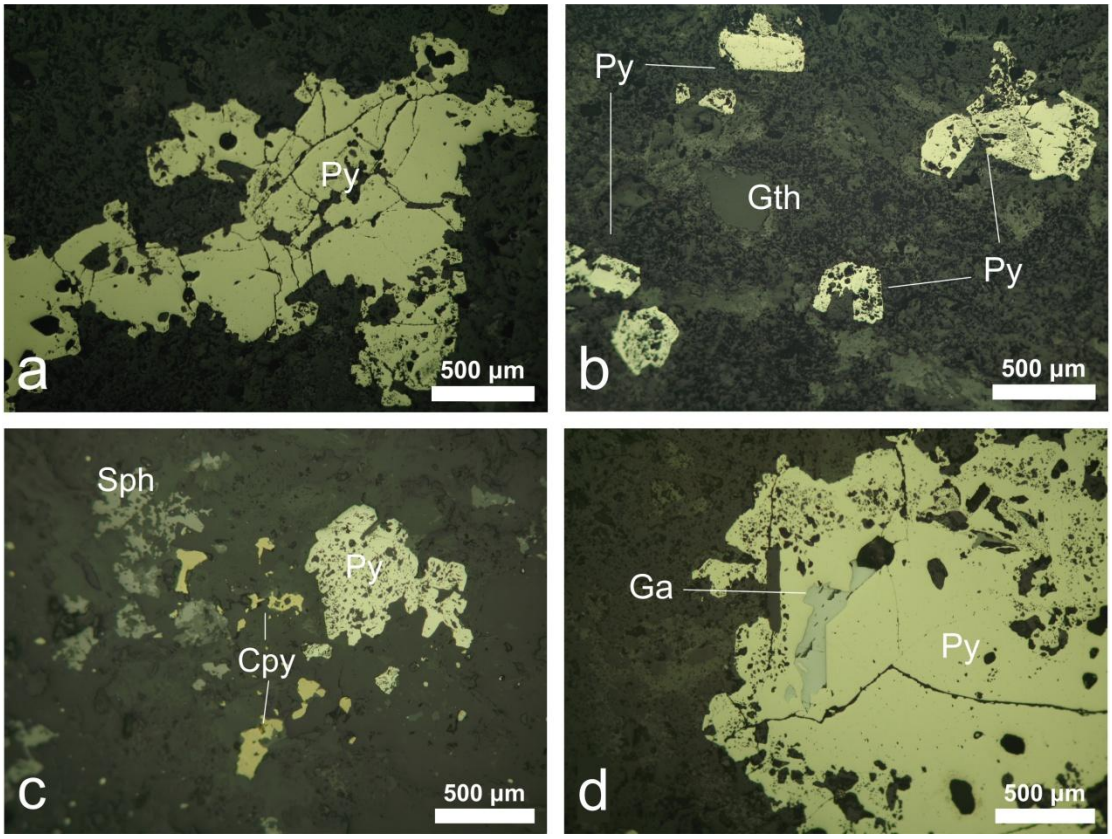

Figure 8.4. Photomicrographs of the primary mineralization in the qtz-monzonite (Nicols //). a Pyrite (Py) in a vein. b. Disseminated euhedral pyrite (Py) and goethite (Gth). c. Disseminations of chalcopyrite (Cpy) coexisting with pyrite (Py) and sphalerite (Sph). d. Galena (Ga) filling interstices in pyrite.

At deeper parts, pyrite forms disseminations and small intergrowths ranging in length from 400 μm up to 0.5 cm. In many cases pyrite is extensively replaced by chalcopyrite which was later replaced by chalcocite (Fig. 8.5a). In these cases, chalcopyrite rather replaces than cements the fractured pyrite grains. Pyrite forms 1 cm wide small intergrowths and disseminations of euhedral crystals (Fig. 8.5b). Up to the depth of 166 m pyrite is massive and euhedral forming small stocks up to 2 cm in width and lacking any specific texture.

Within the metamorphic basement rocks pyrite appears moderately oxidized up to the depth of 53 m. Disseminated small stocks of pyrite (up to 0.6 mm) and veins up to 2 mm wide dominate the rock (Fig. 8.5c). Deeper within the metamorphic basement rocks, at the outer parts of the porphyry system pyrite is observed in up to 1 cm wide veins and as disseminations which gradually with depth, decrease in sizes up to 1 mm. At the depth of 73 m large pyrite grains are replaced by chalcopyrite which

was later replaced by chalcocite and are set in a dark rock mass (Fig. 8.5d). Beneath 73 m within a vein-style mineralization pyrite occurs as inclusions of euhedral crystals (80 to 100 μm wide) in sphalerite and rarely within the rock mass.

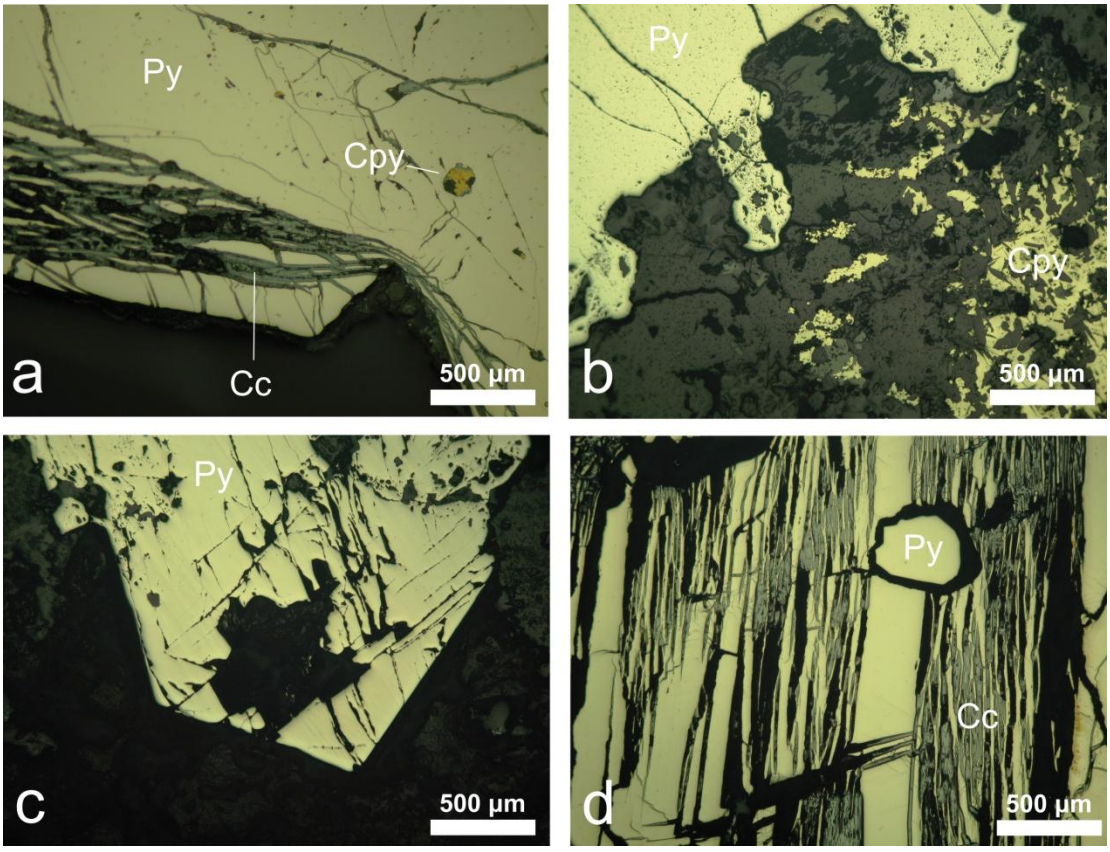

Figure 8.5. Photomicrographs of the primary mineralization in the trachydacite porphyry (Nicols //). a. Cataclastic deformation texture of pyrite (Py) intersected by chalcopyrite which has totally replaced by chalcocite (Cc), and a chalcopyrite (Cpy) inclusion. b. Corroded pyrite (Py) and chalcopyrite (Cpy). c. Euhedral pyrite. d. Pyrite (Py) was replaced by chalcopyrite which was later replaced by chalcocite (Cc).

Chalcopyrite is the second most abundant sulfide mineral of the Vathi porphyry mineralization and is intergrown with pyrite, molybdenite, bornite, pyrrhotite and sphalerite. It is found in all the alteration zones. It mainly occurs as anhedral disseminated grains up to 200 μm in size. Near the surface is rare due to the intense oxidation process. In these cases usually only relicts of chalcopyrite cores remain, rimmed by goethite. In depth, at the primary ore zone, chalcopyrite occurs as disseminated irregular small stocks up to 300 μm in size and as rounded inclusions (<20 μm in width) in pyrite grains (Fig. 8.5a). Chalcopyrite grains are constantly replaced by chalcocite and minor covellite (Fig. 8.6a,b). Beneath Ragian 1 Hill at a

depth between 97.8 and 166 m chalcopyrite exhibits vein and disseminated mineralization styles. At the depth of 97.8 m in the drilling D1 mineralized veins reaching 0.5 cm in width, host chalcopyrite with pyrite inclusions (10-20 μm in size) (Fig. 8.6c). In deeper levels disseminations and small intergrowths of chalcopyrite are widespread and dominate the rock mass. Locally stockworks with chalcopyrite, euhedral quartz and mica are present. Sometimes chalcopyrite coexists with molybdenite. Chalcopyrite was also observed at the outer parts of the porphyry system. Between the depth of 53 and 73 m, dispersed chalcopyrite (up to 400 μm in size) is intergrown with sphalerite (Fig. 8.6d). Below 73 m chalcopyrite appears in rare disseminations which are replaced by chalcocite.

Magnetite is rather rare and is associated with the potassic-sericitic alteration (Fig. 8.7a). It is observed in both the surface and in the drill core samples as subhedral to euhedral crystals. At the depth of 59.90 m within the trachydacite porphyry, magnetite co-exists with disseminated and massive pyrite and minor chalcopyrite. Magnetite is also found in depths from 53 to 60 m in depth at the outer parts of the porphyry system, with pyrite, chalcopyrite and traces of stibnite.

Molybdenite is associated with chalcopyrite and pyrite where it occurs as inclusions (Fig. 8.7b). It was mainly observed in the trachydacite porphyry between 47 and 93 m. Small, less than 30 μm in length, disseminated, molybdenite plates are widespread throughout the rock mass. Euhedral molybdenite plates (~ 20 μm in size) occur also at 139.50 m in the trachydacite porphyry. They appear as inclusions in chalcopyrite and the rock mass. At the outer parts of the porphyry system molybdenite was also observed as disseminations (~ 59.90 m) in the rock mass along with prismatic or oval-shaped rutile.

Bornite is intergrown with chalcopyrite and pyrite and is present as rounded inclusions in chalcopyrite. It was observed constantly rimmed by chalcocite. It varies in size between 15 and 100 μm (Fig. 8.6b). Exsolution lamellae of chalcopyrite were observed in bornite in samples from D1 drill at 47 m depth.

Pyrrhotite is present at depths below 166 m, intergrown with pyrite and chalcopyrite. This assemblage is found in massive sulfide veinlets approximately 1 cm wide rimmed by coarse euhedral quartz crystals ranging in size between 0.3 and 1 cm (Fig. 8.8b). Between the quartz crystals pyrrhotite is intergrown with anhedral to euhedral pyrite (<50 μm in size), chlorite and minor chalcopyrite (40-80 μm in length) (Fig. 8.8c,d).

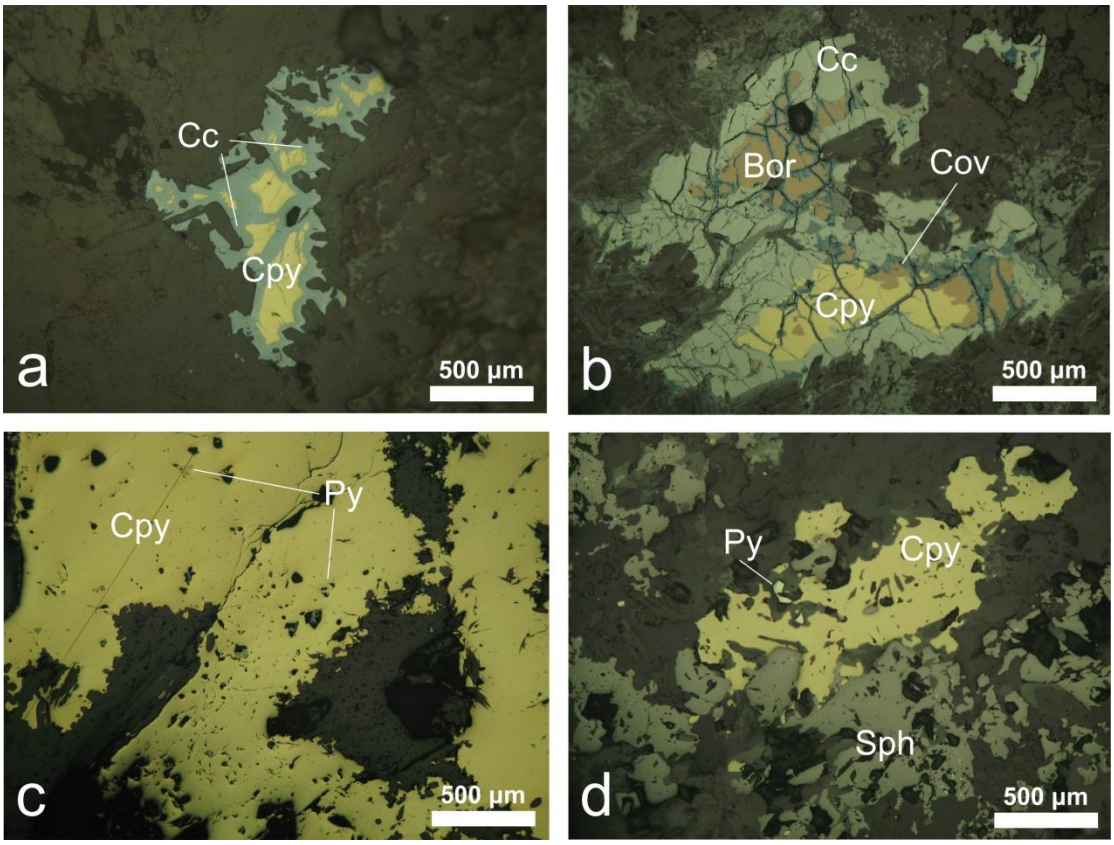

Figure 8.6. Photomicrographs of the primary mineralization in the trachydacite porphyry (Nicols //). a. Chalcopyrite (Cpy) rimmed by chalcocite (Cc). b. Chalcopyrite (Cpy) and bornite (Bor) replaced by chalcocite (Cc) and covellite (Cov). c. Chalcopyrite with small pyrite (Py) inclusions. d. Sphalerite (Sph) intergrown with chalcopyrite (Cpy) and pyrite (Py).

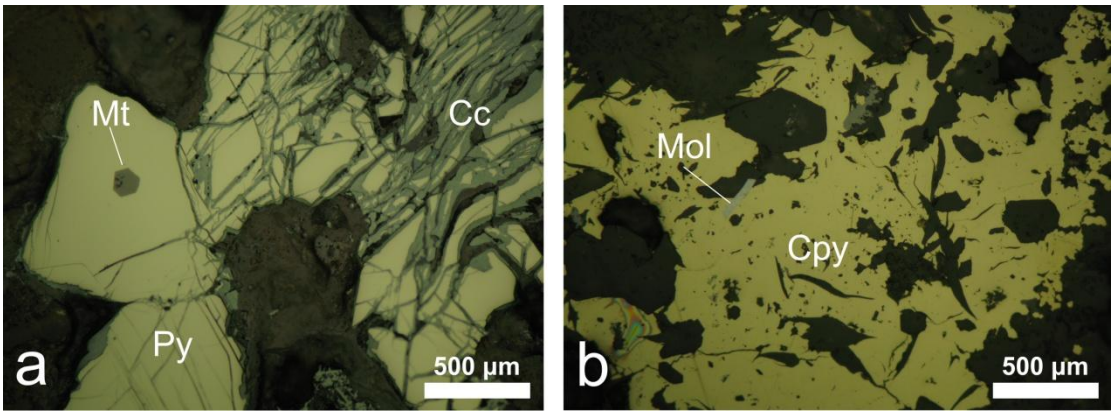

Figure 8.7. Photomicrographs of the mineralization in the trachydacite porphyry in depth (Nicols //). a. Pyrite (Py) with an euhedral magnetite (Mt) inclusion and chalcocite (Cc) which has replaced the chalcopyrite. b. Molybdenite (Mol) plates in chalcopyrite (Cpy).

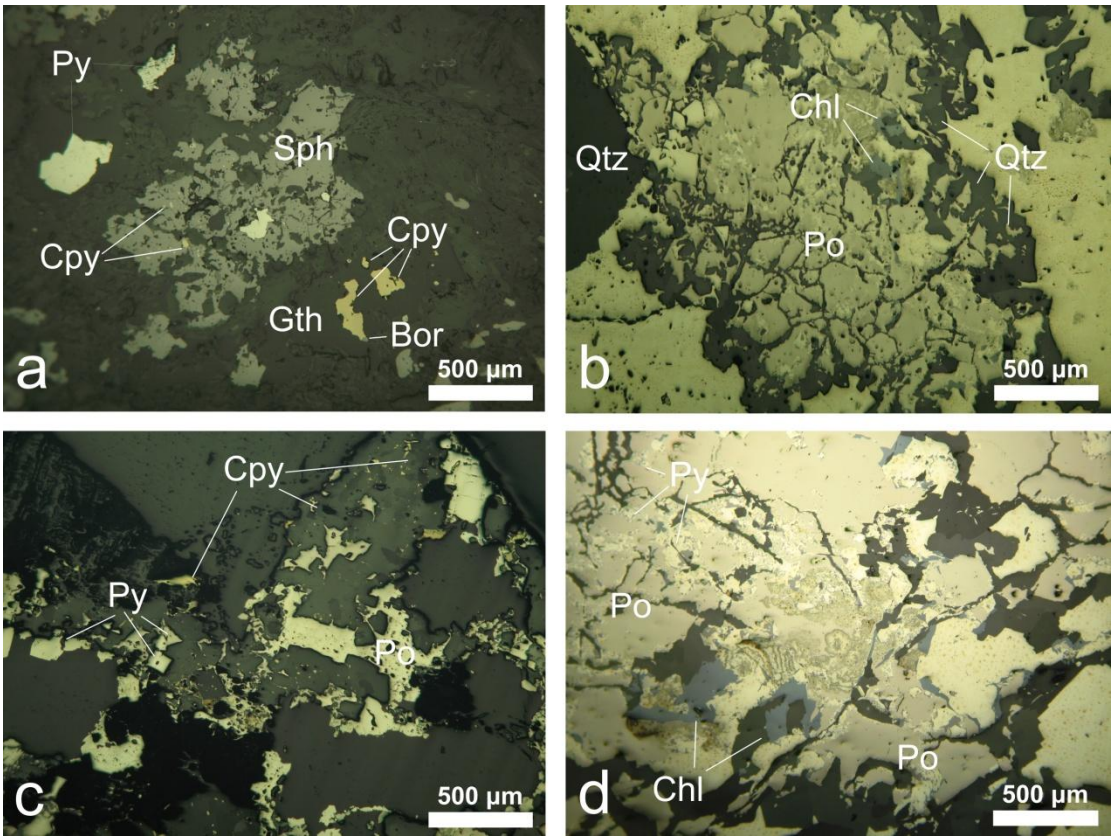

Figure 8.8. Photomicrograph of the mineralization in the trachydacite porphyry in depth (Nicols //). a. Bornite (Bor) in chalcopyrite coexisting with sphalerite (Sph), pyrite (Py) and chalcopyrite (Cpy) inclusions. Chalcopyrite and pyrite are replaced by goethite (Gth). b. Pyrrhotite (Po) is intergrown with pyrite (Py) and chlorite (Chl) rimmed by quartz (Qtz). c. Pyrrhotite (Po) is intergrown with euhedral pyrite (Py) and chalcopyrite (Cpy). d. Pyrrhotite (Po) is intergrown with pyrite (Py) and chlorite (Chl).

Galena is intergrown with pyrite, sphalerite and chalcopyrite and it is related to the sericitic alteration zone. In the near the surface samples galena was mainly observed within the pyrite veins of the qtz-monzonite. It is developed as fillings up to 50 μm wide within interstices and fractures of the pyrite (Fig. 8.4d). This suggests the late formation of galena. Microscopic study of drill core samples showed that galena is also present in depth at the outer parts of the porphyry system. At the depth of 73 m of D5 drilling, galena is present filling interstices and empty spaces between oxidized pyrite grains (Fig. 8.9a). Beneath the depth of 73 m within a massive vein-style mineralization (~ 1 to 3 mm wide) galena was observed mainly associated with sphalerite and quartz as irregular grains (50-200 μm wide). Locally, galena is found as irregular inclusions (10-20 μm wide) in sphalerite.

Sphalerite is rare near the surface and is related to the sericitic alteration zone. It is mainly observed as large anhedral grains with pyrite and chalcopyrite inclusions (Fig. 8.8a). At the depth of 73 m at D5 drilling sphalerite occurs as dark grey irregular grains bearing pyrite (<20 μm in width) and minor chalcopyrite inclusions and it is intergrown with chalcopyrite (Fig. 8.9b). Beneath the depth of 73 m within the massive vein-style mineralization (~ 1 to 3 mm wide) sphalerite is the dominant sulfide mineral. Sphalerite is intergrown with chalcopyrite, galena, arsenopyrite, and minor euhedral pyrite, while euhedral quartz covers the walls of the vein (Fig. 8.9c,d). Sphalerite bears less than 10 μm wide, rounded, inclusions of chalcopyrite (Fig. 8.9d).

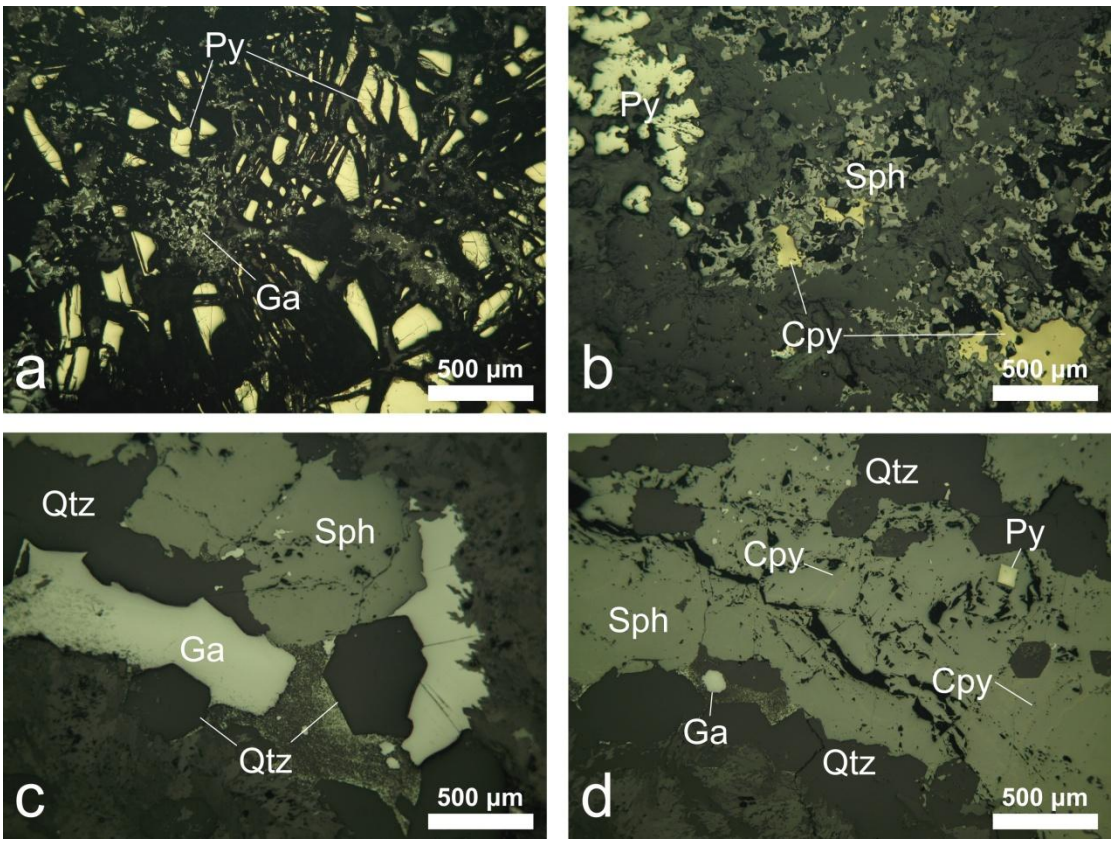

Figure 8.9. Photomicrographs of the mineralization in depth of the outer parts of the porphyry system (Nicols //). a. Galena (Ga) as inclusions in oxidized pyrite (Py). b. Sphalerite (Sph) intergrown with chalcopyrite (Cpy). c. Vein-type mineralization with sphalerite (Sph), galena (Ga) and quartz (Qtz). d. Vein-type mineralization with sphalerite (Sph), galena (Ga), euhedral pyrite (Py), chalcopyrite (Cpy) inclusions and quartz (Qtz).

Arsenopyrite was observed at the outer parts of the Vathi porphyry system in a vein-style mineralization with sphalerite and galena. It forms mainly prismatic and

rhombic euhedral crystals (up to 500 μm in length) (Fig. 8.10a). It also occurs in micro-cavities throughout the rock mass along with quartz (Fig. 8.10b).

Stibnite occurs in traces (<50 μm in size) within fractures in the trachydacite porphyry (Fig. 8.10c). Stibnite co-exists with pyrite and chalcopyrite, although it is not intergrown with them. In addition it does not develop any relation with any other ore mineral. This, along with the occurrence of stibnite within fractures of the rock suggests a late development of this mineral during the ore forming processes.

Native gold is found at a depth of 139.5 m within the potassic-sericitic alteration zone of the trachydacite porphyry. It forms tiny, oval shaped, shinny grains less than 5 μm in length (Fig. 8.10d).

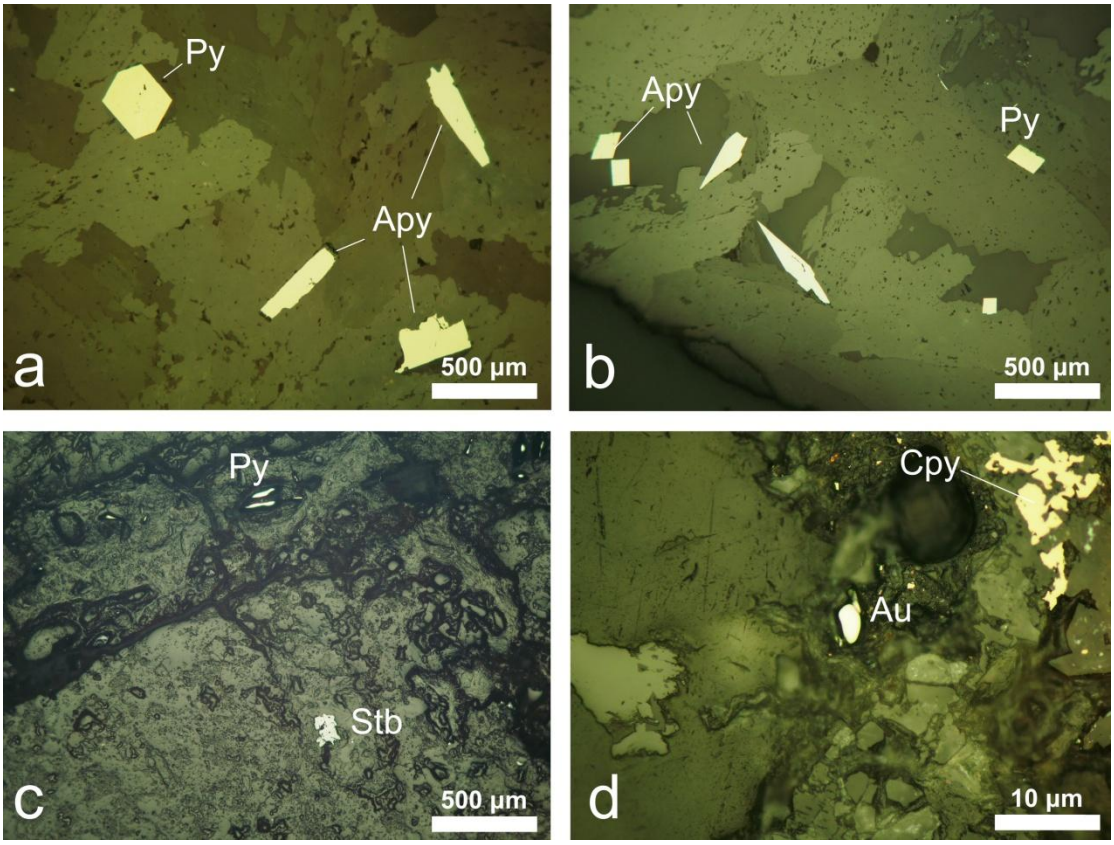

Figure 8.10. Photomicrographs of the mineralization in depth (Nicols //). a,b. Arsenopyrite (Apy) and pyrite (Py) in the rock mass forming respectively cubic to dodecahedral and rhombic euhedral crystals. c. Stibnite (Stb) traces occur at the rock mass. d. A tiny rounded native gold (Au) grain.

8.3. SECONDARY ORE MINERALS

Moderate to strong supergene weathering and alteration processes have affected, almost entirely, the mineralization and an extended, approximately up to a depth of

100 m at Ragian 1 Hill, oxidation zone has developed (Fig. 8.11a). Within the oxidation zone the main secondary minerals found include: hematite + goethite + malachite + azurite + cuprite + torbernite and meta-torbernite, while also native copper and native gold occur (Fig. 8.11b,c,d). A secondary enrichment zone is developed locally approximately between the depth of 90 and 100 m and consists mainly of chalcocite and covellite (Markoulis, 1970; this study).

Hematite and goethite are the main oxidation products of pyrite and chalcopyrite within the oxidation zone (Fig. 8.12). At the surface oxidizing and leaching processes have affected and often completely removed pyrite (Fig 8.13a). Consequently, hematite and goethite were formed. Hematite is found only at the surface. It is observed as sheets and as botryoidal to granular aggregates. Within rock discontinuities hematite appears as radial and bushy aggregates of platy sheets. At deeper parts, pyrite and chalcopyrite are replaced only by goethite. In the fault zones at the surface goethite is the dominant mineral produced by the oxidation and in some cases it forms masses up to 20 cm in width (Fig. 8.11b). At the depth of 16 m at the drilling D2 in a mass of goethite within a discontinuity of the trachydacite porphyry a veinlet of *native gold* is reported by Markoulis (1970). Goethite also forms aggregates in micro-cavities and replacements forming pseudomorphs after pyrite (Fig. 8.13b). In depth, goethite was observed in reniform masses along with tabular rutile. Hematite is developed in flakes and radial forms in micro-cavities and in altered rock-forming minerals along with sericite and Ti-minerals (Fig. 8.13c,d).

Malachite appears as massive, botryoidal aggregations and acicular to tabular-prismatic crystals filling interstices and fractures of the rock (Fig. 8.11c). Malachite and minor *azurite* encrustations are widely present along the east hill sides of Ragian 1 Hill (Fig. 8.11d). Their presence is significant along the phreato-magmatic breccia and the trachydacite porphyry.

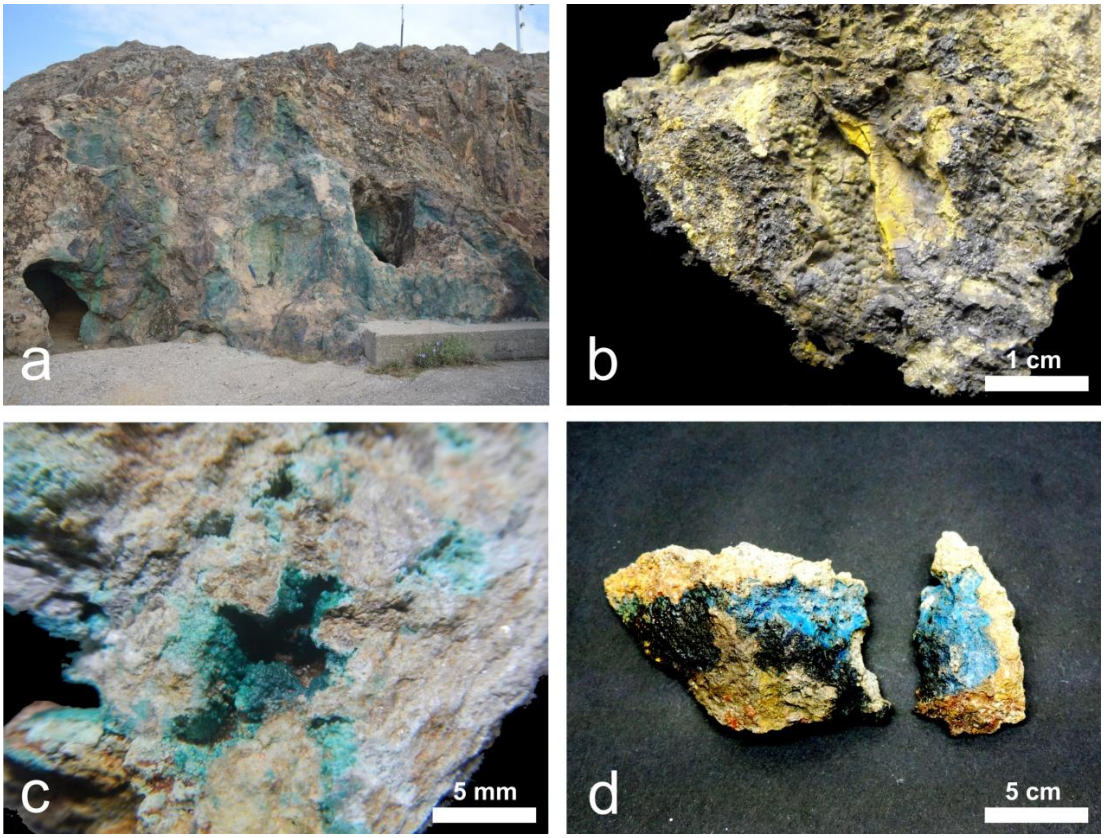

Figure 8.11. a. Ancient galleries for gold extraction extent throughout Ragian 1 Hill. b. Botryoidal aggregations of goethite in envelope-like fissure with earthy goethite and minor hematite. c. Botryoidal malachite in rock cavities. d. Encrustations of azurite.

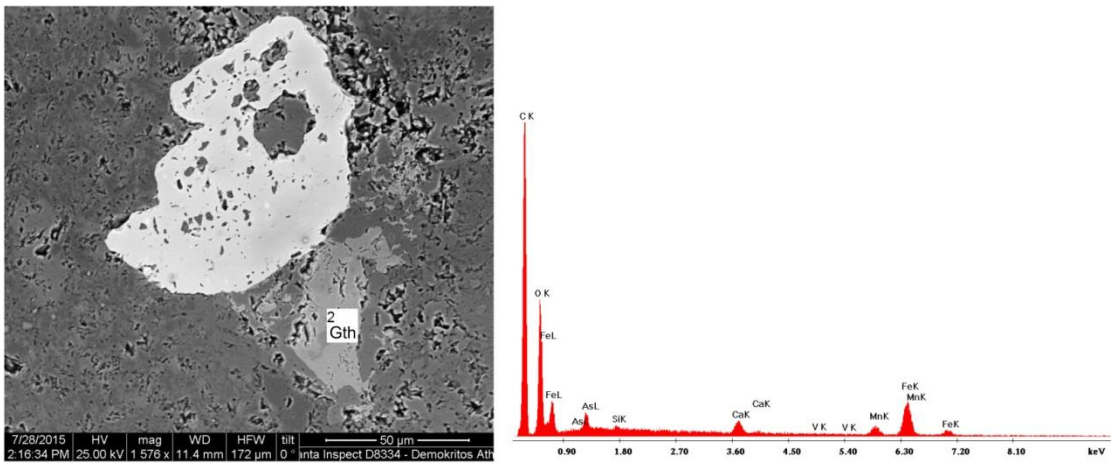

Figure 8.12. Backscattered image of pyrite (bright grey) and goethite from the qtz-monzonite (left). A qualitative analysis using SEM-EDS revealed elevated ratios of As and Mn participating in the crystal structure of the goethite (right).

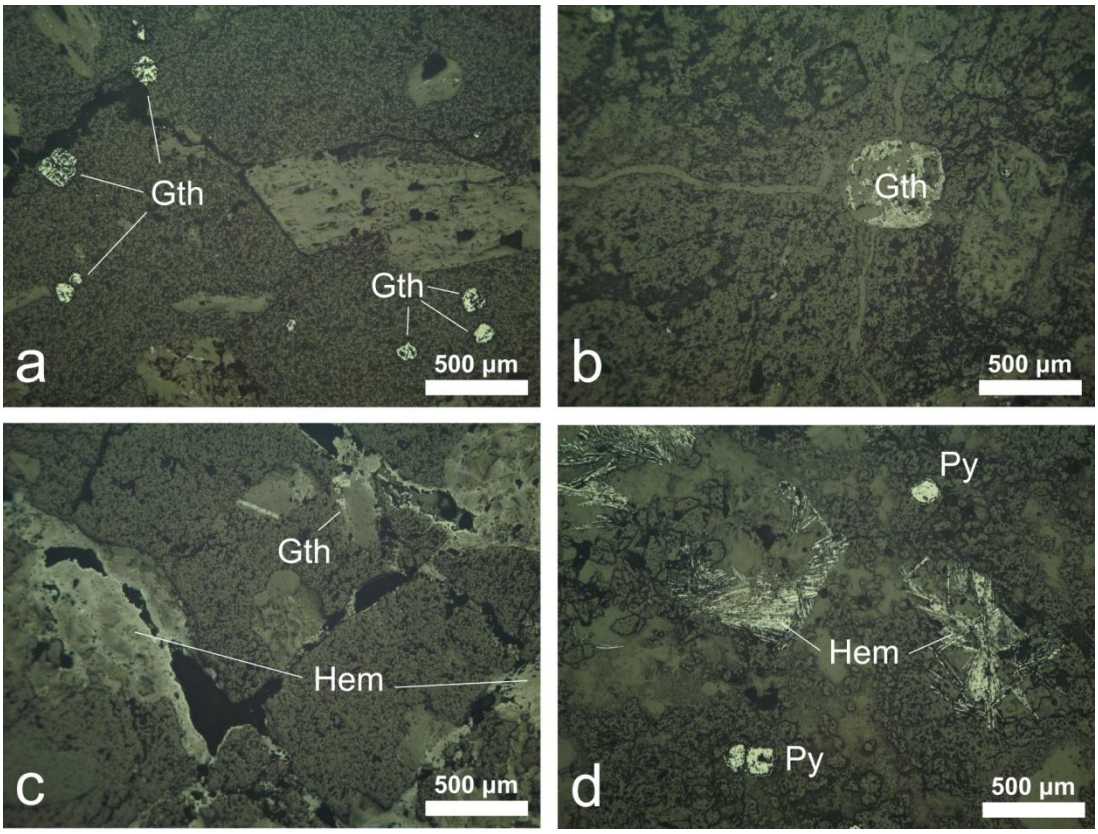

Figure 8.13. Photomicrographs of the oxidized pyrite mineralization of the trachydacite porphyry (Nicols //). a,b. Disseminated goethite (Gth) after pyrite. c. Hematite (Hem) and goethite (Gth) in micro-cavities. d. Goethite (Gth) after pyrite and hematite (Hem) as sheets within altered rock-forming minerals.

Cuprite presence gradually rises with depth (Markoulis, 1970). Between 90 and 92 m of depth it was observed forming veinlets. It fills rock fractures along with minor irregular segregations of chalcocite and covellite. *Native copper* appears as small disseminated grains in cuprite.

Chalcocite and covellite are observed in the secondary enrichment zone. The presence of both minerals drastically increases below 60 m in depth and are mostly found at the depth of 90 m (Fig. 8.14). They are always alteration products of chalcopyrite and bornite.

A restricted, unique in Greece, turqoise occurrence is found at the east side of Ragian 1 Hill first reported by Dimitriadis (1973) (Fig. 8.15a). It appears in veinlets and encrustations exhibiting characteristic pale colors and forming hexagonal pseudo-morphs after apatite (Sklavounos et al., 1992). In addition to turqoise various, small occurrences of LILE- and HFSE-rich (mainly Sr, Nb, Ce, Th, La, U) phosphate

carbonates and multiple oxides (e.g. woodhouseite, senaite), were observed between other minerals such as sericite or filling the empty spaces between them (Fig. 8.15b).

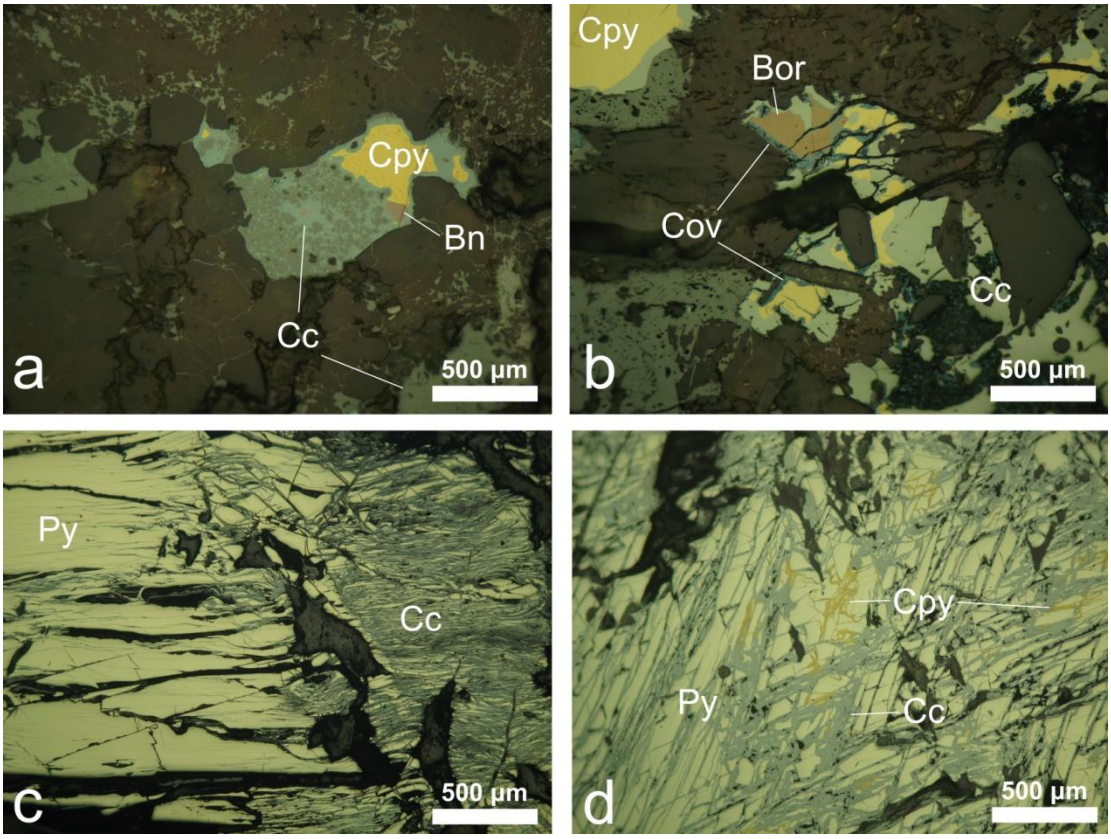

Figure 8.14. Photomicrographs of the supergene mineralization in the trachydacite porphyry in depth. a. Chalcopyrite (Cpy) and bornite (Bor) are replaced by chalcocite (Cc) b. Chalcopyrite (Cpy) and bornite (Bor), are replaced by chalcocite (Cc) and covellite (Cov). c. Secondary chalcocite (Cc) in pyrite (Py). d. Chalcopyrite (Cpy) in pyrite (Py) is replaced by chalcocite (Cc).

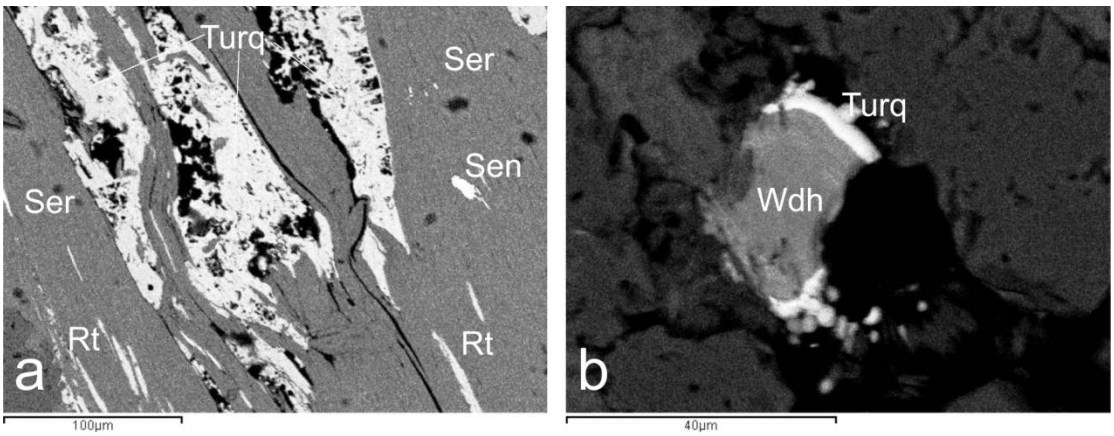

Figure 8.15. Backscattered images and SEM-EDS analyses confirmed the presence of turqoise (Turq) within empty spaces in sericite (a) and as encrustations on other

minerals (b). Senaite (Sen) and rutile (Rt) formed as a result of the Ti removal of the parental mica during alteration (Rimsaite 1973) (a), as well as woodhouseite (Wdh) were also observed (b).

8.4. ORE MINERALIZATION GEOCHEMISTRY

The distribution of basic and precious metals within the Vathi porphyry system is well correlated with the hydrothermal alteration zones and the ore mineralization. It is also affected by the structural trends which controlled the intrusion of the magmatic rocks and the formation of the porphyry system. Oxidation and secondary enrichment processes have further affected the metal distribution. Surface samples were analyzed and spatial distribution maps for the elements Cu, Mo, Au and U were constructed (Fig. 8.17).

Surface samples are locally enriched in Cu, Mo, Au, U, Pb, Zn and Ag. The highest concentrations of these metals are mainly associated with the sericitic alteration zone at the eastern part of the trachydacite porphyry at Ragian 1 Hill (Fig. 8.17). Copper is also enriched at the central area of the hill, while weak anomalies of gold and uranium were observed along and around the qtz-monzonite dikes.

On average, the following measurements were obtained from the Vathi porphyry system 2607 ppm Cu, 335 ppm Mo, 0.73 ppm Au, 106 ppm U, 182 ppm Pb, 90 ppm Zn and 0.12 ppm Ag based on the chemical analyses obtained from 24 surface mineralized samples. Metal concentrations of representative samples from both the trachydacite porphyry and the qtz-monzonite are shown in Table 1. The metal concentrations of the adjacent schists are significantly diminished. The chemical analysis of a representative sample gave 28.29 ppm Cu, 1.02 ppm Mo, 0.01 ppm Au, U up to 106 ppm, 16.98 ppm Pb, 44.4 ppm Zn, while Ag was below detection limit. These values are considered between the lowest for the Vathi porphyry system and for the area of Ragian 1 and 2 Hills (Fig. 8.17). Although, chemical analyses of schists in contact with the trachydacite porphyry exhibit elevated metal concentrations (e.g. 1338 ppm Cu).

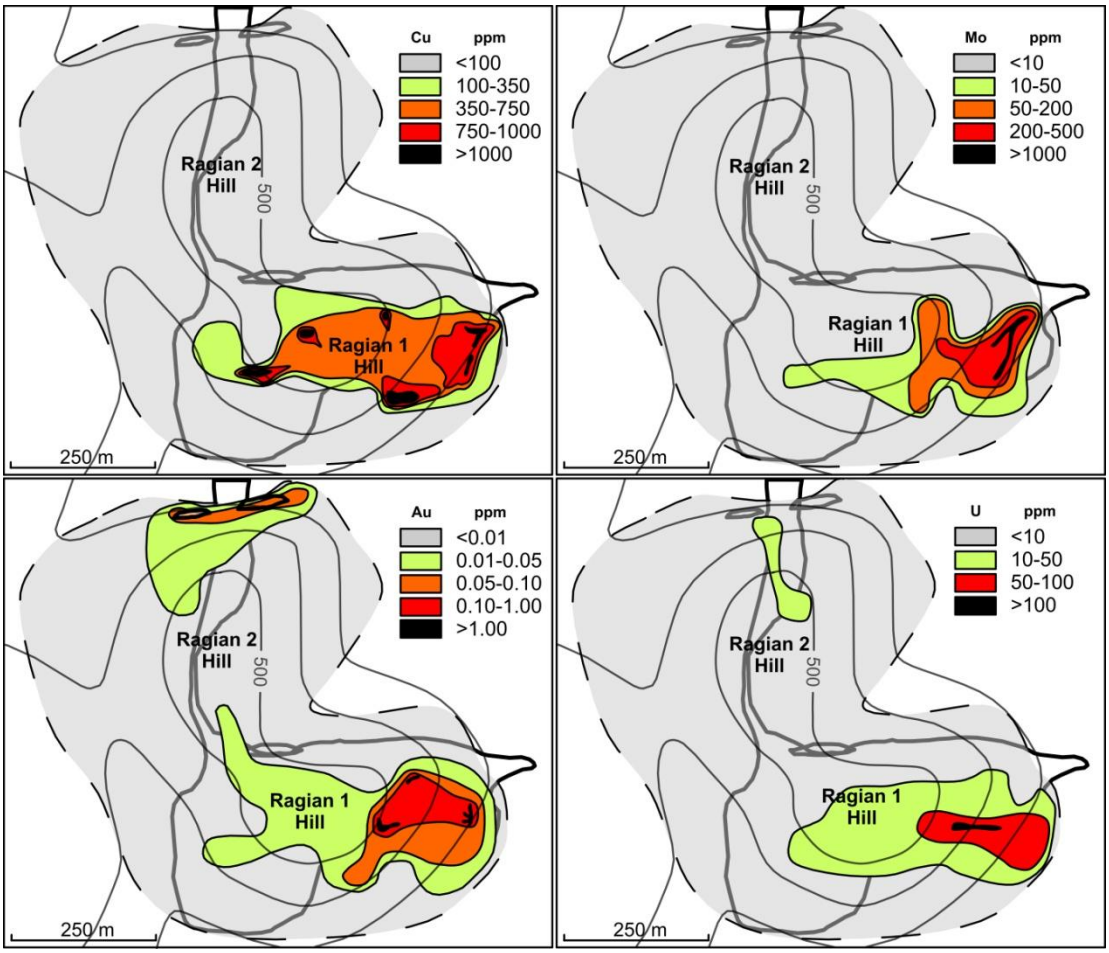

Figure 8.17. The metal distribution throughout Ragian Hills is strongly affected by local tectonic structures, oxidation and secondary enrichment processes.

The analyzed qtz-monzonite samples are characterized by significantly low copper (up to 109.19 ppm) and molybdenum (up to 4.96 ppm) contents and by slightly anomalous gold (up to 0.02 ppm) and uranium (up to 21.4 ppm) contents (Table 1; Fig. 8.17). In contrary, the trachydacite porphyry appears more enriched in base and precious metals. However, it exhibits significant spatial variations in metal concentrations (Fig. 8.17).

The geochemical investigation of samples from the propylitic-sericitic alteration zone of the trachydacite porphyry revealed weak geochemical anomalies. Maximum contents of 1502 ppm for Cu, 29.97 ppm for Mo, 0.03 ppm for Au, 11.8 ppm for U, 10.50 ppm for Pb, 37 ppm for Zn and 0.1 ppm for Ag were found. Sericitized rock samples exhibit higher concentrations. On average copper reaches up to 1296.48 ppm, Mo up to 45.75 ppm, Au up to 0.04 ppm, U up to 18.9 ppm, Pb up to 36.45 ppm, Zn up to 34.9 ppm and Ag up to 0.56 ppm. However, this enrichment should be

addressed to the later sericitic alteration and the secondary oxidation processes. The intense feldspar-destructive area of the sericitic alteration exhibits in comparison to the other alteration zones the highest metal concentrations. On average, copper ranges up to 1398 ppm, Mo up to 311 ppm, Au up to 1.185 ppm, U up to 59 ppm, Pb up to 239.16 ppm, Zn up to 102.7 ppm and Ag up to 0.83 ppm. In general, the metal content becomes higher from west to east along the sericitic alteration zone.

The pheato-magmatic breccia contains significant concentrations in base and precious metals in comparison to these from the qtz-monzonite and the trachydacite porphyry. Concentrations of as much as 722.3 ppm Cu, 340.7 ppm Mo, 0.724 ppm Au, 40.5 ppm U, 27.51 ppm Pb, 33.5 ppm Zn and 3.51 ppm Ag. In addition, it exhibits significantly enriched concentrations in As (61.1 ppm), V (205 ppm), U (40.5 ppm), Rb (321.4 ppm), In (0.81 ppm) as well as in La (613.1 ppm), Ce (894 ppm), Pr (79.1 ppm), Nd (211.1 ppm) and Gd (12.7 ppm).

Finaly, the highest metal contents measured for the Vathi porphyry system was 9297 ppm Cu, 340.7 ppm Mo, 6.996 ppm Au, 328.6 ppm U, 1399.48 ppm Pb, 234 ppm Zn, and 4.2 ppm Ag. However, these chemical analysis results refer to oxidized samples of the trachydacite porphyry. The strong oxidizing processes along with the present of tectonic structures drastically controlled the secondary metal distribution throughout Ragian 1 Hill.

CHAPTER 9. STRUCTURAL CONTROL STUDY

The southern part of SMM in Bulgaria, FYROM and Greece comprises similar tectonic features that are mainly characterized by the effects of differential vertical tectonic movements. These motions are related to normal and oblique fault zones in strike-slip fault settings and to secondary Riedel faults and shear zones as a consequence of the Tertiary-Quaternary extensional tectonics (Pavlides et al., 1988; Kilias et al., 1999; Dumurdzanov et al., 2004; Volkov et al., 2010; Kounov et al., 2010; Siron et al., 2014).

The northern region of the Greek SMM is characterized by four groups of faults (Pavlides and Mountrakis, 1987; Pavlides et al., 1988; Voidomatis, 1990; Kilias et al., 1999). These groups comprise normal faults trending E-W, NW-SE and NE-SW, and N-S trending strike-slip faults. The NE-SW trending group of faults occurs only in the northern part of the Greek SMM. The NW-SE and the NE-SW faults comprise

distinct sinistral strike-slip and significant dextral strike-slip components, respectively (Pavlides et al., 1988). According to Kondopoulou and Westphal (1986), these tectonic features are the result of the clockwise and the counterclockwise rotations of the southern and northern part of the SMM in Greece. Pavlides et al. (1988) proposed that the faults formed between Eocene and Late Miocene times.

On a local scale at the Ragian 1 and Ragian 2 Hills of Vathi, these tectonic settings are represented by NE-SW, NW-SE, and almost E-W trending faults (Fig. 9.1). The NE-SW and the almost E-W trending faults dip to NW and to SSW, respectively. On average, the first group strikes N52E and dips 51^{o} to the NW, whereas the second group strikes N76E and dips 70^{o} to the SSW. The NW-SE trending faults strike on average N25W and dip 60^{o} to the ENE-E. Field observations suggest that the E-W trending faults should be considered extensive tectonic settings, which favored the intrusion of the magmatic rocks and the enhanced hydrothermal fluid circulation (Fig. 9.1). The NW-SE and the NE-SW trending faults –most probably refer to compressive tectonic structures– also contributed to the fluid circulation and to the deposition of ore mineralization (Fig. 9.1).

The magmatic rocks, the phreato-magmatic breccia, the hydrothermal alterations, the D-type and the oxidized veins exhibit a close relation to the mentioned regional tectonic settings. The qtz-monzonite occurs in narrow, elongated, dikes which trend E-W. Locally, the qtz-monzonite appears affected by an intense high-temperature potassic alteration set in a cataclastic environment (Fig. 9.2). Macroscopically, angular quartz and augen aggregates of quartz are observed and they are evidence of the intense structural control. Throughout the trachydacite porphyry several tectonic structures are present fragmenting especially Ragian 1 Hill (Fig. 9.1). Additionally, the mineralized phreato-magmatic breccia intrudes the trachydacite porphyry along an E-W direction. This direction is similar to the direction of the faults which control the qtz-monzonite intrusions and therefore a possible genetical association is suggested. At the east side of Ragian 1 Hill a network of faults occurs within the area of the most intense sericitic alteration zone emphasizing on a significant structural control of the hydrothermal alteration zones. Furthermore, stockwork and fault-hosted sheeted quartz D-type veins with oxidized mineralization outcrop in the eastern part of the Vathi porphyry system (Fig. 9.3). They are structurally controlled by an E-W trending fault zone dipping at average 60^{o} to the SSW. This tectonic feature structurally

dominates the north hillside of Ragian 1 Hill and is followed by numerous similar yet minor, parallel to sub-parallel tectonic features.

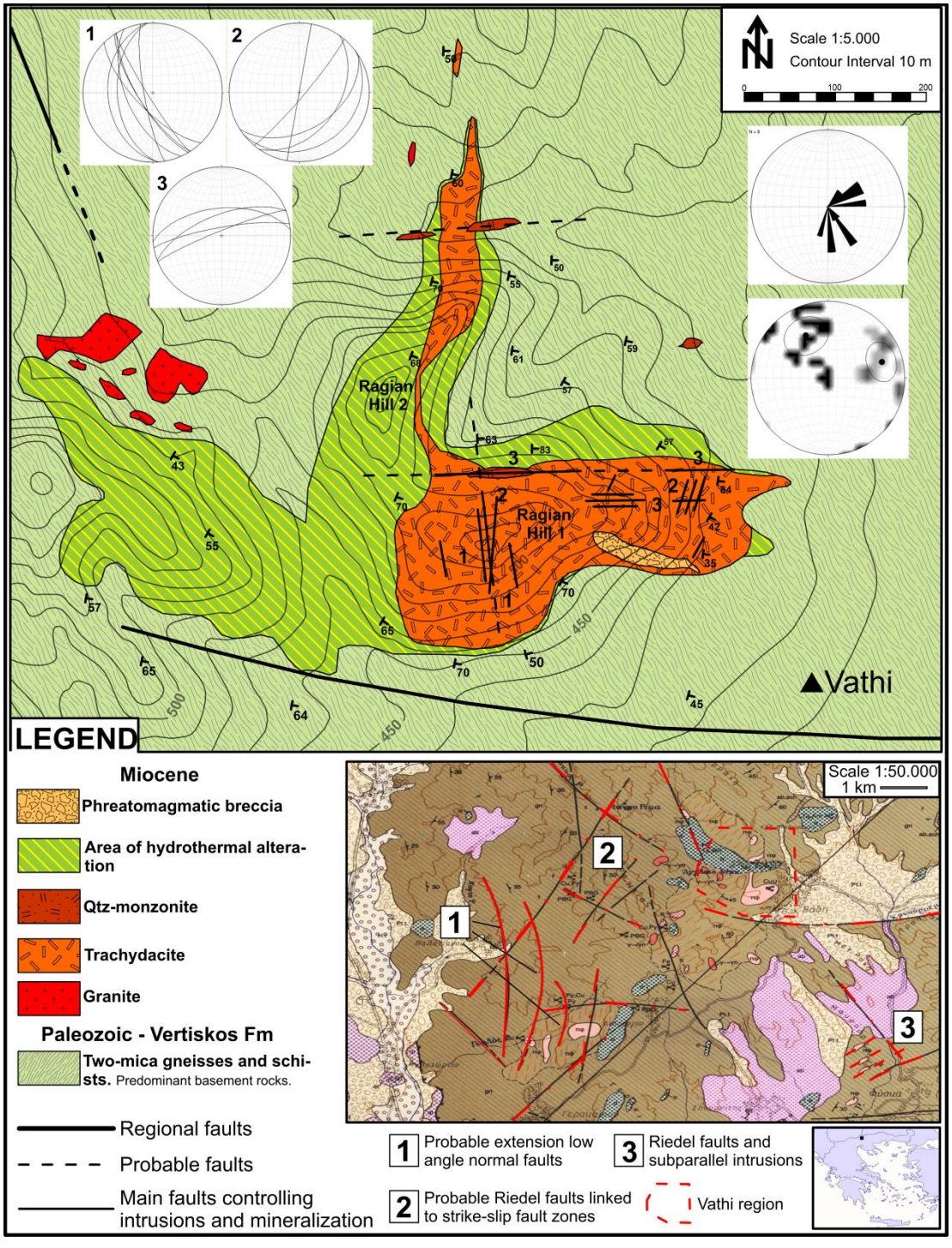

Figure 9.1. Vathi Ragian 1 and 2 Hills tectonic map. NW-SE, NE-SW and almost E-W faults are depicted through stereographic projections, a dip-slip cumulative rose diagram and a dip-slip cumulative pole density diagram. Also, a district scale tectonic interpretation is proposed based on the existing tectonic analysis for the Serbo-Macedonian Massif (IGME 1:50.000 map sheet Xerson; Kilias et al., 1999).

Finally, the extended presence of secondary ore minerals is linked to the NW-SE and the NE-SW trending faults. These compressive tectonic structures are characterized by the occurrence of hematite, goethite and malachite (Fig. 9.4). Along Ragian 1 Hill they bear several marks of the ancient mining activities.

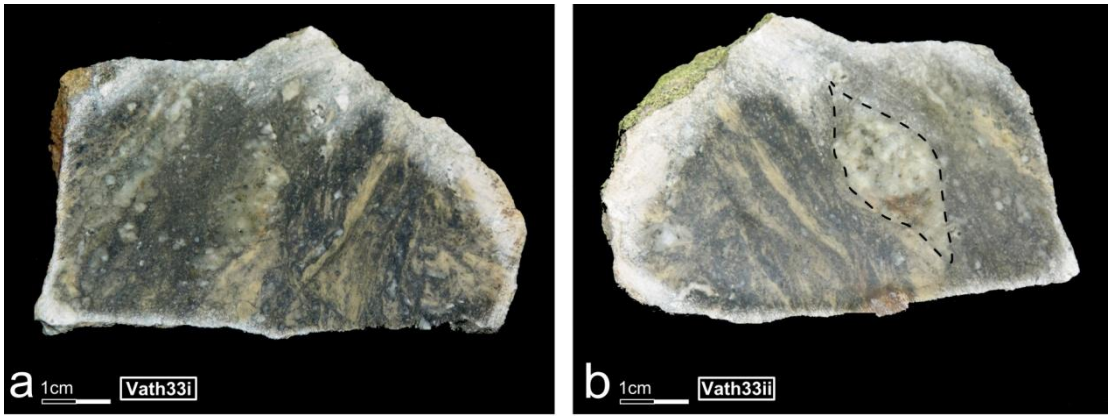

Figure 9.2a,b. Intensively potassically altered qtz-monzonite samples occurring along the E-W striking fault zone. Angular and sub-angular quartz crystals are widespread as well as eye-shaped (b) quartz aggregates.

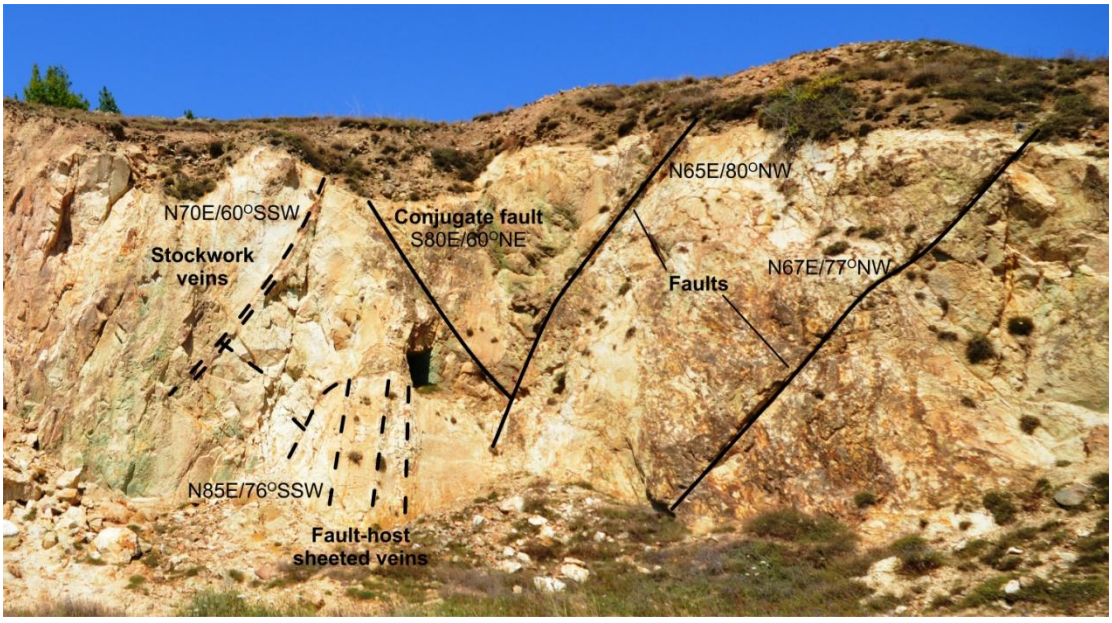

Figure 9.3. Fault-hosted sheeted and stockwork veins (dashed lines) consisting of quartz, sericite and oxidized mineralization. Malachite impregnations cover the wall rocks. NE-SW striking normal faults are also highlighted.

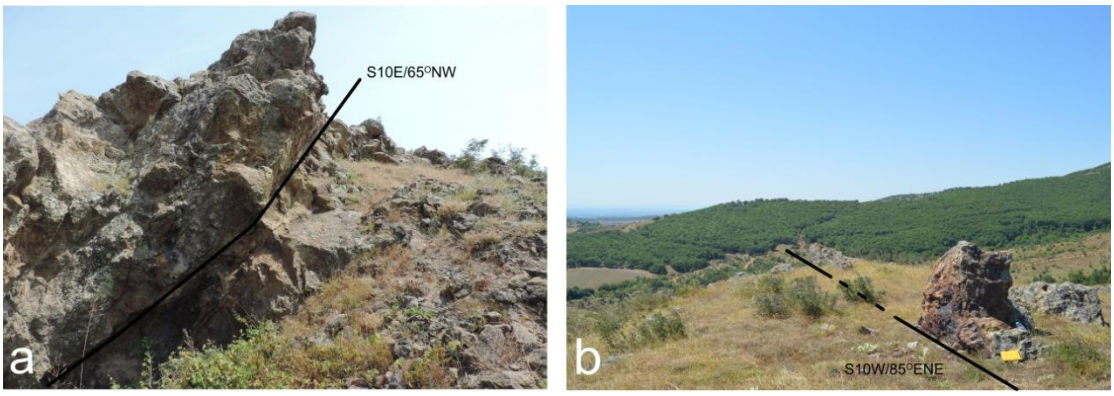

Figure 9.4a,b. NW-SE and NE-SW faults crosscutting the trachydacite porphyry. They bear significant amounts of hematite and goethite.

CHAPTER 10. DISCUSSION

The intrusion of co-magmatic, calc-alkaline to alkaline I-type granitoids directly or indirectly related to subduction, of intermediate to felsic compositions, in shallow depths usually result in the formation of porphyry type deposits (Sinclair, 2007; Seedorf, 2008; Sillitoe, 2010; Ridley, 2013). Disseminated and stockwork-type ore textures are distinctive characteristics of these types of deposits together with the hydrothermal alteration zoning patterns within the intrusive rocks and outwards (Sillitoe, 2010; Ridley, 2013). The abundant volumes of H_2O- Cl- and S-bearing fluids enriched in fluid–mobile elements such as K, Rb, Cs, Ca, Sr, Ba, U, B, Pb, As, Sb, Tl, and possibly Cu, Au and PGEs, are incorporated in the magmas and in the subsequent ore mineralization. These components are fluxed from the dehydrating subducting slab into the mantle wedge metasomatizing it (Richards, 2011). The subduction-modified lower lithosphere of the upper plate constitutes an additional fluid and element source during the post-collisional stage (Sillitoe, 2010; Richards, 2011). In particular, the lower crustal amphibolitic cumulate roots of former arc magmatic complexes are remelted under relatively low fS_2 conditions, whereas active subduction S-fluxes are missing. These areas bear a sparse (yet enriched in chalcophile and highly siderophile elements e.g. Au, Ni) sulfide content which is residual from fractionation of previous arc magmas (Richards, 2005; 2011; 2013; Richards and Mumin, 2013). Hence, these fluids tend to form post-subduction porphyry deposits enriched in Au and PGEs (Richards, 2009).

Well-known examples of deposits of this category are the Roşia Montană porphyry Cu-Au and Kisladag porphyry Au along the Western Tethyan Metallogenic

Belt (Richards, 2011). The above geochemical processes, set in an exceptional post-collisional geotectonic environment, resulted in the formation of several Tertiary porphyry deposits along northern Greece e.g. Skouries, Fisoka, Maronia, Pagoni Rachi, Fakos and Stipsi (Kroll, 2002; Melfos et al., 2002; Voudouris and Alfieris, 2005; Voudouris et al. 2009; Fornadel et al. 2012).

On the SiO_2 vs V/Sc diagram, a relatively fresh sample from the qtz-monzonite of Vathi plots together with other porphyry Cu-Au deposits (Fig. 10.3). The V/Sc ratio can be applied due to its high resistance to distribution by moderate hydrothermal alteration fluids (Loucks, 2015). Thus, it can provide independent corroboration of the Cu prospectivity of igneous suites, which manifests the fertility of the magma below Vathi (Loucks, 2015). According to Frei (1992) the elevated Fe^{3+} and Mg^{2+}/Fe^{2+} ratio, as well as the greater than 1000 ppm ranging sulfur values prove the mineralized character of the qtz-monzonite intrusion of Vathi. Based on the results presented above and on the geophysical study of the area (Thanasoulas, 1979) it is suggested that the mineralization is genetically linked to the subvolcanic qtz-monzonite dikes and is partly hosted in the deep to shallow subvolcanic trachydacite porphyry. The significant local enrichment of the sericitic alteration zone in Cu, Au, Mo, and U should be linked to supergene processes. The close association of the secondary alteration minerals -K-feldspar and biotite- with the Cu mineralization in the qtz-monzonite dikes and the relatively high Cu-Au grades suggest that the volatile fluids were possibly exsolved from the magma (Gustafson and Hunt, 1975; Sillitoe, 2010). The mineralization forms disseminations (up to 30 vol%), veins, stockworks, and small stocks.

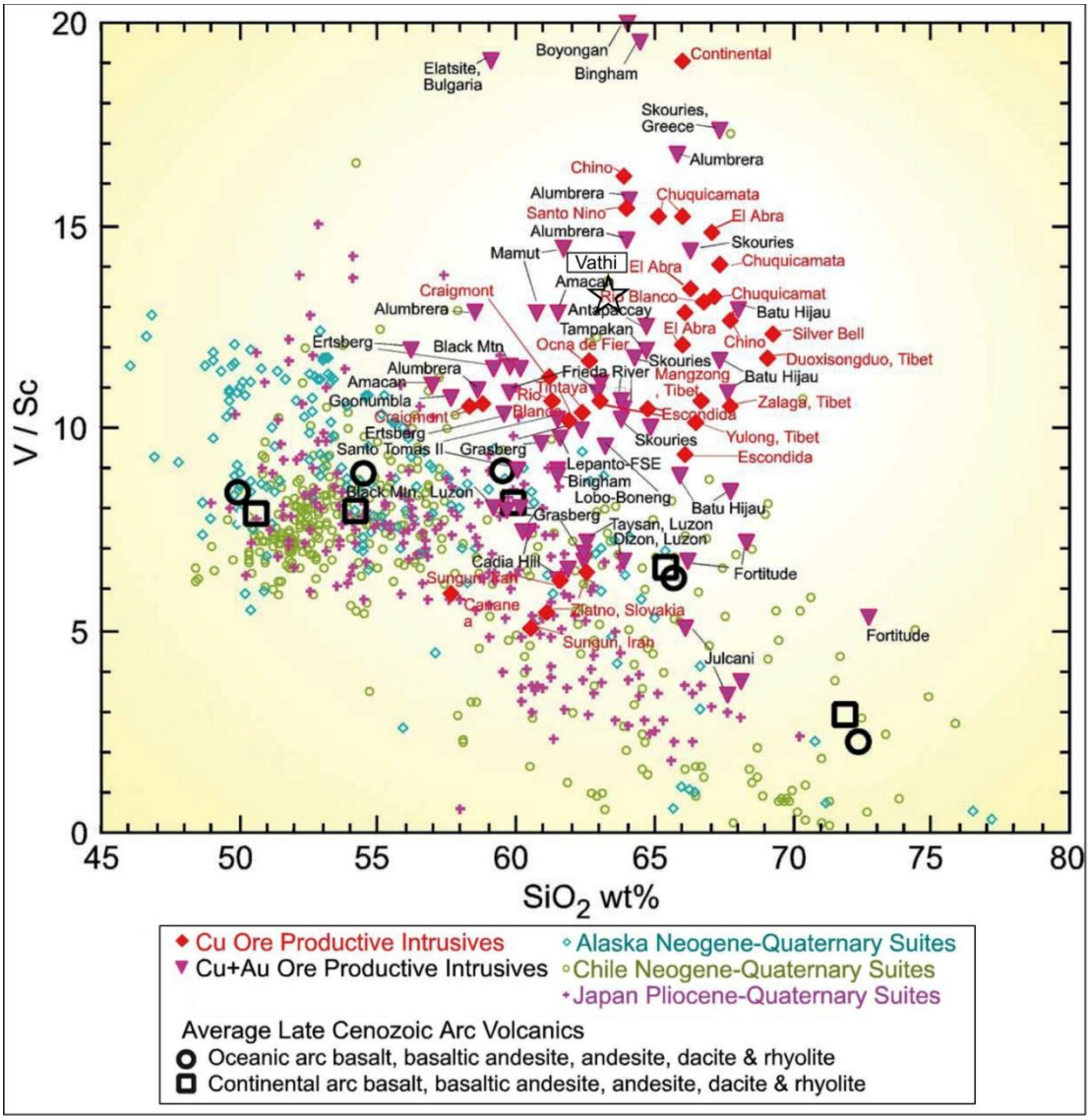

Figure 10.3. The global reference suite of porphyry Cu ore deposits classification based on whole-rock V/Sc ratios vs SiO_2 wt%. Prospective Cu-Au deposits are characterized worldwide by V/Sc > 10 ratios. The Vathi qtz-monzonite (Vath30) has V/Sc = 13.27 and is plotte among the magmatically fertile and prospective Cu-Au ore deposits (pink rhombuses) (Loucks, 2015).

Geotectonic settings, structural control and magma emplacement

The Serbo-Macedonian Massif is part of the Rhodope Metamorphic Province and shares the same magmatic to hydrothermal history to the adjacent Rhodope Massif since the Eocene, as a consequence of the subduction of the Vardar ocean plate below the Eurasian continent (Himmerkus et al., 2009; Kydonakis et al., 2014). The subduction zone migration to SSE since Eocene driven by slab roll-back, asthenospheric upwell and slab break-off, has repeatedly resulted in the formation of major Cu-Au porphyry systems in southeastern Europe during Tertiary (de Boorder et

al., 1998; von Quadt et al., 2005; Burg, 2012; Kaiser-Rohrmeier et al., 2013). At these ongoing accretional or collisional geotectonic settings, critical to the formation of the Tertiary Cu-Au porphyry deposits was the decrease of the African-Eurasian convergence rate up to 1.5 cm/yr in a time period of 10 Ma (Bertrand et al., 2014).

The Oligocene-Miocene ore mineralization of the Serbo-Macedonian metallogenic province (SMMP) is connected to post-collisional Tertiary back-arc magmatism, which is the result of the contemporaneous district crustal scale geotectonic settings (Lips, 2002; Neubauer, 2002). This post-collisional event was characterized by the strong structural control of low to middle angled detachment faults, caused by the N–S extension and the exhumation of the Rhodope and Serbo-Macedonian Massifs (Kilias et al., 1999; Krohe and Mposkos, 2002). Relative to the Serbo-Macedonian Massif collapse are the Strymon-Kerdylion detachment faults separating the Serbo-Macedonian Massif from the Rhodope Massif (Dinter and Royden, 2002; Killias et al., 1999; 2015). According to Schenker et al. (2012), the intrusion of magmas in these massifs was controlled by such contemporaneous detachment faults.

The main phase of the mineralized intrusion along the Serbo-Macedonian Massif is geochronologically spanned in a time period between Middle Oligocene and Middle Miocene (30-17 Ma) (Frei, 1992; Gilg and Frei, 1994). According to Pavlides et al. (1990) the activation of brittle faults striking E–W, NW–SE and NE–SW as a result of the N-W extension is placed around the Early Oligocene. These faults are linked to shear and strike–slip tectonic settings and are probably related to North Aegean Trough, with several of them being still active (Pavlides et al., 1990; Mouslopoulou et al., 2014). Gilg (1993) and Gilg and Frei (1994) suggested that these faults acted as channel ways for the upwelling magmas, controlling thus the circulation of the magmatic – hydrothermal fluids. A characteristic example of this structural control mechanism has been recently described by Bristol et al. (2015) for the formation of the Stanos shear-zone hosted Cu-Au-Bi-Te mineralization at the southern SMMP. Hahn et al. (2012) correlating these results with the Eocene-Miocene geotectonic evolution of Serbo-Macedonian Massif proposed that the older (around Eocene) intrusions are linked to the exhumation of the Serbo-Macedonian Massif from the Rhodope Metamorphic Complex, while the younger (around Miocene) intrusions were formed after the final positioning of the Serbo-Macedonian Massif. During this stage a dominant structural event was the reactivation of several

detachment faults as normal faults connected or related to strike-slip fault zones and Riedel faults, e.g Strymon Fault System (Kilias et al., 1999; Koukouvelas and Aydin, 2002; Chatzipetros et al., 2012; Mouslopoulou et al., 2014) (Fig. 10.2). Thus, it is highlighted that along with the crustal scale tectonic structures, the regional and district scale tectonic structures are key factors controlling the formation of several ore deposits types during post-collisional stages (Tosdal and Richards, 2001; Richards, 2003).

Vathi magmatic complex was emplaced in such environment of post-subduction tectonic extension which was followed by the development of local transpressional and transtensional tectonic settings, during Miocece (Fig. 10.2). Several deep to shallow subvolcanic stock-like bodies, plugs and dikes varying in composition from granodiorite and monzodiorite to quartz-monzonite and from rhyodacite to trachydacite porphyries intruded the metamorphic basement rocks at the broader area of Vathi (Filippidis et al., 1988; Frei, 1992; this study). Their emplacement was structurally controlled by the development of regional tectonic settings which is in accordance with the contemporaneous district tectonic settings. The E-W, NW-SE and NE-SW trending fault system favored the emplacement of the trachydacite porphyry and the qtz-monzonite and the formation of the porphyry style mineralization by channeling the magmatic-hydrothermal fluids and the meteoric waters circulation.

The qtz-monzonite dikes at Vathi are genetically related with the mineralization and intruded into the earlier volcanic rocks and the basement metamorphic rocks of the Vertiskos Unit, under subvolcanic conditions during Burdigalian between 18±1/2 - 17±2/2 Ma, based on U-Pb zircons ratios by Frei (1992). The presence of the phreato-magmatic breccia suggests that some of these dikes may have vented themselves. However, as the drill core description from D1 drilling revealed most of them were terminated upwards beneath the paleosurface and now some are exposed due to erosion (see Fig. 8.1). Detailed geological mapping revealed that the intrusions were favored by regional tectonics. Ore-related qtz-monzonites are oval, steep, dike-like bodies characterized microscopically by porphyritic textures. This could be attributed to the fast ascent of magma in an extensional regime and the consequent crystallization at shallow depths. A similar mechanism is described by Melfos et al. (2002) for the porphyritic microgranite of Maronia, NE. Greece.

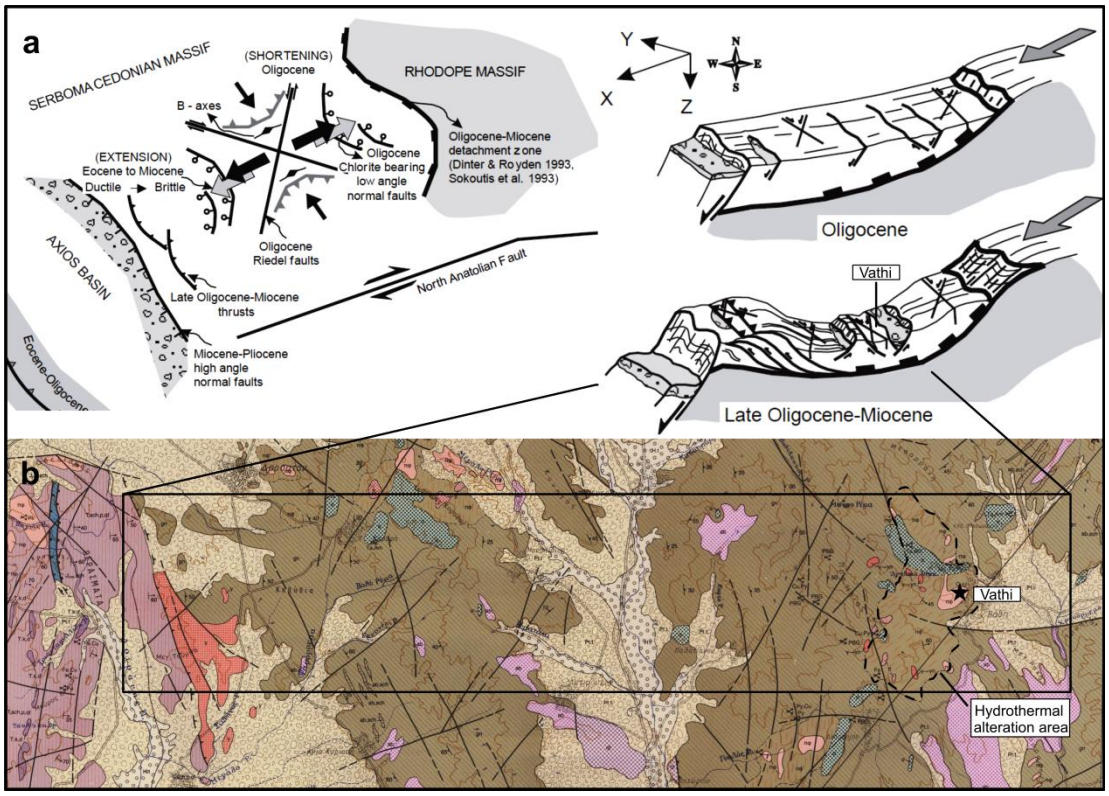

Figure 10.2. The correlation between the Eocene - Miocene geotectonic evolution model of the Serbo-Macedonian Massif (a) and the tectonic emplacement of the Vathi magmatic complex (b) in the broader region of the NW Greek Serbo-Macedonian Massif (Herson map sheet; 1:50.000; Ioannidis and Kelepertzis, 1974; tectonic settings reconstruction; Kilias et al., 1999).

No relation was observed between the qtz-monzonites and the granites outcropping westwards of Ragian 1 and 2 Hills (Fig. 5.1). Furthermore, the qtz-monzonites appearing as a dike and stock-like bodies northwestwards of Ragian 1 Hill should be highlighted (Filippidis et al., 1988). Consequently, the existence of similar in composition intrusive and extrusive rocks which share the same age as well as their spatially closely related emplacement as finger-like projections, favored by regional tectonics, implies the existence of a magma chamber in depth. This is something rather common along the Serbo-Macedonian metallogenic province e.g. Buchim Cu-Au-porphyry deposit, FYROM (Serafimovski et al., 2010).

The magmatic rocks related to the Vathi porphyry system have been previously characterized as rhyodacite (Andronopoulos, 1967; Melidonis, 1968) or latite (Frei, 1992) and as qtz-monzonite (Filippidis et al. 1988). In the present study we classify the first rock as trachydacite porphyry based mainly on the geochemistry and the petrography. The trachydacite porphyry represents an old volcanic to subvolcanic

magmatic phase, which was probably extruded subaerially during the early magmatic activity forming a volcanic dome. The geophysical study carried out by Thanasoulas (1979) revealed that the trachydacite porphyry dips to the west deeper than 240 m. A qtz-monzonite stock was previously described by Filippidis et al. (1988), NW from the study area. At the Vathi porphyry system two qtz-monzonite outcrops from the Ragian 1 and 2 Hills are reported for the first time. Taking into consideration the suggestions by Sillitoe (2010) we can assume that at the Vathi porphyry system the emplacement of the qtz-monzonite took place possibly 0.5 to 3 Ma after the emplacement of the trachydacite porphyry between 18.5 and 21 Ma. The overall short timeline of the magmatic activity in the area could explain the dwarf volumes of magma and the dwarf porphyry style mineralization (Serafimovski et al., 2010; Ducea et al., 2015).

Hydrothermal fluids circulation and source of metals

The close spatial distribution of the ore assemblages and the lack of quartz veins or other magmatic rock dikes truncated by the qtz-monzonites suggest that there was not any significant amount of volatile fluids flow during the porphyry mineralization formation. These characteristics support that volatile fluids possibly circulated as a volatile bubble suspension (Cashman and Mangan, 1994; Proffett, 2003). However, the significant amount of mineralization hosted in the trachydacite porphyry suggests that probably moderate amounts of fluids and volatiles were exsolved from the porphyry magma beneath the trachydacite porphyry. Phase separation is a common process during the mineralization in the porphyry type deposits (Hedenquist et al., 1998; Heinrich, 2005; Sillitoe, 2010). Along with the regional tectonic structures the exsolving hydrous fluids and silicate melts during the crystallization of the qtz-monzonite intrusions at shallow depths favored the hydraulic stress of the host trachydacite porphyry and the formation of a dense system of discontinuities in the rock. This process enhanced the permeability of the host-rock and the major part of the chalcopyrite, pyrite, molybdenite, and bornite mineralization in depth was deposited along fractures and cracks.

Phase separation is essential for Au deposition in porphyry systems, which follows the deposition of Cu in high temperatures (Hedenquist et al., 1998; Ulrich et al., 1999). Despite the lack of geochemical data in depth, the optical microscopy study of the Vathi mineralization revealed the presence of native gold grains co-existing

with equal quantities of pyrite and chalcopyrite. Based on chemical analyses of the surface samples, Au concentration reaches on average 0.73 ppm, and the Au/Cu ratio (~ 0.8:1.0) is in good agreement with the proposed 0.8:1.0 to 1:1 ratios by Kirkham and Sinclair (1995) and Kesler et al. (2002). These ratios represent the worldwide moderate to high-grade porphyry mineralizations (Sinclair, 2007). The highest gold contents in Vathi are found within the most oxidized rock samples, along fault systems and along the phreato-magmatic breccia. This is common at the upper parts of the porphyry systems or beneath the lithocaps (Sillitoe, 2010), where a sharp drop in Au solubility occurs due to intense phase separation in upflow conduits or due to admixture of the ascendant fluids with meteoric water (Heinrich, 2005; Sillitoe, 2010). In addition, Au precipitation along phreato-magmatic breccias is favored by the permeable textures created by the periodic catastrophic release of build-up volatiles, which is also the case study at the Vathi phreato-magmatic breccia.

Molybdenum and base metals Fe, Pb, Zn, and As precipitation and distribution follow the proposed models by Sillitoe (2010) and Richards (2011). Molybdenum precipitates in depth after copper, while Fe, Pb, Zn, and As form minerals at the upper, outer and adjacent areas of the intrusions. Frei (1992), based on Pb isotopes, showed that the basement rocks of Vertiskos Unit contributed in base metals to the ascending magmatic melts enriching them especially in Cu, Pb and Zn. Moreover the same author suggested that this enrichment took place by assimilation of wall rocks by magma and not by the pre-Tertiary ore mineralization. Although crustal scale extensional structures can provide path ways to the ascending mantle derived magmas, limiting crustal interaction usually an assimilation with the crust may occur (Richards et al., 2003; Richards, 2011). Assimilation grants to the ascending magma fractionated trace elements patterns and evolved, namely crustal and isotopic signatures. Thus, the Vathi porphyry system is enriched in large-ion lithophile (LIL) elements and in heavy field strength (HFS) elements. Rb, Cs, Ba and Zr, Nb, Th, U are the most enriched incompatible elements. A significant enrichment is observed also in the REEs La (up to 613.1 ppm), Ce (up to 894 ppm), Pr (up to 79.1 ppm), Nd (up to 211.1 ppm) and Gd (up to 12.7 ppm), as well as in Ti (up to 7040 ppm) and P (up to 1340 ppm). These geochemical and metal enrichment characteristics, when compared to the rock geochemistry, the ore type, and the ongoing geotectonic settings, suggest that Vathi porphyry deposit shares several common characteristics with the proposed model for the other mildly alkaline to alkaline porphyry deposits

(Zhenhua et al., 2003; Richards et al., 2012; Richards and Mumin, 2013). It should be memtnioned that the alkaline porphyry deposits are described as the link between MH-IOCG (magmatic-hydrothermal iron oxide-copper-gold) deposits and Cu-porphyry deposits (Tornos et al., 2010; Teixeira et al., 2015) and their case study needs careful data interpretation (Yigit, 2009).

Uranium exhibits moderately to highly enriched concentrations in Vathi magmatic rocks following the development of the ore mineralization. Uranium ranges in the qtz-monzonite and the trachydacite porphyry between 14 to 106 ppm. However in the phreato-magmatic breccia and along the mineralized tectonic structures, U reaches 328 ppm which is expressed by the presence of the autunite group minerals, torbernite and meta-torbernite (Andronopoulos, 1967; Stavropodis and Kotopouli, 1972; Stergiou et al., 1993). Uranium enrichment is rather an uncommon characteristic for porphyry systems and a dominant constitute of the MH-IOCG deposits (Richards and Mumin, 2013). Uranium tends to be enriched in the alkaline intrusions and several alkaline porphyry deposits have been reported containing elevated uranium values (Kolessar, 1970; Rice et al., 1985; Bi et al., 2002; Sillitoe, 2002). Uranium enrichment in Vathi could be the result of the final stages of crystallization of the mildly alkaline magma combined with the activity of deep sheeted faults. The final-stage cupola rapture exsolved residual and accumulated magmatic fluids enriched in uranium which were set in a fluid circulation network controlled by the tectonic structures. Rice et al. (1985) described a similar mechanism resulting in uranium enrichment for an alkaline porphyry molybdenum system at Central City, Colorado, while Persianis et al. (2010) highlights the importance of tectonic structures in redistribution and uranium mineral formation for the Stratoni granodiorite in Chalkidiki, N. Greece. This channel network enhancing the rock permeability should also be critical to the secondary enrichment of torbernite at the average depth of 73 m through a mechanism similar to this of roll-front uranium deposits (Robb, 2013). The Vathi system hosts the only known U-bearing porphyry mineralization in Greece. In contrary, at the SMMP of Serbia and FYROM several U mineralizations exist which are linked to magmatic complexes and porphyry subvolcanic to volcanic intrusions (Raducinović, 1974; Radosavljević et al., 2013).

Formation of the ore assemblages

Disseminations, veinlets and small stocks of pyrite and minor chalcopyrite at the surface and of chalcopyrite-bornite-molybdenite-magnetite in depth are the typical textures and mineral paragenesis in Vathi and this is in agreement with the model of the porphyry deposits described by Sillitoe (2010). Near 750^{o}C volatile fluids migrating upward from the solidified porphyries through fractures, slowly cooled and gradually stabilized, depositing Cu-sulfides (Sillitoe, 2010). Molybdenite due to different chemical complexing and probably assisted by progressive increase of the Mo/Cu ratio in the residual parental melt was deposited during the late stages of the bulk formation of potassic mineral assemblages (Candela and Holland, 1986; Sillitoe, 2010). Tiny and sporadic euhedral pyrite disseminations were deposited outwards in places of extensive groundwater and magmatic fluids mingling following the development of propylitic alteration zone (Sillitoe, 2010). Below 350°C, a single-phase, low- to moderate salinity liquid resulted in the formation of late stage high-sulfidation pyrite-minor chalcopyrite mineralization being followed by galena and sphalerite. These are common minerals of the late stages of porphyry system and are the result of Zn, Pb, Ag and Mn accumulation in the residual ore forming solution (Ulrich et al., 1999; Wilkinson et al., 2008; Sillitoe, 2010). Thus, these minerals appear mostly irregular filling empty spaces among or within the previously crystallized minerals. In general, the Zn-Pb-Cu-Ag±Au paragenesis is developed as subepithermal veins or in skarn formation depending on the wall rock type at the periphery of the porphyry systems following the development of the propylitic alteration zone, at lower temperatures (Sinclair, 2007; Sillitoe, 2010). Furthermore, as Proffett (2003) reports for Alumbrera Cu-Au deposit, galena and sphalerite presence could be linked to less pervasive feldspar destructive processes while pyrite occurrence is linked to more pervasive environments. In addition, sphalerite, galena, carbonate minerals and euhedral quartz could form late-stage veins exhibiting open-space filling textures (Proffett, 2003). This could also be suggested for Vathi deposit as euhedral quartz was found in small geodes along with completely oxidized Pb-Zn-sulfides.

The Vathi porphyry system is characterized by extended dispersed pyrite and D-type veins in the marginal trachydacite porphyry wall rocks. These characteristics are common during the development of the late-stage overprinting sericitic alteration zone (Sillitoe, 2010). At the surface, the peripheral, low pyrite shell and pyrite shell ore grade zones were observed following the telescoped overgrowth of the alteration

zones, while in depth the transition from the pyrite shell to the ore shell ore grade zone was documented (Lowell and Guilbert, 1970; Sillitoe, 2010).

In depth three more ore parageneses were observed in the drill cores. They include chalcopyrite-pyrite-molybdenite±stibnite disseminations and massive sphalerite-galena±arsenopyrite and pyrite-pyrrhotite-chalcopyrite veins and veinlets. The two first ore parageneses are common at the upper and peripheral parts of a porphyry system (Sinclair, 2007; Sillitoe, 2010). However, the pyrite-pyrrhotite-chalcopyrite mineralization is rather uncommon. Pyrrhotite veins rimmed by euhedral quartz are usually observed in reduced and not in oxidized Cu-Au-porphyry systems (Rowins, 1999; 2000). The reduced environment lowers S and Cu solubility in the magmatic melt (Cao et al., 2014). The S^{2-} becomes the dominant sulfur species in it and potentially isolates sulfides from the magma during migration (Cao et al., 2014). As a consequence massive pyrrhotite can be deposited between 350 and 600^{o}C. In contrary, at oxidized environments the system is enriched in Cl^{-} and depleted in S^{2-} (Rowins, 2000). This increases Cu solubility and during the potassic alteration, chalcopyrite and/or bornite are deposited instead of pyrrhotite (Rowins, 2000). Additionally, pyrrhotite has been reported from the biotite-actinolite alteration zone linked to alkaline porphyry systems and from peripheral to porphyry-Au deposit quartz stockwork veins (Sillitoe, 2002; Sidorov et al., 2006). This could implies, a relatively reduced parental magmatic source for the magmatic fluids which formed the mineralization at Vathi. However, intrusion activity may has continued after the development of the porphyry system and resulted in the formation of an overprinting epithermal mineralization (Corbett and Leach, 1998; Hedenquist et al., 1998; Müller et al., 2002). Thus, the mineral sequence of stibnite, sphalerite, galena, arsenopyrite and pyrrhotite from the shallower to the deeper parts could represent an overprinting epithermal mineralization (Hedenquist and Lowenstern, 1994; Sillitoe, 1999).

Post-depositional oxidizing processes have affected the entire Vathi porphyry system resulting in an in situ oxidation of the mineral assemblages (Chavez, 2000). Acidic fluids circulation resulting from the oxidation of the hypogene dispersed pyrite of the low pyrite and of the pyrite shells dissolved and redistributed downwards the metal ions of the hypogene mineralization according to specific chemical reactions (John et al., 2010). The oxidized zone includes mainly goethite, hematite, cuprite, native copper and meta-torbernite, torberinte, malachite and minor limonite, azurite and turqoise and is locally enriched in Ag, Au, U and REEs. A narrow secondary

enrichment zone is observed including chalcocite and covellite. This narrow enrichment zone indicates the existence of a relatively shallow water table (Hartley and Rice, 2005).

Alteration zones

Ore deposition and alteration zones exhibit a well documented connection. Potassic alteration and sericitic alteration are invariably associated with the main sulfide mineralization, while propylitic alteration bears minor amounts of pyrite mineralization.

The potassic-sericitic alteration is characterized by secondary K-feldspar and biotite. It was formed during the same time period with qtz-monzonite emplacement and is developed within the intrusions. This indicates also the outermost infringement limits of the magmatic fluids. Potassic fluid migration is observed only along the E-W trending fault at Ragian 1 Hill. Euhedral quartz, biotite and massive chalcopyrite and pyrite in rock cavities characterize the ore assemblage of the deep potassic-sericitic alteration.

The propylitic-sericitic alteration is characterized by the presence of epidote and chlorite (Thompson and Thompson, 1998; Sillitoe, 2010). It was probably contemporaneous with the latest stage of the potassic alteration and the Cu-Au mineralization but older than the sericitic alteration. Pyrite and chalcopyrite are found in traces which possibly indicate insignificant amounts of sulfur in the hydrothermal fluids or a heating process or both (Hemley et al., 1992).

The sericitic alteration is expressed by the almost complete replacement of K-feldspars and by the extensive presence of sericite and euhedral quartz in the ground mass. Kaolinite, dolomite and rutile are also minor diagnostic phases (Thompson and Thompson, 1998; John et al., 2010; Sillitoe, 2010). The sericitic alteration overprints both the potassic and the propylitic alteration zones. In contrast to the depleted in sulfur propylitic alteration zone, the areas of sericitic alteration zone exhibiting the strongest feldspar destructive textures bear a relatively high sulfur content (S= ~1.30 wt%). The magmatic fluids activity which resulted in the formation of this alteration zone during the late phases of the porphyry system was mainly channeled by the major E-W trending fault at the eastern part of Ragian 1 Hill. Within this tectonic structure numerous sheeted and stockwork quartz veins are located, while abundant D-type veins are present transecting the wall rocks in perpendicular patterns. Finally,

if the eastward areas of intense sericitic alteration are compared to other areas of Ragian 1 and 2 Hills, and by assuming a unique oxidation rate for the entire area, it could be proposed that these late fluids introduce and remobilize relatively moderate Cu contents.

Based on the above described results of the field and the laboratory studies, a provisional schematic insight on the major components of the magmatic-hydrothermal-structural history of the Vathi deposit is illustrated in the following figure (Fig. 10.1).

Proposals for future exploration

The Kilkis mining district hosts several Tertiary mineralized intrusions and mineralizations set in wide areas of alteration zones such as these of Gerakario, Pontokerasia and Vathi. A dense network of faults and fault intersections is related to these wide areas controlling most times the emplacement of the magmatic rocks and the patterns of the alteration zones. The Vathi magmatic complex is one of the most promising areas for future exploration for porphyry type ore mineralizations as it is exceptionally enriched in Cu, Au, Mo, U, and REEs. Based on the unpublished reports of the Institute of Geology and Mineral Exploration (IGME) the porphyry system at Vathi has never been explored thoroughfully (Melidonis, 1968; Andronopoulos, 1967; Markoulis, 1970). In fact, the old drill core exploration project was targeted on the uraniferous deposit concluding that it is of minor significance (Markoulis, 1970). Although since the early 70s Armstron (1974) and Nininger (1974) have pointed out the future significance of large size low-grade porphyry and porphyry like deposits in uranium production. Therefore further exploration on Vathi mineralization could be suggested using modern methods.

In particular, any future exploration planning should be targeted on further correlations between the intrusions and the extension of drill workings in depth. This could result in a more thoroughly reconstructed model for the area, which could describe in detail any possible exploitation potential. It should be highlighted that the Vathi porphyry deposit shares several features in common in terms of age, alkali- and REE- enrichment with the porphyry Cu-Au deposits of the adjacent Chalkidiki district (e.g Skouries, Fisoka). Consequently, the entire Greek Serbo-Macedonian metallogenic province could be a promising future exploration target for gold and probably PGEs as Eliopoulos et al. (2014) propose.

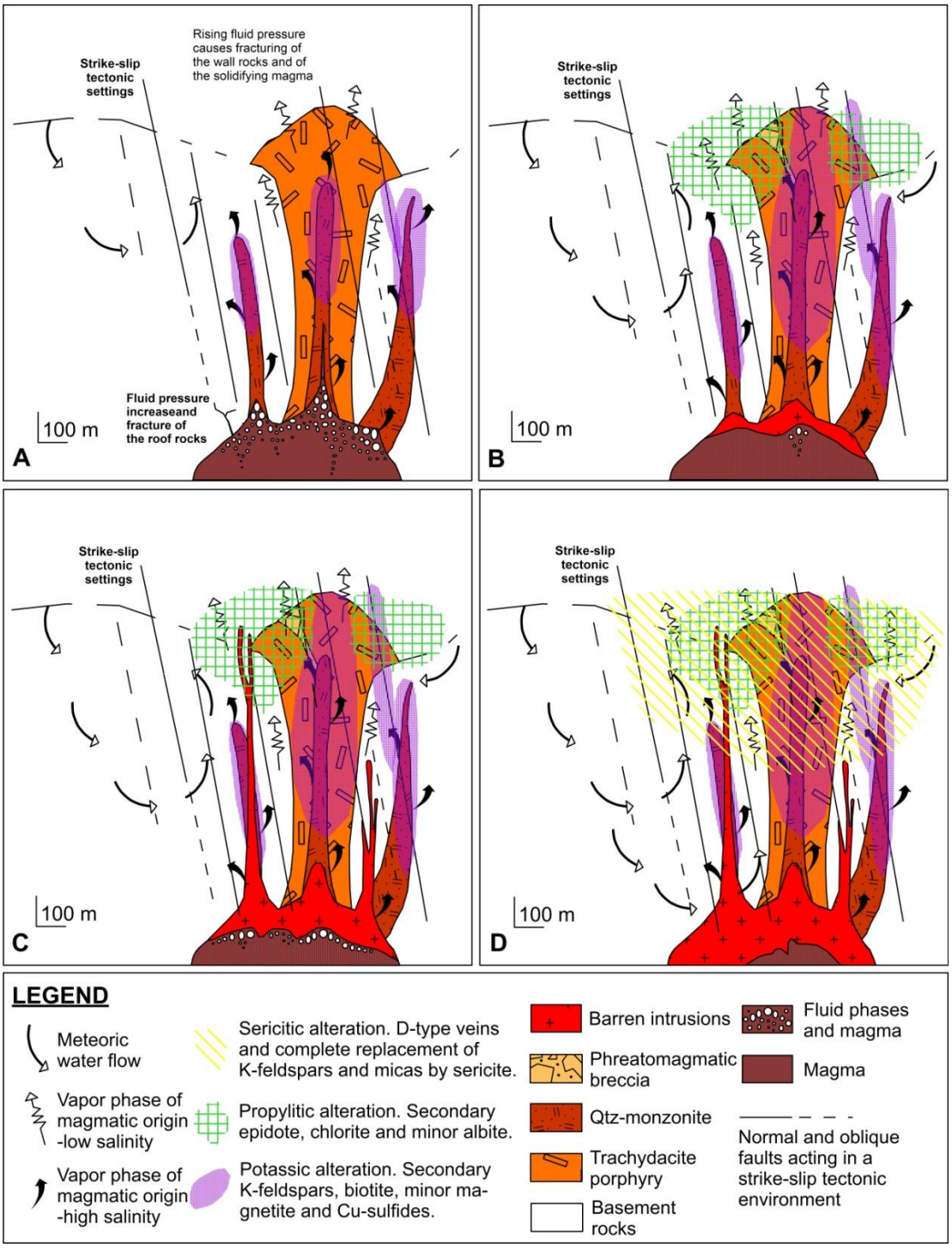

Figure 10.1. Schematic model of the emplacement of the magmatic rocks, the ore mineralization and the alteration zones at Vathi along a N-S cross-section. A. Tectonic instability forwards the fast ascent of the magma (the position of faults is indicative), the finger-like qtz-monzonite dikes are emplaced, potassic alteration mineral assemblage starts being deposited and ground water is heated and circulates. B. The potassic mineral assemblage crystallization continuous, heated ground water and low salinity vapor phase of magmatic origin propylitize mainly the trachydacite porphyry partly overprinting the potassic mineral assemblages. C. Depleted in Cu

magmatic fluids previously accumulated beneath cupola exsolve and form the barren intrusions. Faults advance. D. Sericitic alteration covers the entire area of the Vathi magmatic complex. Intense feldspar destructive phenomena, late disseminated pyrite mineralization and D-veins occur at the trachydacite porphyry. Groundwater circulates in deeper levels along faults, depletes U and transfers it to the surface forming the uraniferous mineralization in the porphyry trachydacite.

CHAPTER 11. CONCLUSIONS

The Vathi porphyry Cu–Au±U±Mo mineralization occurs in the Serbo-Macedonian metallogenic province of the Tertiary Western Tethyan Metallogenic Belt. It is extended around Ragian 1 and Ragian 2 Hills mainly hosted by a trachydacite porphyry and genetically linked to subvolcanic qtz-monzonite dikes (18-17 Ma), which intrude the two-mica gneiss and schists of the crystalline basement of the Vertiskos Unit and the trachydacite porphyry. Both magmatic intrusions are characterized as generally silica-saturated and exhibit alkali-calcic to high-K alkaline chemical affinities.

The emplacement of the magmatic rocks was structurally controlled by three major fault groups, with E-W, NW-SE and NE-SW structural trending, as the result of the Tertiary evolution of the Serbo-Macedonian Massif. The qtz-monzonite appears as fault-controlled, narrow, elongated, dikes and stocks and is affected by potassic alteration which is overprinted by a sericitic alteration. The trachydacite porphyry is affected locally by a propylitic alteration which is overprinted by an extended and locally very strong sericitic alteration characterized by feldspar-destructive processes and silicification. Late stockwork, sheeted veins and oxidized quartz-pyrite D-veins, which trend ENE-WSW, outcrop adjacent to the trachydacite porphyry. The ENE-trending hydrothermally altered phreato-magmatic breccia crosscut the trachydacite porphyry and is related to the qtz-monzonite. The breccia consists of angular fragments of trachydacite and basement metamorphic rocks cemented by clays, white mica and quartz, and disseminations of oxidized mineralization. Hematite, goethite and malachite fill fractures of the breccia and form extended encrustations.

At the Vathi porphyry system the potassic-sericitic alteration is linked to an ore assemblage including chalcopyrite + bornite + molybdenite + magnetite, while the sericitic alteration zone is associated with the ore assemblages of chalcopyrite + pyrite

+ molybdenite ± stibnite, pyrite + pyrrhotite + chalcopyrite, and sphalerite + galena ± arsenopyrite. The ore assemblages pyrite + pyrrhotite + chalcopyrite and sphalerite + galena ± arsenopyrite mainly occur below a depth of 166 and 73 m respectively. Additionally, the first is centered to the porphyry system, while the second is developed at the peripheries of the system. At the surface, the observed mineralization is characterized by relict disseminated pyrite and chalcopyrite and minor sphalerite and galena. These ore minerals are usually linked to the potassic-sericitic alteration zone.

The trachydacite porphyry is affected by extended supergene oxidation processes averaging 90 m deep and expressed by the dominant presence of malachite, azurite, hematite, goethite, cuprite, native copper, native gold and meta-torbernite. A restricted secondary enrichment zone, approximately 2 m thick, occurs beneath the oxidation zone including, chalcocite and covellite. Surface oxidized samples contain in average 2607 ppm Cu, 335 ppm Mo, 182.5 ppm Pb, 89.9 ppm Zn and 118 ppm Ag and up to 7 ppm Au (in average 0.73 ppm), up to 330 ppm U, up to 500 ppm La, and up to 715 ppm Ce.

Throughout the broader area of NE Kilkis a dense network of faults and fault intersections occur accompanied by several ore types that form an extensive zone of exploration area associated with the Kilkis ore district. The Vathi porphyry style mineralization is unusual and exceptionally enriched in U and REEs. It shares several features in common with the Skouries porphyry Cu-Au deposit, in the adjacent Chalkidiki ore district, and is a promising future exploration target for gold.

REFERENCE

Agostini, S., Doglioni, C., Innocenti, F., Manetti, P., and Tonarini, S., 2010, On the geodynamics of the Aegean rift, Tectonophysics, v. 488, p. 7-21.

Anderson, D.L., 2007, New theory of the Earth, Cambridge University Press, Cambridge, 384 p.

Andronopoulos, B., 1968, The uranium mineralization at Vathi, Kilkis, IGSR unpubl. Report, Athens (in Greek), 12 p.

Armstron, F.C., 1974, Uranium resources of the future-"porphyry"uranium deposits, Formation of uranium ore deposits symposium, International Atomic Energy Agency, Athens, Greece.

Berger, B.R., Ayuso, R.A., Wynn, J.C., and Seal, R.R., 2008, Preliminary model of porphyry copper deposits: U.S. Geological Survey, Open-File Report, 2008–1321, p. 55.

Bertrand, G., Guillou-Frottier, L., and Loiselet, C., 2014, Distribution of porphyry copper deposits along the western Tethyan and Andean subduction zones: Insights from a paleotectonic approach, Ore Geology Reviews, v. 60, p. 174-190.

Bi, X., Cornell, D.H., and Hu, R., 2002, REE composition of primary and altered feldspar from the mineralized alteration zone of alkaline intrusive rocks, western Yunnan Province, China, Ore Geology Reviews, v. 19, p. 69-78.

Bonev, N., Dilek, Y., Hanchar, J. M., Bogdanov, K., and Klain, L., 2012, Nd–Sr–Pb isotopic composition and mantle sources of Triassic rift Units in the Serbo-Macedonian and the western Rhodope Massifs (Bulgaria–Greece), Geological Magazine, v. 149, p. 146-152.

Bonin, B., Sekkal, A.-A., Bussy, F., Ferrag, S., 1998, Alkali-calcic and alkaline post-orogenic (PO) granite magmatism: petrologic constraints and geodynamic settings, Lithos, v. 45, p. 45-70.

Bristol, S.K., Spry, P.G., Voudouris, P.Ch., Melfos, V., Mathur, R.D., Fornadel, A.P., and Sakellaris, G.A., 2015, Geochemical and geochronological constraints on the formation of shear-zone hosted Cu–Au–Bi–Te mineralization in the Stanos area, Chalkidiki, northern Greece, Elsevier, Ore Geology Reviews, v. 66, p. 266–282.

Brun, J.P., and Sokoutis, D., 2007, Kinematics of the southern Rhodope Core Complex (North Greece), International Journal of Earth Sciences, v. 99, p. 109–138.

Brun, J.-P. and Faccenna, C., 2008, Exhumation of high-pressure rocks driven by slab rollback, Earth and Planetary Science Letters, v. 272, p. 1–7.

Burg, J.-P., 2002, Tectonic processes, *in* Encyclopedia of Life Support Systems (EOLSS), Developed under the Auspices of the UNESCO, Eolss Publishers Co. Ltd., Oxford, UK, http://www.eolss.net/.

Burg, J.P., 2012, Rhodope: From Mesozoic convergence to Cenozoic extension, Review of petro-structural data in the geochronological frame, Journal of the Virtual Explorer, v. 39, p. 1–44.

Candela, P.A., and Holland, H.D., 1986, A mass transfer model for copper and molybdenum in magmatic hydrotheral systems: The origin of porphyry-type ore deposits, Economic Geology, v. 81, p. 1−19.

Cao, M., Qin, K., Li, G., Jin, L., Evans, N.J., and Yang, X., 2014, Baogutu: an example of reduced porphyry Cu deposit in western Junggar, Ore Geology Reviews, v. 56, p. 159-180.

Carten, R.B., White, W.H., and Stein, H.J., 1993, High-grade, graniterelated molybdenum systems: classification and origin, in Kirkham, R.V., Sinclair, W.D., Thorpe, R.I., and Duke, J.M., eds., Mineral Deposit Modeling: Geological Association of Canada, Special Paper, v. 40, p. 521-554.

Cashman, K.V., and Mangan, M.T., 1994, Physical aspects of magmatic degassing II, Constraints on vesiculation processes from textural studies of eruptive products: Reviews in Mineralogy, v. 30, p. 447–478.

Cathles, L.M., and Shannon, R., 2007, How potassium silicate alteration suggests the formation of porphyry copper deposits begins with the nearly explosive but barren expulsion of large volumes of magmatic water, Earth and Planetary Science Letters, v. 262, p. 92−108.

Chatzipetros, A., Kiratzi, A., Sboras, S., Zouros, N., and Pavlides, S., 2013, Active faulting in the north-eastern Aegean Sea Islands, Tectonophysics, v. 597, p. 106-122.

Chávez, W.X., Jr., 2000, Supergene oxidation of copper deposits—Zoning and distribution of copper oxide minerals, Society of Economic Geologists Newsletter, v. 41, p. 10–21.

Christofides, G., D'amico, C., Del Moro, A., Eleftheriadis, G., and Kyriakopoulos, C., 1990, Rb/Sr geochronology and geochemical characters of the Sithonia plutonic complex (Greece), European Journal of Mineralogy, v. 2, p. 79–87.

Condie, K., C., 1997, Plate tectonics and crustal evolution, Butterworth-Heinemann, Oxford, 282 p.

Corbett, G.J., and Leach, T.M., 1998, Southwest Pacific gold-copper systems: Structure, alteration and mineralization, Special Publication, Society of Economic Geologists, v. 6, 238 p.

Dal Piaz, G., V., Bistacchi, A., and Massironi, M., 2003, Geological outline of the Alps, Episodes, v. 26, p. 175-180.

Davies, J., H. and von Blanckenburg, F., 1995, Slab breakoff: A model of lithosphere detachment and its test in the magmatism and deformation of collisional orogens, Earth and Planetary Science Letters, 129, 85-102.

de Boorder, H., Spakman, W., White, S.,H., and Wortel, M.,J.,R., 1998, Late Cenozoic mineralization, orogenic collapse and slab detachment in the European Alpine Belt, Earth and Planetary Science Letters, v. 164, p. 569-575.

de Launay, L., 1913, Traité de métallogénie: gîtes minéraux et métallifères: gisements, recherche, production et commerce des minéraux utiles et minerais, description des principales mines (3 volumes), Ch. Béranger, Paris, 934 p.

de Wet, AP., Miller, A, Bickle, M.J., and Chapman, H.J., 1989, Geology and geochronology of the Amea, Sithonia and Ouranopolis intrusions, Chalkidiki Peninsula, Northern Greece, Tectonophysics, v. 161, p. 65-79.

de Vos, W., Batista, M. J., Demetriades, A., Duris, M., Lexa, J., Lis, J., Marsina, K., O'Conor, P.J., 2005, Metallogenic mineral provinces and world class ore deposits in Europe, Geochemical Atlas of Europe, v. 1, p. 43-49.

Dilek, Y., Shallo, M., and Furnes, H., 2005, Rift-drift, seafloor spreading, and subduction zone tectonics of Albanian ophiolites, International Geology Review, v. 47, p. 147–176.

Dilek, Y., 2006, Collision tectonics of the Mediterranean region: Causes and consequences, Geological Society of America, Special Paper, 409.

Dilek, Y., Altunkaynak, S., and Oner, Z., 2009, Syn-extensional granitoids in the Menderes core complex and the late Cenozoic extensional tectonics of the Aegean province, Special Publications, Geological Society, London, v. 321, p. 197–223.

Dimitriadis, S., 1973, Callait (turquoise) in a weathered trachyte rock of Vathi Kilkis area, Annales Geologiques des Pays Helleniques, v. 25, p. 328-332 (in Greek).

Dimitriadis, S., and Godelitsas, A., 1991, Evidence for high pressure metamorphism in the Vertiskos Group of the Serbomacedonian Massif: The eclogite of Nea Roda, Chalkidiki, Bulletin of Geological Society of Greece, v. 25, p. 67-80.

Dimou, E., 1989, Native minerals in rocks and mineralizations of Greece and their significance, Bulletin of the Geological Society of Greece, v. XXIII/2, p. 207-223.

Dinter, D.A., and Royden, L., 1993, Late Cenozoic extension in northeastern Greece: Strymon Valley detachment system and Rhodope metamorphic core complex, Geology, v. 21, p. 45-48.

Dixon, J. and Dimitriadis, S., 1984, Metamorphosed ophiolitic rocks from the Serbo – Macedonian Massif, near Lake Volvi, North – East Greee, Journal of Geological Society, Special Publication, v. 17, p. 603-618.

Doglioni, C., Agostini, S., Crespi, M., Innocenti, F., Manetti, P., Riguzzi, F., and Savaşçin, M.Y., 2002, On the extension in western Anatolia and the Aegean sea. Journal of Virtual Explorer, v. 8, p. 169–184.

Ducea, M.N., Paterson, S.R., and DeCelles, P.G., 2015, High-volume magmatic events in subduction systems, Elements, v. 11, p. 99-104.

Duggen, S., Hoernle, K., Van Den Bogaard P., and Garbe-Schonberg, D., 2005, Post-collisional transition from subduction to intraplate-type magmatism in the westernmost mediterranean: evidence for continental-edge delamination of subcontinental lithosphere, Journal of Petrology, v. 46, p. 1155–1201.

Dumurdzanov, N., Serafimovski, T., and Burchfiel, B.C., 2004, Evolution of the Neogene-Pleistocene basins of Macedonia, Geological Society of America, Digital Map and Chart Series, v. 1, p. 1-20.

Duretz, T., Schmalholz, M., and Gerya, T.,V., 2012, Dynamics of slab detachment, Geochemical, Geophysics, Geosystem. v. 13, p. 17.

Economou-Eliopoulos, M., and Eliopoulos, D., 1993, Platinum, palladium and gold content in the porphyry-Cu systems of the Vertiskos formations, Serbo-Macedonian Massif, Bulletin of the Geological Society of Greece, v. XXVIII/2, p. 393-405.

Einaudi M.T., 1997, Mapping altered and mineralized rocks: An introduction to the Anaconda method: Unpublished report, Stanford, California, Department of Geological and Environmental Sciences, Stanford University, 16 p.

Eldorado Gold SA, 2016, http://www.eldoradogold.com/assets/operations-and-projects/europe/default.aspx.

Eliopoulos, D.G., and Economou-Eliopoulos, M., 1991, Platinum-group element and gold contents in the Skouries porphyry copper deposit, Chalkidiki peninsula, northern Greece, Economic Geology, v. 86, p. 740-749.

Eliopoulos, D.G., Economou-Eliopoulos, M., and Zelyaskova-Panayiotova, M., 2014, Critical factors controlling Pd and Pt potential in porphyry Cu–Au deposits: evidence from the Balkan Peninsula, Geosciences, v. 4, p. 31-49.

Filippidis, A., Kougoulis, C., Michailidis, K., 1988, Sr-bearing stilbite in a quartz-monzonite from Vathi, Kilkis, Northern Greece, Schweizerische Mineralogische und Petrographische Mitteilungen, v. 68, p. 67-76.

Frei, R., 1992, Isotope (Pb, Rb-Sr,S,O,C,U-Pb) geochemical investigations on Tertiary intrusives and related mineralizations in the Serbomacedonian Pb-Zn, Sb+Cu-Mo metallogenic province in Northern Greece, Swiss Federal Institute of Technology (ETH) Zurich, Switzerland, Ph.D. Thesis, 231 p.

Frei, R., 1996, The extend of inner mineral isotope equilibrium: a systematic bulk U-Pb and Pb step leaching (PbSL) isotope study of individual minerals from a Tertiary granite of lerissos (northern Greece), European Journal of Mineralogy, v. 8, p. 1175–1189.

Fornadel, A.P, Voudouris, P, Spry P.G, and Melfos, V., 2012, Mineralogical, stable isotope and fluid inclusion studies of spatially related porphyry Cu-Mo and epithermal Au-Te mineralization, Fakos Peninsula, Limnos Island, Greece, Mineralogy and Petrology, v. 105, p. 85-111.

Fytikas, M., Innocenti, F., Manetti, P., Mazzuoli, R., Peccerillo, A., and Villari, L., 1984, Tertiary to Quaternary Evolution of Volcanism in the Aegean region, *in* Dixon, J.E., Robertson, A.H.F., (Eds.), The Geological evolution of the Eastern Mediterranean: Geological Society Special Publication, v. 17, p. 687–699.

Gilg, H.A., 1993, Geochronology (K–Ar), fluid inclusion, and stable isotope (C, O, H) studies of skarn, porphyry copper, and carbonate hosted Pb–Zn (Ag–Au) replacement deposits in the Kassandra mining district (eastern Chalkidiki, Greece), Swiss Federal Institute of Technology (ETH) Zurich, Switzerland, Unpublished Ph.D. thesis, 153 pp.

Gilg, H.A., and Frei, R., 1994, Chronology of magmatism and mineralization in the Kassandra mining area, Greece: The potentials and limitations of dating hydrothermal illites, Geochimica et cosmochimica acta, v. 58, p. 2107-2122.

Green, T.H., and Pearson, N.J., 1985, Experimental determination of REE partition coefficients between amphibole and basaltic to andesitic liquids at high pressure, Geochimica et Cosmochimica Acta, v. 49, p. 1465–1468.

Gupta, A.K., and Fyfe, W.S., 2003, The young potassic rock, Ane Books, New Delhi, 370 pp.

Gustafson, L.B., and Hunt, J.P., 1975, The porphyry copper deposit at El Salvador, Chile, Economic Geology, v. 70, p. 857- 912.

Gustafson, L.B., 1978, Some major factors of porphyry copper genesis, Economic Geology, v. 73, p. 600−607.

Hahn, A., Rankin, A., Treloar, P., Naden, J., Forward, P., and Kilias, S.P., 2010, Hydrothermal Pb-Zn-Au-Ag and Cu-Au mineralisation in the Kassandra mine district, N. Greece: a metallogenetic model with regional economic implications?, Abstract Volume of the XIX Carpatho-Balkanian Geological Association Congress, v. 39 , p. 151-152.

Hahn, A., Naden, J., Treloar, P.J., Kilias, S.P., Rankin, A.H., and Forward, P., 2012, A new time frame for the mineralization in the Kassandra mine district, N Greece: deposit formation during metamorphic core complex exhumation, Journal of Earth Sciences, v. 96, p. 1079-1099.

Harangi, S., Downes, H., and Seghedi, I., 2006, Tertiary–Quaternary subduction processes and related magmatism in the Alpine–Mediterranean region. Geological Society, London, Memoirs, v. 32, p. 167–190.

Harris, N.B.W., Pearce, J.A., Tindle, A.G., 1986, Geochemical characteristics of collision-zone magmatism, Geological Society, London, Special Publications, v. 19, p. 67-81.

Hartley, A.J., and Rice, C.M., 2005, Controls on supergene enrichment of porphyry copper deposits in the Central Andes—A review and discussion, Mineralium Deposita, v. 40, p. 515–525.

Hastie, A.R., Kerr, A.C., Pearce, J.A., Mitchell, S.F., 2007, Classification of altered volcanic island arc rocks using immobile trace elements: development of the Th-Co discrimination diagram, Journal of Petrology, v. 48, p. 2341-2357.

Hedenquist, J.W., and Lowenstern, J.B., 1994, The role of magmas in the formation of hydrothermal ore deposits, Nature, v. 370, p. 519-527.

Hedenquist, J.W., Arribas Jr.,A., and Reynolds, J.R., 1998, Evolution of an intrusion-centered hydrothermal system: Far Southeast–Lepanto porphyry and epithermal Cu–Au deposits, Philippines, Economic Geology, v. 93, p. 373–404.

Heinrich, C.A., 2005, The physical and chemical evolution of low-salinity magmatic fluids at the porphyry to epithermal transition: a thermodynamic study, Mineralium Deposita, v. 39, p. 864–889.

Hemley, J.J., Cygan, G.L., Fein, J.B., Robinson, G.R., and D'Angelo, W.M., 1992, Hydrothermal ore-forming processes in the light of studies in rock buffered systems: I. Iron-copper-zinc-lead sulfide solubility relations, Economic Geology, v. 87, p. 1–22.

Henley, R.W., and Berger, B.R., 2012, Pyrite–sulfosalt reactions and semimetal fractionation in the Chinkuashih, Taiwan, copper–gold deposit: a 1 Ma paleo-fumarole." Geofluids, v. 12.3, p. 245-260.

Herodotus, The Histories, A.D. Godley, v. 5.17, s. 2.

Hestie, A.R., Kerr, A.C., Pearce, J.A., and Mitchell, S.F., 2007, Classification of Altered Volcanic Island Arc Rocks using Immobile Trace Elements: Development of the Th-Co Discrimination Diagram, Journal of Petrology, v. 48, p. 2341-2357.

Heuret, A., and Lallemand, S., 2005, Plate motions, slab dynamics and back-arc deformation, Physics of the Earth and Planetary Interiors, v. 149, p. 31–51.

Himmerkus, F., Reischmann, T., and Kostopoulos, D., 2006, Late Proterozoic and Silurian basement Units within the Serbo-Macedonian Massif, northern Greece: the significance of terrane accretion in the Hellenides, Special Publications, Geological Society, London, v. 260, p. 35–50.

Himmerkus, F., Anders, B., Reischmann, T., and Kostopoulos, D., 2007, Gondwana-derived terranes in the northern Hellenides, Geological Society of America Memoirs, v. 200, p. 379-390.

Himmerkus, F., Reischmann, T., and Kostopoulos, D., 2009a, Serbo-Macedonian revisited: a Silurian basement terrane from northern Gondwana in the Internal Hellenides, Greece, Tectonophysics, v. 473, p. 20-35.

Himmerkus, F., Reischmann, T., and Kostopoulos, D., 2009b, Triassic rift-related meta-granites in the Internal Hellenides, Greece, Geological Magazine, v. 146, p. 252-265.

Hou, Z., Ma, H., Khin, Z., Zhang, Y., Wang, M., Wang, Z., and Pan, G., 2003, The Himalayan Yulong porphyry copper belt; product of largescale strike-slip faulting in eastern Tibet, Economic Geology, v. 98, p. 125-145.

Ioannidis, K., and Kelepertzis, A., 1974, Herson, Geological map 1:50.000, IGME, Athens.

Jankovic, S., 1977, The copper deposits and geotectonic setting of the Tethyan Eurasian Metallogenic Belt, Mineralium Deposita, v. 12, p. 37–47.

Jankovic, S., 1986, Tetheyan Eurasian metallogenic belt: relations of mineral associations and their tectonic setting, Geotectonica et Metallogenia, v. 10, p. 99–124.

John, D.A., Ayuso, R.A., Barton, M.D., Blakely, R.J., Bodnar, R.J., Dilles, J.H., Gray, Floyd, Graybeal, F.T., Mars, J.C., McPhee, D.K., Seal, R.R., Taylor, R.D., and Vikre, P.G., 2010, Porphyry copper deposit model, chap. B of Mineral deposit models for resource assessment: U.S. Geological Survey, Scientific Investigations Report, 2010–5070–B, 169 p.

Jolivet, L., and Faccenna, C., 2000, Mediterranean extension and the Africa-Eurasia collision. Tectonics, v. 19, p. 1095–1106.

Jolivet, L., 2001, A comparison of geodetic and finite strain pattern in the Aegean, geodynamic implications, Earth Planetary Science Letters, v. 187, p. 95–104.

Jolivet, L., Faccenna, C., Huet, B., Labrousse, L., Pourhiet, L., Lacombe, O., Lecomte, E., Burov, E., Denèle, Y., Brun, J.-J., Philippon, M., Paul, A., Salaün, G., Karabulut, H., Piromallo, C., Monié, P., Gueydan, F., Okay, A., Oberhänsli, R., Pourteau, A., Augier, R., Gadenne, L., and Driussi, O., 2013, Aegean tectonics: Strain localisation, slab tearing and trench retreat, Tectonophysics, v. 597-598, p. 1-33.

Joplin, G., A., 1968, The shoshonite association – a review, Journal of Geological Society of Australia, v. 15, p. 275-294.

Kalogeropoulos, S.I., Kilias, S.P., Bitzios, D.C., Nicolaou, M., and Both, R.A., 1989, Genesis of the Olympias carbonate-hosted Pb-Zn (Au, Ag) sulfide ore deposit, eastern Chalkidiki Peninsula, northern Greece, Economic Geology, v. 84, p. 1210-1234.

Kalogeropoulos, S.I., Frei, R., Nikolaou, M., and Gerouki, F., 1990, Origin and metallogenetic significance of the Tertiary Stratoni "Granodiorite", Chalkidiki, N. Greece: isotopic and chemical evidence, Bulletin of the Geological Society of Greece, v. 26, p. 23-38.

Kerrich, R., Goldfarb, R.J., and Richards, J.P., 2005, Metallogenic provinces in an evolving geodynamic framework, Economic geology, v. 100, p. 1097-1136.

Kesler, S.E., Chryssoulis, S.L., and Simon, G., 2002, Gold in porphyry copper deposits: its abundance and fate, Ore Geology Reviews, v. 21, p. 103.

Kilias, A., Falalakis, G., and Mountrakis, D., 1997, Alpine tectonometamorphic history of the Serbomacedonian metamorphic rocks: Implication for the Tertiary unroofing of the Serbomacedonian-Rhodope metamorphic complexes (Macedonia, Greece), Mineral Wealth, Athens, v. 105, p. 32-50.

Kilias, A., Falalakis, G., Mountrakis, D., 1999, Cretaceous–Tertiary structures and kinematics of the Serbomacedonian metamorphic rocks and their relation to the exhumation of the Hellenic hinterland (Macedonia, Greece), International Journal of Earth Sciences, v. 88, p. 513–531.

Kilias, A., Falalakis, G., Sfeikos, A., Papadimitriou, E., Vamvaka, A., and Gkarlaouni, C., 2013, The Thrace basin in the Rhodope province of NE Greece - A tertiary supradetachment basin and its geodynamic implications, Tectonophysics, v. 595–596, p. 90–105.

Kilias, A.D., Vamvaka, A., Falalakis, G., Sfeikos, A., Papadimitriou, E., Gkarlaouni, C.H., and Karakostas, B., 2015, The Mesohellenic Trough and the Paleogene Thrace Basin on the Rhodope Massif, their Structural Evolution and Geotectonic Significance in the Hellenides, Journal of Geology and Geosciences, v.4, p. 198.

Kockel, F., and Walther, H.W., 1967, Der Rhyolith von Strimonikon, sein tektonischer Rahmen und die junge Lagerstättenbildung in seiner Umgebung (Zentral Mazedonien, Griechenland), Bulletin of the Geological Society of Greece, v. **7**, p. 1–16.

Kockel, F., and Mollat, H., 1972, Zangliverion, Geological map 1:50.000, IGME, Athens.

Kockel, F., Mollat, H., and Antoniadis, P., 1974, Peninsula of Sithonia, Geological map 1:50.000, IGME, Athens.

Kockel, F., Mollat, H., and Gundlach, H., 1975, Hydrothermally altered and (copper) mineralized porphyritic intrusions in the Serbo-Macedonian Massif (Greece), Mineralium Deposita, v. 10, p. 195-204.

Kockel, F., Mollat, H., and Antoniadis, P., 1978a, Arnaea, Geological map 1:50.000, IGME, Athens.

Kockel, F., Mollat, H., and Antoniadis, P., 1978b, Ierissos, Geological map 1:50.000, IGME, Athens.

Kockel, F., Mollat, H., and Walther, H.W., Antoniadis, P., and Ioannidis, K., 1978c, Stavros, Geological map 1:50.000, IGME, Athens.

Kockel, F., Mollat, H., and Walther, H.W., Antoniadis, P., and Ioannidis, K., 1978d, Stratoniki, Geological map 1:50.000, IGME, Athens.

Kockel, F., and Ioannidis K., 1979a, Kilkis, Geological map 1:50.000, IGME, Athens.

Kochel, F., Mollat, H., Antoniadis, P., and Ioannidis, K., 1979b, Lachanas, Geological map 1:50.000, IGME, Athens.

Kockel, F., Mollat, H., Antoniadis, P., and Ioannidis, K., 1979c, Sochos, Geological map 1:50.000, IGME, Athens.

Kolessar, J., 1970, Geology and copper deposits of the Tyrone district, Guidebook of the Tyrone-Big Hatchet Mountains-Florida Mountains Region, New Mexico Geological Society Guidebook, v. 21, p. 127-132.

Kondopoulou, D., and Westphal, M. (1986), Paleomagnetism of the Tertiary intrusives from Chalkidiki (northern Greece), Journal of Geophysics-Zeitschrift fur Geophysik, v. 59, p. 62-66.

Kourou, A., 1991, Lithology, tectonics, geochemistry and metamorphism of a sector of the west part of the Vertiskos Group, The area NE of the lake Agios Vasilios (Koronia), Ph.D. dissertation, AUTh, Thessaloniki, p. 481, (in Greek).

Koukouvelas, I.K., and Aydin, A., 2002, Fault structure and related basins of the North Aegean Sea and its surroundings, Tectonics, v. 21, p. 10-1.

Kounov, A., Seward, D., Burg, J. P., Bernoulli, D., Ivanov, Z., and Handler, R., 2010, Geochronological and structural constraints on the Cretaceous thermotectonic evolution of the Kraishte zone, western Bulgaria, Tectonics, v. 29.

Krohe, A., and Mposkos, E., 2002, Multiple generations of extensional detachments in the Rhodope Mountains (northern Greece): evidence of episodic exhumation of high-pressure rocks, Special Publication, Geological Society of London, v. 204, p. 151-178.

Kroll, T., Müller, D., Seifert, T., Herzig, P.M., and Schneider, A., 2002, Petrology and geochemistry of the shoshonite-hosted Skouries porphyry Cu-Au deposit, Chalkidiki, Greece, Mineralium Deposita, v. 37, p. 137-144.

Kydonakis, K., Gallagher, K., Brun, J.-P., Jolivet, M., Gueydan, F., and Kostopoulos, D., 2014, Upper Cretaceous exhumation of the western Rhodope Metamorphic Province (Chalkidiki Peninsula, northern Greece), Tectonics, v. 33.

Kydonakis, K., Brun, J. P., Sokoutis, D., and Gueydan, F., 2015, Kinematics of Cretaceous subduction and exhumation in the western Rhodope (Chalkidiki block), Tectonophysics, v. 665, p. 218-235.

Le Bas, M,.J., Le Maitre, R.,W., Streckeisen, A., and Zanettin, B., 1986, A chemical classification of volcanic rocks based on the total alkali-silica diagram, Journal of Petrology, v. 27, p. 745-750.

Le Maitre, R.,W., 1989, A Classification of igneous rocks and glossary of terms, Blackwell, Oxford, 193 pp.

Lindgren, W., 1933, Mineral deposits (4th ed.; 3d impression revised), New York, McGraw-Hill, 930 p.

Lips, A.L., 2002, Correlating magmatic–hydrothermal ore deposit formation over time with geodynamic processes in SE Europe, Geological Society of London, Special Publication, v. 204, p. 69–79.

Logan, J.M., and Mihalynuk, M.G., 2014, Tectonic controls on Early Mesozoic paired alkaline porphyry deposit belts (Cu-Au ± Ag-Pt-Pd-Mo) within the Canadian Cordillera, Economic Geology, v. 109, p. 827-858.

Loucks, R.R., 2015, Distinctive composition of copper-ore forming arc magmas, Australian Journal of Earth Sciences, v. 61, p. 5-16.

Lowell, J.D., and Guilbert, J.M., 1970, Lateral and vertical alteration-mineralization zoning in porphyry ore deposits, Economic Geology, v. 65, p. 373–408.

MacDonald, G.D., and Arnold, L.C., 1994, Geological and geochemical zoning of the Grasberg Igneous Complex, Irian Jaya, Indonesia, Journal of Geochemical Exploration, v. 50, p. 143-178.

Mao, J., Pirajno, F., Lehmann, B., Luo, M., and Berzina, A., 2014, Distribution of porphyry deposits in the Eurasian continent and their corresponding tectonic settings, Journal of Asian Earth Sciences, v. 79, p. 576-584.

Makris, J., 1985, Geophysics and geodynamic implications for the evolution of the Hellenides, Geological evolution of the Mediterranean Basin, Springer Verlag, New York, p. 231-248.

Marchev, P., Kaiser-Rohrmeier, M., Heinrich, C., Ovtcharova, M., von Quadt, A., and Raicheva, R., 2005, Hydrothermal ore deposits related to post-orogenic extensional magmatism and core complex formation: The Rhodope Massif of Bulgaria and Greece, Ore Geology Reviews, v. 27, p. 53-89.

Markoulis, M., 1970, The carried out exploration program at Vathi on behalf of the Greek Atomic Energy Commission (EEAE) targeting the uraniferous mineral assemblages of the region, IGSR unpublished report, Athens, 35 p, (in Greek).

McInnes, I.A., Evans, N.J., Fu, F.Q., Garwin, S., Belousova, E., Griffin, W.L., Bertens, A., Sukarna, D., Permanadewi, S., Andrew, R.L., and Deckart, K., 2005, Thermal history analysis of selected Chilean, Indonesian and Iranian porphyry Cu-Au-Mo deposits, *in* Porter, T.M., ed., Super porphyry copper and gold deposits: A global perspective, Adelaide, PGC Publishing, v. 1, p. 27−42.

Melidonis, N., 1968, Geological mapping of Vathi, Kilkis, IGSR unpublished report, Athens, 20 p, (in Greek).

Melidonis, N.G., 1972, Geological structure and mineralization of the Pontokerasia area (Central Macedonia, Greece), Annales Geologiques Des Pays Helleniques, v. 24, p. 323-393, (in Greek with English abstract).

Melfos V., Vavelidis M., Arikas K., 2001, A new occurrence of argentopentlandite and gold from the Au-Ag-rich copper mineralisation in the Paliomylos area, Serbomacedonian Massif, Central Macedonia, Greece, Bulletin of the Geological Society of Greece, v. XXXIV/3, p. 1065-1072.

Melfos, V., Vavelidis, M., Christofides, G., Seidel, E., 2002, Origin and evolution of the Tertiary Maronia porphyry copper-molybdenum deposit, Thrace, Greece, Mineralium Deposita, 37, 648-668.

Melfos, V. and Voudouris, P.,Ch., 2012, Geological, Mineralogical and Geochemical Aspects for Critical and Rare Metals in Greece, Minerals, v. 2, p. 300-317.

Mouslopoulou, V., Saltogianni, V., Gianniou, M., and Stiros, S., 2014, Geodetic evidence for tectonic activity on the Strymon Fault System, northeast Greece, Tectonophysics, v. 633, p. 246-255.

Mposkos, E., 1983, A mineralogical study of the Au–Ag–Bi–Te–Cu–Co–Ni–As–S ore mineralization in Macedonia, Chemie der Erde, v. 42, p. 281–296.

Müller, D., Kaminski, K., Uhlig, S., Graupner, T., Herzig, P.M., and Hunt, S., 2002, The transition from porphyry-to epithermal-style gold mineralization at Ladolam, Lihir Island, Papua New Guinea: a reconnaissance study, Mineralium Deposita, v. 37, p. 61-74.

Neubauer, F., 2002, Evolution of late Neoproterozoic to early Paleozoic elements in central and southeast Alpine mountain belts: review and synthesis, Tectonophysics, v. 352, p. 87–103.

Neubauer, F., Heinrich, C.A., and Geode ABCD working group, 2003, Late Cretaceous and Tertiary geodynamics and ore deposit evolution of the Alpine–Balkan–Carpathian–Dinaride orogen, Mineral exploration and sustainable development, Millpress, Rotterdam, p.1133-1136.

Nininger, R.D., 1974, The world uranium supply challenge-an appraisal, Formation of uranium ore deposits symposium, International Atomic Energy Agency, Athens, Greece.

Pamic, J., Balen, D., and Herak, M., 2002, The Zagorje-Mid-Transdanubian Zone: origin and geodynamic evolution of Late Paleogene magmatic associations along the Periadriatic- Sava-Vardar magmatic belt, Geodinamica Acta, v. 15, p. 209-231.

Panagos, A., Pe, G.G., and Varnavas, S.P., 1978, The volcanic rocks of Strymonikon – Metamorphosis, Central Macedonia, Greece, Chemie der Erde, v. 37, p. 50-61.

Pan-European Code for Reporting of Exploration Results, Mineral Resources and Reserves [Online], http://46.32.234.2/perc/documents/PERC_REPORTING_CODE_jan2009.pdfwww.perc.co (accessed Mar. 27, 2012).

Papazachos, B.C., Karakostas, V.G., Papazachos, C.B., Scordilis, E.M., 2000, The geometry of the Wadati-Benioff zone and lithospheric kinematics in the Hellenic arc, Tectonophysics, v. 319, p. 275–300.

Paraskevopoulos, G.M., 1958, On the genesis of the W-Sb-ore deposits of the Lachanas region, Central Macedonia, Annales Geologique Des Pays Hellenique, v. 9, p. 227-241.

Pavlides, S.B., and Mountrakis, D.M., 1987, Extensional tectonics of northwestern Macedonia, Greece, since the late Miocene, Journal of Structural Geology, v. 9, p. 385-392.

Pavlides, S. B., Kondopoulou, D. P., Kilias, A. T., and Westphal, M., 1988, Complex rotational deformations in the Serbo-Macedonian massif (north Greece): structural and paleomagnetic evidence, Tectonophysics, v. 145(3), p. 329-335.

Pavlides, S., Mountrakis, D., Kilias, A., and Tranos, M., 1990, The role of strike-slip movements in the extensional area of Northern Aegean (Greece), A case of transtensional tectonics, Annales Tectonicae, Special Issue, v.4, p. 196–211.

Pe-Piper, G., and Piper, D.J., 2002, The igneous rocks of Greece, Gebrüder Borntraeger, Berlin, 573 p.

Pe-Piper, G., and Piper, D. J., 2006, Unique features of the Cenozoic igneous rocks of Greece, Geological Society of America Special Papers, v. 409, p. 259-282.

Peccerillo, A., and Taylor, S.R., 1976, Geochemistry of Eocene calc-alkaline volcanic rocks of the Kastamonu area, northern Turkey, Contributions to Mineralogy and Petrology, v. 58, p. 63-81.

Persianis, D., Katsikis, I., and Karageorgiou, D., 2010, The genetic hypothesis of the uraniferus mineralization, eastern Chalkidiki (Northern Greece), Bulletin of the Geological Society of Greece, v. 43, p. 2692-2701.

Perugini, D., Poli, G., Christofides, G., Eleftheriadis, G., Koroneos, A., Soldatos, T., 2004, Mantle-derived and crustal melts dichotomy in northern Greece: spatiotemporal and geodynamic implications, Geological Journal, v. 39, p. 63-80.

Petrascheck, W.E., 1965, Typical features of metallogenetic provinces, Economic Geology, v. 60, p. 1620-34.

Proffett, J.M., 2003, Geology of the Bajo de la Alumbrera porphyry copper-gold deposit, Argentina, Economic Geology, v. 98, p. 1535-1574.

Pirajno, F., 2009, Hydrothermal processes and mineral systems, Springer, Netherlands, p. 1250.

Radosavljević, S.A., Stojanović, J.N., Radosavljević-Mihajlović, A.S., and Kašić, V.D., 2013, Polymetallic mineralization of the Boranja orefield, Podrinje Metallogenic District, Serbia: zonality, mineral associations and genetic features, Periodico di Mineralogia, v. 82. p. 61-87.

Raducinović, D., 1974, Zletovska Reka uranium deposit, *in* proceedings of: Formation of uranium ore deposits, International Atomic Energy Agency, 6-10 May, Athens.

Rice, C.M., Harmon, R.S., and Shepherd, T.J., 1985, Central City, Colorado; the upper part of an alkaline porphyry molybdenum system, Economic Geology, v. 80, p. 1769-1796.

Richards, J.P., 2003, Tectono-magmatic precursors for porphyry Cu–(Mo–Au) deposit formation, Economic Geology, v. 98, p. 1515–1533.

Richards, J.P., 2005, Cumulative factors in the generation of giant calc-alkaline porphyry Cu deposits, *in* Porter, T.M., ed., Super porphyry copper and gold deposits: A global perspective, Linden Park, South Australia, Porter Geoscience Consulting Publishing, v. 1, p. 7–25.

Richards, J.P., 2009, Postsubduction porphyry Cu-Au and epithermal Au deposits: Products of remelting of subduction-modified lithosphere, Geology, v. 37, p. 247-250.

Richards, J.P., 2011, Magmatic to hydrothermal metal fluxes in convergent and collided margins, Ore Geology Reviews, v. 40, p. 1-26.

Richards, J.P., Spell, T., Rameh, E., Razique, A., and Fletcher, T., 2012, High Sr/Y magmas reflect arc maturity, high magmatic water content, and porphyry Cu±Mo±Au potential: examples from the Tethyan arcs of Central and Eastern Iran and Western Pakistan, Economic Geology, v. 107, p. 295-332.

Richards, J.P., 2013, Giant ore deposits formed by optimal alignments and combinations of geological processes, Nature Geoscience, v. 6, p. 911–916.

Richards, J.P., and Mumin, A.H., 2013, Magmatic-hydrothermal processes within an evolving Earth: Iron oxide-copper-gold and porphyry Cu±Mo±Au deposits, Geology, v. 41, p. 767-770.

Ridley, J., 2013, Ore deposit geology, Cambridge University Press, 409 p.

Rimsaite, J., 1973, Natural alteration of mica of mica and reactions between released ions in mineral deposits, Clays and Clay minerals, v. 23, p. 247-255.

Robb, L., 2013, Introduction to ore-forming processes, John Wiley & Sons, 384 p.

Kaiser-Rohrmeier, M., von Quadt, A., Driesner, T., Heinrich, C. A., Handler, R., Ovtcharova, M., Ivanov, Z.,Petrov, P., Sarov, St., and Peytcheva, I., 2013, Post-orogenic extension and hydrothermal ore formation: High-precision geochronology of the central rhodopian metamorphic core complex (Bulgaria-Greece), Economic Geology, v. 108, p. 691-718.

Rowins, S.M., 1999, Reduced porphyry copper-gold deposits: A newly recognized style of gold mineralization, Geological Society of America, Abstracts with Programs, v. 31, p. A-92.

Rowins, S.M., Reduced porphyry copper-gold deposits: A new variation on an old theme, Geology, v. 28, p. 491-494.

Sagui, C.L., 1928, The ancient mining works of Cassandra, Greece, Economic Geology, v. 23, p. 671-680.

Schenker, F.L., Gerya, T., and Burg, J.-P., 2012, Bimodal behavior of extended continental lithosphere: modeling insight and application to thermal history of migmatitic core complexes, Tectonophysics, v. 579, p. 88–103.

Schildgen, T.F., Yıldırım, C., Cosentino, D., and Strecker, M.R., 2014, Linking slab break-off, Hellenic trench retreat, and uplift of the Central and Eastern Anatolian plateaus, Earth-Science Reviews, v. 128, p. 147–168.

Seedorff, E., Barton, M.D., Stavast, W.J.A., and Maher, D.J., 2008, Root zones of porphyry systems: Extending the porphyry model to depth, Economic Geology, v. 103, p. 939−956.

Serafimovski, T., Stefanova, V., and Volkov, A.V., 2010, Dwarf copper-gold porphyry deposits of the Buchim-Damjan-Borov Dol ore district, Republic of Macedonia (FYROM), Geology of Ore Deposits, v. 52, p. 179-195.

Sidiropoulos, N., 1991, Lithology, geochemistry, tectonics and metamorphism of the Northewestern part of the Vertiskos Group, The area of the Disoro (Krousia) Mountain, North of Kilkis, AUTh, Thessaloniki, Ph.D. dissertation, p. 592, (in Greek).

Sidorov, A.A., Tomson, I.N., Savva, N.E., Volkov, A.V., Prokofev, V.Y., and Kolova, E.E., 2006, Relation between porphyry deposits and their vein satellites, Doklady earth sciences, v. 409, p. 859-863.

Sievers, H., and Buijs, B., 2011, Defining critical raw materials, European Commission, European Union Policy on Natuaral Resources.

Sillitoe, R.H., and Bonham, H.F., Jr., 1984, Volcanic landforms and ore deposits: Economic Geology, v. 79, p. 1286-1298.

Sillitoe, R.H., 1993, Gold-rich porphyry copper deposits: geological model and exploration implications, *in* Kirkham, R.V., Sinclair, W.D., Thorpe, R.I., and Duke, J.M., eds., Mineral Deposit Modeling: Geological Association of Canada, Special Paper, v. 40, p. 465-478.

Sillitoe, R.H., 1999, Styles of high-sulphidation gold, silver and copper mineralisation in porphyry and epithermal environments, Pacrim'99 Congress, Bali, Indonesia, Parkville, Australasian Institute of Mining and Metallurgy, p. 29-44.

Sillitoe, R.H., 2002, Some metallogenic features of gold and copper deposits related to alkaline rocks and consequences for exploration, Mineralium Deposita, v. 37, p. 4-13.

Sillitoe, R., H., 2010, Porphyry Copper Systems, Economic Geology, v. 105, p. 3–41.

Sinclair, W.D., 2007, Porphyry deposits, *in* Goodfellow, W.D., ed., Mineral Deposits of Canada: A Synthesis of Major Deposit-Types, District Metallogeny, the

Evolution of Geological Provinces, and Exploration Methods: Geological Association of Canada, Mineral Deposits Division, Special Publication, v. 5, p. 223-243.

Singer, A.D., Berger, I.V., Moring, C.B., 2005, Porphyry copper deposits of the world: database, map, and grade and tonnage models, *in* US Geological Survey, Open-File Report, 2005–1060.

Siron, C. R., Thompson, J. F., Rhys, D., Baker, T., Russell, S., Tsitsanis, P., and Randall, S., 2014, Structural framework of the Stratoni fault corridor, Kassandra mining district, Northern Greece, *in* 2014 GSA Annual Meeting in Vancouver, British Columbia.

Siron C. R., Thompson, J. F., Baker, T., Friedman, R., Tsitsanis, P., Russell, S., Randall, S., Mortensen, J. K., 2016, Magmatic and metallogenic framework of Au-Cu porphyry and polymetallic carbonate-hosted replacement deposits of the Kassandra mining district, Northern Greece, SEG Special Publication, Tethyan Tectonics and Metallogeny, SEG 2016 Conference, Çeşme, Turkey.

Sklavounos, S., Ericsson, T., Filippidis, A., Michailidis, K., and Kougoulis, C., 1992, Chemical, X-ray and Mössbauer investigation of a turquoise from the Vathi area volcanic rocks, Macedonia, Greece, Neues Jahrbuch für Mineralogie Monatshefte, v. 10, p. 469–480.

Soldatos T., Koroneos A., Christofides G., Del-Moro A., 2001, Rb-Sr geochronology and origin of the Elatia Plutonite (Hellenic Rhodope Massif, N. Greece) constrained by new Sr isotopic data, Neues Jahrbuch für Mineralogie (Abh.), v. 176, p. 179-209.

Stavropodis. J.D., and Kotopouli, K., 1972, Autunite – a new uranium mineral for Greece, Annales Geologiques Des Pays Helleniques, v. 24, p. 424-432, (in Greek with English abstract).

Stergiou, A., 1995, "CRYST" Program for crystallinity determination, by XRD profile fitting, Thessaloniki, Department of Physics, Aristotle University of Thessaloniki.

Stergiou, A.C., Rentzeperis, P.J., and Sklavounos, S., 1993, Refinement of the crystal structure of metatorbernite, Zeitschrift für Kristallographie, v. 205, p. 1-7.

Stern, R., J., 2002, Subduction zones, Reviews of Geophysicists, v. 40, p. 1012.

Sutphin, D.M., Hammarstrom, J.M., Drew, L.J., Large, D.E., Berger, B.B., Dicken, C.L., and DeMarr, M.W., with contributions from Billa, M., Briskey, J.A.,

Cassard, D., Lips, A., Pertold, Z., and Roşu, E., 2013, Porphyry copper assessment of Europe, exclusive of the Fennoscandian Shield, U.S. Geological Survey, Scientific Investigations Report, 2010–5090–K, 197 p., and GIS data.

Tămaș, Călin G., and Jean P. Milési, 2012, Hydrovolcanic Breccia Pipe Structures-General Features and Genetic Criteria. I. Phreatomagmatic Breccias, Studia UBB Geologia, v. 47, p. 127-147.

Tarkian, M., and Stribrny, B., 1999, Platinum-group elements in porphyry copper deposits: A reconnaissance study, Mineralogy and Petrology, v. 65, p. 161–183.

Taylor, S.R., and McLennan, S.M., 1985, The continental crust; Its composition and evolution; an examination of the geological record preserved in sedimentary rocks, Blackwell, Oxford, 312 p.

Teixeira, N.A., Ganade, C.E., Matos, F., Campos, L.D., and Carvalho, M.T., Naves de, 2015, Alkaline Porphyry Copper Deposits and IOCG – What is the link?, Institutional Repository of Geosciences, 4 p.

Thanasoulas, K., 1979, Geophysical study at the volcanic rocks area of Vathi, Kilkis, National Institut of Geology and Mineral Exploration, Athens, 17 p., (in Greek).

Thymiatis, G., 1995, The ore mineralization in Laodikino–Lipsidri area, Kilkis district, Macedonia, north Greece, Aristotle University of Thessaloniki, Greece, Ph.D. thesis, 260 p, (in Greek with English abstract).

Thompson, A.J.B., and Thompson, J.F.H., 1998, Atlas of alteration: A field guide to hydrothermal alteration minerals, Geological Association of Canada, Vancouver, p. 119.

Tirel, C., Gueydan, F., Tiberi, C., and Brun, J.-P., 2004, Aegean crustal thickness inferred from gravity inversion, Geodynamical implications, Earth and Planetary Science Letters, v. 228, p. 267–280.

Tompouloglou, C., 1981, Les minéralisations tertiares, type cuivre porphyrique, du massif Serbo-Macédonien (Macédoine, Grèce) dans leur context magmatique (avec un traitement géostatistique pour les données du prospect d'Alexia), Ecole National Supérieure des Mines de Paris, France, Ph.D. thesis, 204 p (in French).

Tornos, F., Velasco, F., Barra, F., and Morata, D., 2010, The Tropezón Cu–Mo–(Au) deposit, Northern Chile: the missing link between IOCG and porphyry copper systems?, Mineralium Deposita, v. 45, p. 313-321.

Tosdal, R.M., and Richards, J.P., 2001, Magmatic and structural controls on the development of porphyry Cu-Mo-Au deposits, *in* Richards, J.P., Tosdal, R.M., (Eds.), Structural Controls on Ore Genesis, Society of Economic Geologists Reviews, v. 14, p. 157–181.

Tranos, M.D., Kachev, V.N., and Mountrakis, D.M., 2008, Transtensional origin of the NE-SW Simitli basin along the Strouma (Strymon) Lineament, SW Bulgaria, Journal of Geological Society London, v. 165, p. 499-510.

Tranos, M.D., Eleftheriadis, G.E., and Kilias, A.A., 2009, Philippi granitoid as a proxy for the Oligocene and Miocene crustal deformation in the Rhodope Massif (Eastern Macedonia, Greece), Geotectonic Research, v. 96, p. 69-85.

Tranos, M.,D., and Lacombe, O., 2014, Late Cenozoic faulting in SW Bulgaria: Fault geometry, kinematics and driving stress regimes, Implications for late orogenic processes in the Hellenic hinterland, Journal of Geodynamics, v. 74, p. 32– 55.

Ulrich, T., Gunther, D., and Heinrich, C.A., 1999, Gold concentrations of magmatic brines and the metal budget of porphyry copper deposits, Nature, v. 399, p. 676–679.

van Hunen, J., and Allen, M.B., 2011, Continental collision and slab break-off: A comparison of 3-D numerical models with observations, Earth and Planetary Science Letters, v. 302, p. 27–37.

Vavelidis, M., Kilias, A., Melfos, V., and Schmidt-Mumm, A., 1996, New investigations in the Au–Ag-bearing Cu mineralization in the Koronouda area, Central Macedonia, northern Greece, Terranes of Serbia: The Formation of the Geologic Framework of Serbia and the Adjacent Regions, Faculty of Mining and Geology, University of Belgrade, p. 317–322.

Vavelidis, M., and Tarkian, M., 1995, Mineralogy of the gold-silver-bearing copper mineralized zones in the Palyopyrgos (Nea Maditos-Stanos) area, Northern Greece, Journal of Mineralogy and Geochemistry, v. 3, p. 133-143.

Vavelidis, M., Melfos, V., and Kilias, A., 1999, The gold-bearing quartz veins in the metamorphic rocks at the Drakontio area, central Macedonia, northern Greece,

in Mineral Deposits, Process to Processing, Eds: Stanley, C.J. et al., p. 209-212.

Vavelidis, M., Melfos, V., and Arikas, K., 2000, Mineralogy and structural control of the Au–Ag-rich copper mineralization in the Serbomacedonian Massif, Paliomylos area, Greece, European Journal of Mineralogy, v. 12, p .22.

Vavelidis, M., 2004, Gold deposits and ancient mining activities in Macedonia and Thrace, Thessalonikeon Polis, v. 14, p. 74-93, (in Greek).

Vavelidis, M., and Andreou, S., 2007, Gold and gold working in Late Bronze Age Northern Greece, Naturwissenschaften, v. 95, p. 361-366.

Veranis, N., and Tsamantouridis, P., 1991, Using panning method to the exploration of auriferous mineralizations of Krousia metallogenic province, IGME, unpubl. Report, Thessaloniki, 15 p., (in Greek).

Voidomatis, P.S., Pavlides, S.B., and Papadopoulos, G.A., 1990, Active deformation and seismic potential in the Serbomacedonian zone, northern Greece, Tectonophysics, v. 179, p. 1-9.

von Quadt, A., Driesner, T., and Heinrich, C.A., 2004, Geodynamics and Ore Deposit Evolution of the Alpine-Carpathian-Balkan-Dinaride Orogenic System, Swiss Bulletin of Mineralogy and Petrology, v. 84, p. 1-2.

von Quadt, A., Moritz, R., Peytcheva, I., and Heinrich, C.A., 2005, Geochronology and geodynamics of calc-alkaline magmatism and Cu-Au mineralization: The Panagyurishte region of the Apuseni-Banat-Timok-Srednogorie Belt (Bulgaria), Ore Geology Reviews, v. 27, p. 95–126.

Volkov, A.V., Serafimovski, T., Alekseev, V.Y., and Tasev, G., 2010, The structural-metallogenic maps of ore districts of FYR of Macedonia, Proceedings of the XIX CBGA Congress, Thessaloniki, Greece, v. 100, p. 359-368.

Voudouris, P., and Alfieris, D., 2005, New porphyry -Cu±Mo occurrences in the north-eastern Aegean, Greece: Ore mineralogy and epithermal relationships, In Mineral Deposit Research: Meeting the Global Challenge, Springer Berlin Heidelberg, p. 473-476,

Voudouris, P.C., Melfos, V., Spry, P.G., Bindi, L., Kartal, T., Arikas, K., Moritz, R., and Ortelli, M., 2009, Rhenium-rich molybdenite and rheniite in the Pagoni Rachi Mo–Cu–Te–Ag–Au prospect, northern Greece: implications for the Re geochemistry of porphyry-style Cu–Mo and Mo mineralization, The Canadian Mineralogist, v. 47, p. 1013-1036.

Voudouris, P., Melfos, V., Spry, P. G., Bindi, L., Moritz, R., Ortelli, M., and Kartal, T., 2013, Extremely Re-rich molybdenite from porphyry Cu-Mo-Au prospects in northeastern Greece: Mode of occurrence causes of enrichment, and implications for gold exploration, Minerals, v. 3, p. 165-191.

Walther, H.J.J., Kochel, F., Leube, A., Korber, H., and Luttig, G., 1970, Sitochorion, Geological map 1:50.000, IGME, Athens.

Whalen, J.B., Anderson, R.G., Struik, L.C., and Villeneuve, M.E., 2001, Geochemistry and Nd isotopes of the Franηois Lake plutonic suite, Endako batholith: host and progenitor to the Endako molybdenum camp, central British Columbia, Canadian Journal of Earth Sciences, v. 38, p. 603-618.

Wilkinson, J.J., Wilkinson, C.C., Vry, V.H., Rusk, B.G., Séguel, J., Zentilli, M., and Jeffries, T.E., 2008, Ore fluid chemistry in super-giant porphyry copper deposits [ext. abs.]: Pacrim Congress 2008, Gold Coast, Queensland, 2008, Extended Abstracts: Melbourne, Australasian Institute of Mining and Metallurgy, p. 295−299.

Wilson, M., and Bianchini, G., 1999, Tertiary–Quaternary magmatism within the Mediterranean and surrounding regions, Tertiary Extension within the Alpine Orogen, Geological Society, London, Special Publications, v. 156, p. 141–168.

Wilson, M., and Downes, H., 2006, Tertiary–Quaternary intra-plate magmatism in Europe and relationship to mantle dynamics, Geological Society, London, Memoirs, v. 32, p. 147–166.

Winter, J.D., 2001, An introduction to igneous and metamorphic petrology: New Jersey, Prentice Hall, 697 p.

Yigit, O., 2009, Mineral deposits of Turkey in relation to Tethyan metallogeny: implications for future mineral exploration, Economic Geology, v. 104, p. 19-51.

Yigit, O., 2012, A prospective sector in the Tethyan Metallogenic Belt: Geology and geochronology of mineral deposits in the Biga Peninsula, NW Turkey, Ore Geology Reviews, v. 46, p. 118-148.

Zagorchev, I., 2007, Structure and tectonic evolution of the Pirin-Pangaion Structural Zone (Rhodope Massif, southern Bulgaria and northern Greece, Geological Journal, v. 29, p. 241 – 268.

Zhang, S.-H., Zhao, Y., Song, B., Hu, J.-M., Liu, S.,-W., Yang, Y.-H., Chen, F.-K., Liu, X.-M., Liu, J., 2009, Contrasting Late Carboniferous and Late Permian–Middle Triassic intrusive suites from the northern margin of the North China craton: Geochronology, petrogenesis, and tectonic implications, Geological Society of America Bulletin, v. 121, p. 181-200.

Zhenhua, Z., Xiaolin, X., Qiang, W., Zhiwei, B., Yuquan, Z., Yingwen, X., Shuangkui, R., 2003, Alkali-rich igneous rocks and related Au and Cu large and superlarge deposits in China**,** Science in China Series D: Earth Sciences**, v.** 46, pp 1-13**.**

Zürcher, L., Bookstrom A.A., Hammarstrom, J.M., Mars, J.C., Ludington, S., Zientek, M.L., Dunlap, P., and Wallis, J.C., with contributions from Drew, L.J., Sutphin, D.M., Berger, B.R., Herrington, R.J., Billa, M., Kuşcu, I., Moon, C.J., and Richards, J.P., 2015, Porphyry copper assessment of the Tethys region of western and southern Asia: U.S. Geological Survey, Scientific Investigations Report, 2010–5090–V, 232 p., and spatial data.